

REF COPY

2

DOT/FAA/CT-88/29

Stall/Spin Aerodynamic Data Project

FAA Technical Center
Atlantic City International Airport
N.J. 08405

AD-A216 610

ERIC
ECTE
05 1990
D CB D

Melvin H. Snyder

Institute for Aviation Research
Wichita State University

September 1989

Final Report

This document is available to the U.S. public through the National Technical Information Service, Springfield, Virginia 22161.

DISTRIBUTION STATEMENT A

Approved for public release
Distribution Unlimited



U.S. Department of Transportation
Federal Aviation Administration

90 01 08 017

NOTICE

This document is disseminated under the sponsorship of the U. S. Department of Transportation in the interest of information exchange. The United States Government assumes no liability for the contents or use thereof.

The United States Government does not endorse products or manufacturers. Trade or manufacturers' names appear herein solely because they are considered essential to the objective of this report.

1. Report No. DOT/FAA/CT-88/29		2. Government Accession No.		3. Recipient's Catalog No.	
4. Title and Subtitle STALL/SPIN AERODYNAMIC DATA PROJECT				5. Report Date September 1989	
				6. Performing Organization Code	
7. Author(s) Melvin H. Snyder				8. Performing Organization Report No. DOT/FAA/CT-88/29	
9. Performing Organization Name and Address Institute for Aviation Research The Wichita State University Wichita, KS 67208				10. Work Unit No. (TRAIS)	
				11. Contract or Grant No.	
12. Sponsoring Agency Name and Address U.S. Department of Transportation Federal Aviation Administration Technical Center Atlantic City International Airport, NJ 08405				13. Type of Report and Period Covered Final 1 Oct. 1986 - 30 Sept. 1988	
				14. Sponsoring Agency Code	
15. Supplementary Notes COTR: John Reed Technical Center					
16. Abstract The purpose of this project was to develop a bank of aerodynamic data including high angle-of-attack aerodynamic characteristics of 2-D airfoils and characteristics of 3-D wings and of complete airplanes beyond the stall. To fill gaps in available literature, flow visualization studies and wind tunnel tests were to be conducted. Also, a flow visualization laboratory was to be established to study wing stall and anti-stall devices. The flow visualization laboratory is in operation. A bank of 2-D high angle-of-attack airfoil data has been compiled. The 3-D data have been acquired; water tunnel and wind tunnel reflection plane tests have been performed and continue. Data obtained indicated that movable leading-edge control surfaces show promise toward the goal of controlled flight beyond the stall.					
17. Key Words Stall, Spin Departure, High Angle of Attack Airfoil Characteristics; Leading-Edge Controls.			18. Distribution Statement Document is available to the public through the National Technical Information Service, Springfield, Virginia 22161		
19. Security Classif. (of this report) Unclassified		20. Security Classif. (of this page) Unclassified		21. No. of Pages 123	22. Price

TABLE OF CONTENTS

	Page
INTRODUCTION	1
Purpose	1
Specific Objectives	1
DISCUSSION	2
Progress in Achieving Objectives	2
Work in Progress	3
RECOMMENDATIONS	4
Planned Future Work	4
Test Proposal	4
Recommendation for 2-D Tests	5
REFERENCES	6
APPENDICES	
A - Compilation of Characteristics of Airfoils at High Angles of Attack	
B - Predicting Optimal Drooped Leading-Edge Extension Length for an NACA 0015 Wing Through Flow Visualization	
C - Experimental Study of Separated Flow Field on an NACA 23024 Right Wing	



Accession For	
NTIS - CRAM	<input checked="" type="checkbox"/>
DTIC - TAB	<input type="checkbox"/>
Unannounced	<input type="checkbox"/>
Justification	
By _____	
Distributed / _____	
Availability Codes	
Dist	Availability Code
A-1	

LIST OF FIGURES

Figure		Page
1a	FluiDyne Water Tunnel	7
1b	Elevation of W.S.U. 2ft. x 3ft. Water Tunnel	8
2a	First Floor Plan of I.A.R.	9
2b	Sketch of Projected Flow Visualization Laboratory	10
3	Lift Coefficient, 2-D compared to 3-D (A.R. = 13.3)	11
4	Lift Distribution in Spanwise Direction	12
5	Wing Sections Pressure Distribution $\alpha = 10$ degrees	13
6	Wing Sections Pressure Distribution $\alpha = 20$ degrees	14
7	Wing Sections Pressure Distribution $\alpha = 30$ degrees	15
8	Leading-edge and Trailing-edge Ailerons	16

INTRODUCTION

PURPOSE

The purpose of this aerodynamic data program is to develop a bank of aerodynamic data to be used by Dr. G. Nagati and his co-workers in developing a stall/spin flight simulator.

This data bank is to include high angle-of-attack aerodynamic characteristics of 2-D airfoils, characteristics of 3-D wings beyond the stall and complete airplane data.

Parallel to the establishing of the data base is the development of a flow visualization laboratory to study wing stall and anti-stall devices.

SPECIFIC OBJECTIVES

A detailed list of objectives of this program includes the following:

1. Search for and acquire literature on stall/spin flight phenomena. Evaluate the literature.
2. Acquire flight test and wind tunnel data on aircraft stalls and spins.
3. Set up a computer library of two-dimensional high angle-of-attack airfoil data and make the data readily available to users.
4. Assemble computer library of three-dimensional wing and airplane data, particularly at high angles of attack.
5. Develop a flow visualization laboratory for use in stall and spin departure studies.
6. Conduct flow visualization studies and wind tunnel tests to fill out gaps in literature.

DISCUSSION

PROGRESS IN ACHIEVING OBJECTIVES

Computer Data Bank. An extensive library of 2-D airfoil data has been acquired and stored in the W.S.U. main frame computer. These data are readily accessed by the flight simulator working group and by others.

A graphic portrayal of these data is given in the report IAR 88-110, "Compilation of Characteristics of Airfoils at High Angles of Attack" (Ref. 1). A draft of this report is attached to this report as Appendix A.

Flow Visualization Laboratory. The Flow Visualization Laboratory consists of a water tunnel, a two-dimensional smoke tunnel, and a three-dimensional smoke tunnel.

The water tunnel was contracted for in Spring, 1987 and delivered to W.S.U. in Summer, 1987. The tunnel is currently housed in a temporary metal building. It will be moved to the Flow Visualization Laboratory in the new Institute for Aviation Research building shortly after the beginning of the year, 1990.

The water tunnel was purchased from the FluidDyne company and is similar to that shown in figure 1a. The design was modified and the W.S.U. water tunnel is 3 feet deep instead of 2 feet to permit model testing at higher angles of attack. An elevation of the tunnel is shown in figure 1b. Although the water tunnel was supplied as a turn-key facility, additional equipment, such as mounting strut extension, and reflection-plane mounting, have been built in the W.S.U. shop to make it more usable.

When the Institute for Aviation Research building is completed in Fall, 1989, the water tunnel will be moved to the Flow Visualization Laboratory on the first floor of that building (see Figure 2a). This 1850 sq. ft. laboratory will also contain a new two-dimensional smoke tunnel. As shown in figure 2b, the water tunnel will be set into a 2 ft. recess in the floor so that the test section will be at eye level. A video recorder and special lights have also been provided.

At present, the 2-D and 3-D smoke tunnels in Wallace Hall are being used. The 3-D tunnel has been overhauled and a new Roscoe smoke generator has been installed.

Flow Visualization Studies. Flow visualization studies have been conducted in the water tunnel to supplement the information available to the flight simulator group. An experiment to optimize the size of drooped leading-edge extensions on a wing (Ref. 2) is included in Appendix B of this report.

Wind Tunnel Tests. To determine the span loading and the stall characteristics of wings at and above the stall, wind tunnel tests of reflection-plane wings have been conducted.

These tests are conducted in the Walter Beech 7 ft. x 10 ft. Wind Tunnel and include force balance tests, pressure surveys, and survey of the wake above and downstream of the stalling wing.

The first test was a reflection-plane test of a 9 inch chord, 60 inch semi-span (Aspect Ratio = 13.3) wing with an NACA 23024 airfoil section. The purposes of the test were (1) to validate the use of strip-a-tube pressure belts in the wind tunnel, (2) to develop a technique for obtaining span lift distribution, (3) to determine effects on span lift-distribution of wing stall, and (4) to provide some configuration of the computer methods being used by the simulator group to determine span loading.

Results of this test are reported in a thesis by Yong Wang (Ref. 3). A briefer report summarizing the thesis is attached as Appendix C.

The second in this series of tests has been completed. A series of leading-edge extension cuffs has been tested on the same wing and the spanwise size and location have been optimized. A thesis by George Ross will report the results in Spring, 1989.

WORK IN PROGRESS

Literature Searches. Intensive literature searches currently underway include:

1. Leading-edge devices, including leading-edge droop, i.e. extension, fixed, controllable and automatically movable.
2. Effects of wing sweep on span loading distribution.

Model Construction. Two new models are being constructed. First is a cambered variable-sweep water tunnel model to visualize high-alpha outboard flow as affected by wing sweep. The second model is a wind tunnel reflection-plane wing equipped with both leading-edge and trailing-edge ailerons. This wing has an NLF(1)-0414 airfoil section to provide contrast to the old low-speed NACA 23024 section already tested. It is equipped with a 20% chord l.e. aileron (may be deflected down 30 deg. and up 15 deg.) and 20% chord t.e. aileron (deflection = \pm 30 deg.).

Test in Progress. A test of three sweepback (sheared) wingtips is being conducted in the water tunnel.

RECOMMENDATIONS

PLANNED FUTURE WORK

The work of this project will continue. A particular direction of this work is pointed up by the thesis of Yong Wang (Appendix C is a summary of that thesis). For his wing, C_L vs. angle of attack is shown in figure 3 compared with $2-D C_q$. Figure 4 shows the spanwise distribution of lift. Below the stall ($\alpha = 4$ degrees and 10 degrees) the usual spanwise distribution on a finite span wing is obtained. Above the stall, however, the distribution is distinctly different. The center of lift is shifted toward the wingtip.

The reason for this shift is shown in figures 5, 6, and 7. The inboard sections stall earlier, and when the complete wing is stalled, there is still positive lift at the tip sections. This greater lift is due largely to the "side-edge lift" (see Ref. 4) created by the vortex suction lift of the wing tip vortex.

Figure 7 shows that while most of the wing is stalled ($\alpha = 30$ degrees) at 10% of chord downstream of leading edge, spanwise stations 90% and 95% are stalled at about 30% or 40%. This delay of the stall outboard has long been the goal of those seeking to prevent spin entry from the stall. Apparently, it occurs with an ordinary straight wing, but spin entry still occurs.

The ailerons are useless because the downstream part of the airfoil (the part where the ailerons are located) is stalled, even though the lift is still high. Deflection of trailing-edge ailerons does not significantly change the lift of the wing.

However, if the pressure distribution is controlled on the first 20% to 25% of the outboard wing sections, large changes in local lift (and wing rolling movement) can be obtained and the aircraft can be controlled through the stall. It is possible that leading-edge ailerons can be developed which can control the aircraft above the stall and thus prevent spin entry of a stalled aircraft.

Leading-edge ailerons may be designed by hinging the forward part of the airfoil. While leading-edge ailerons may be quite effective above the stall, they will probably be not very effective at low angles of attack. The most effective control system will probably incorporate both leading-edge and trailing-edge ailerons as shown in figure 8.

TEST PROPOSAL

The principal investigator and a group of graduate students propose to conduct a systematic investigation of a lateral control system using leading-edge ailerons. The objective is a

system which will provide controlled flight through and beyond the stall. The initial tests will make use of the 3-D reflection plane model currently under construction.

RECOMMENDATION FOR 2-D TESTS

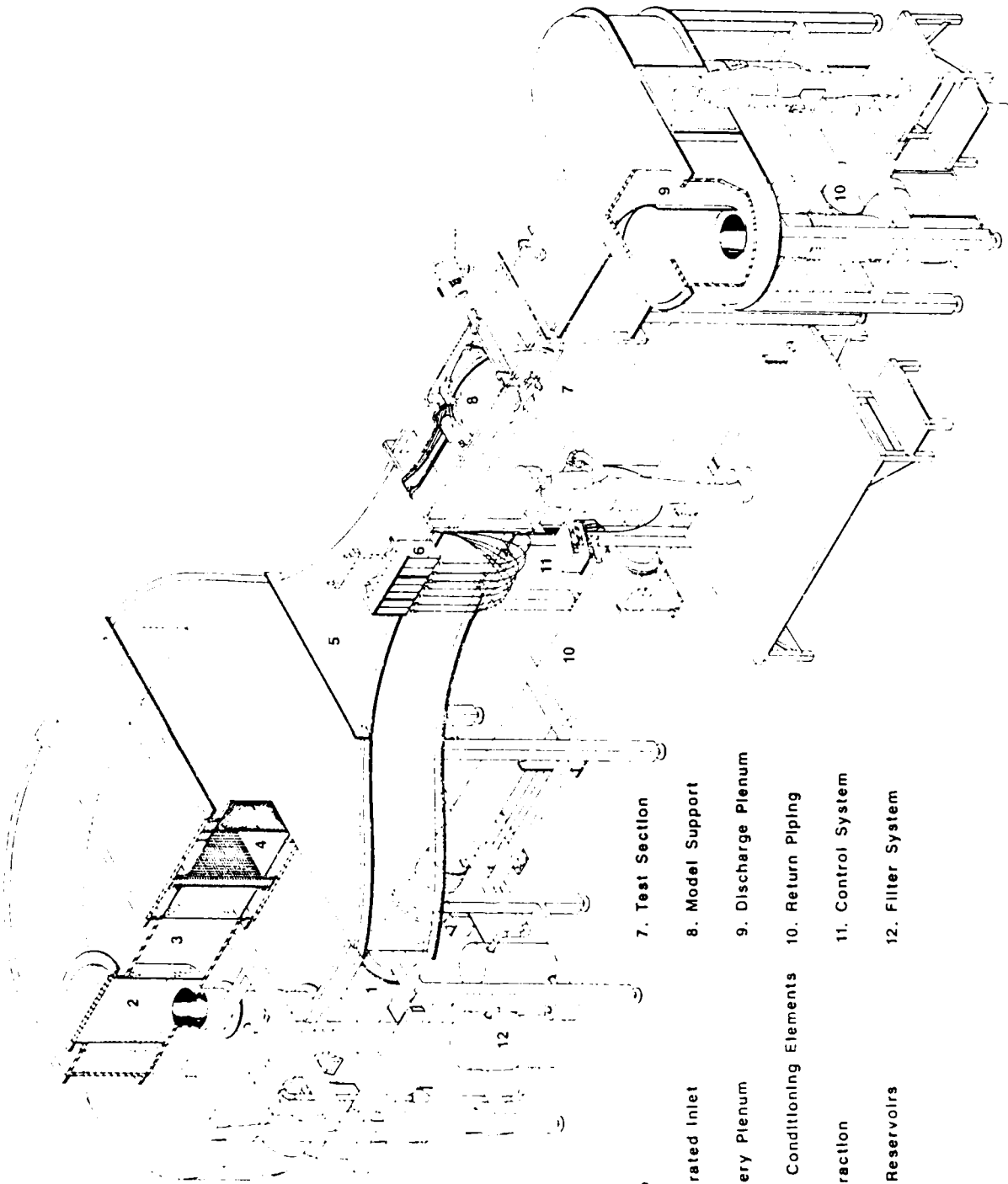
It is recommended that support be obtained to also provide a 2-D model and tests to determine aerodynamic characteristics of a section with positive and negative aileron deflections as follows:

1. Trailing-edge aileron
2. Leading-edge aileron
3. Leading-edge and trailing-edge ailerons acting together

Angles of attack would be from -10 to +45 degrees. Effects of slots and aileron drooping will also be determined. Measurements would include force balance data and surface pressure data. Flow visualization tests would pay particular attention to the wing areas at both ends of the ailerons.

REFERENCES

1. Wang Yong and Melvin H. Snyder; "Compilation of Characteristics of Airfoils at High Angles of Attack"; IAR 88-110, Institute for Aviation Research, The Wichita State University, Wichita, KS, August, 1988.
2. August A. Asay and Melvin H. Snyder; "Predicting Optimal Drooped Leading-Edge Extension Length for an NACA 0015 Wing Through Flow Visualization"; IAR 88-111, Institute for Aviation Research, The Wichita State University, Wichita, KS, May, 1988.
3. Yong Wang; "Experimental Study of Separation Flow Field on NACA 23024 Right Wing"; M.S. Thesis, The Wichita State University, Wichita, KS, July, 1988.
4. John E. Lamar; "Extension of Leading-Edge-Suction Analogy to Wings with Separated Flow Around the Side Edges at Subsonic Speeds"; NASA TR R-428, NASA Langley Research Center.
5. Ira Abbott and A. E. von Doenhoff; Theory of Wing Sections, Dover Publications, Inc., New York, 1959.



KEY:

- 1. Pump
- 2. Perforated Inlet
- 3. Delivery Plenum
- 4. Flow Conditioning Elements
- 5. Contraction
- 6. Dye Reservoirs
- 7. Test Section
- 8. Model Support
- 9. Discharge Plenum
- 10. Return Piping
- 11. Control System
- 12. Filter System

Figure 1a. FluidDyne Water Tunnel.

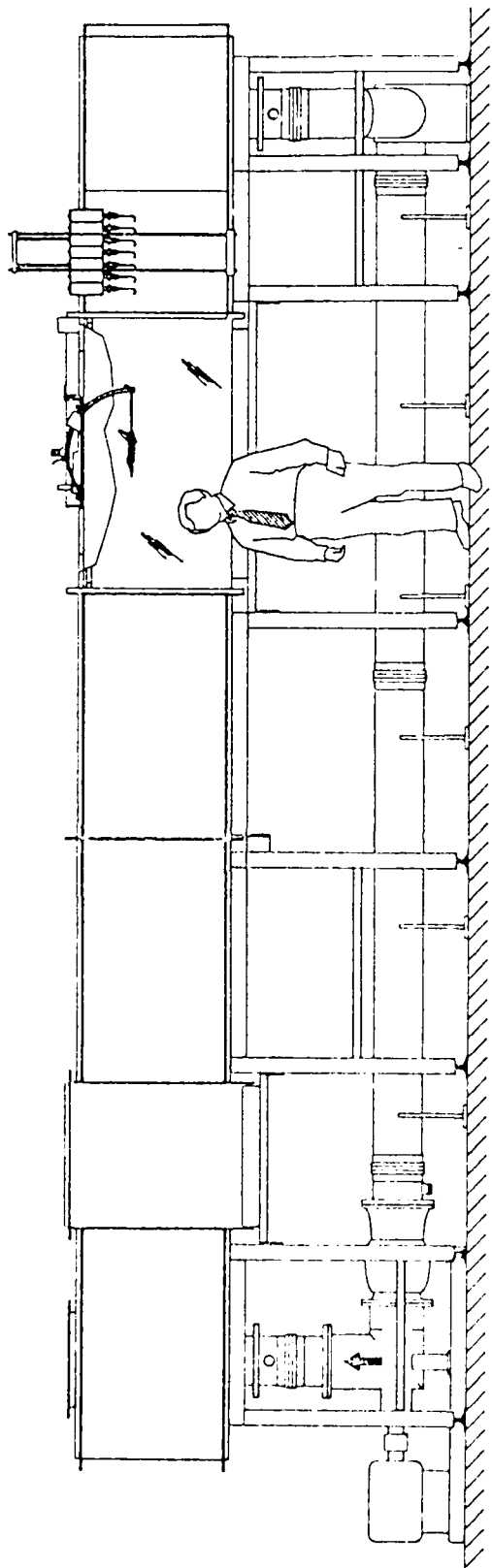


Figure 1b. Elevation of W. S. U. 2 ft. X 3 ft. Water Tunnel.

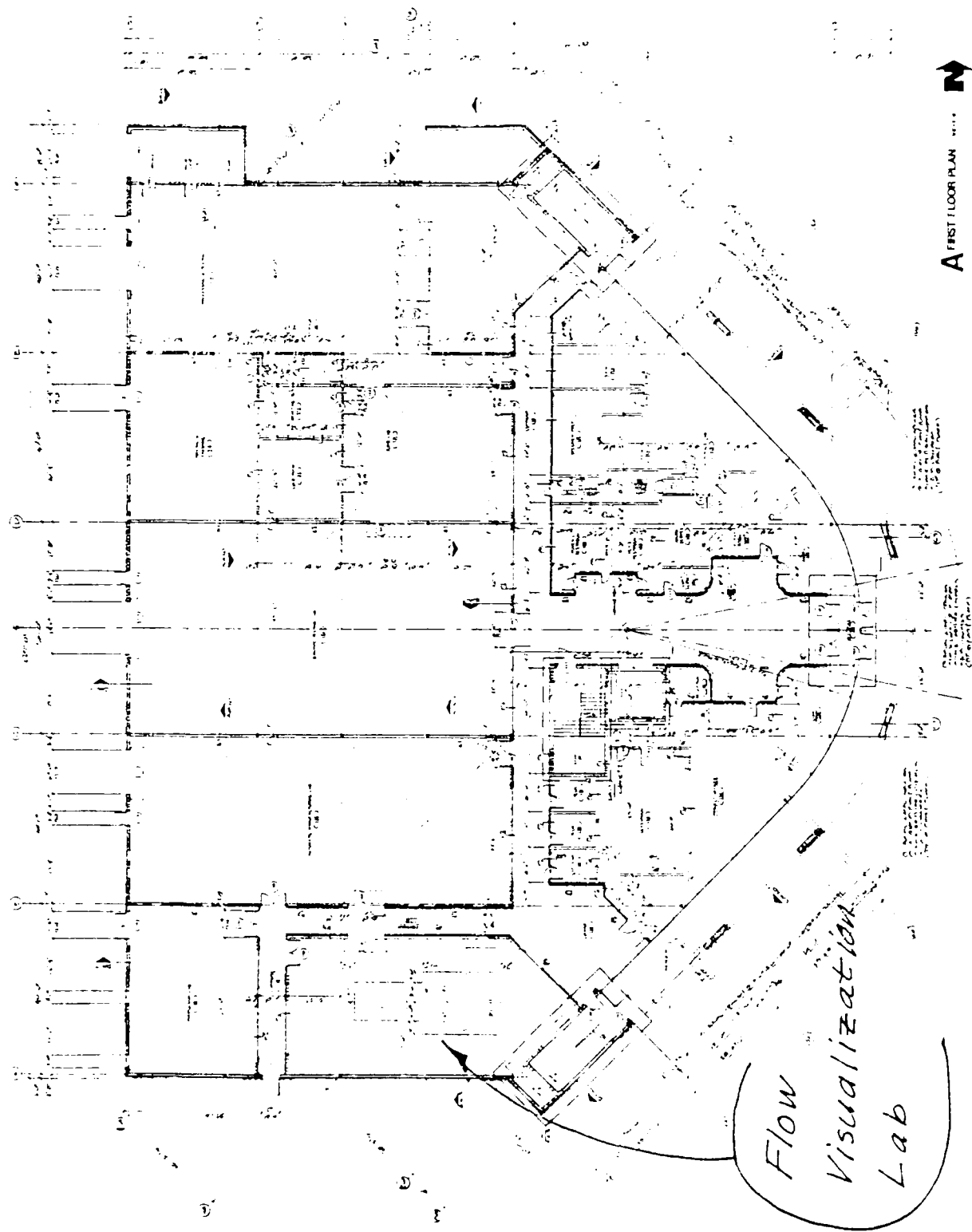


Fig. 2a. First Floor Plan of Aviation Research Building Showing Flow Visualization Lab.

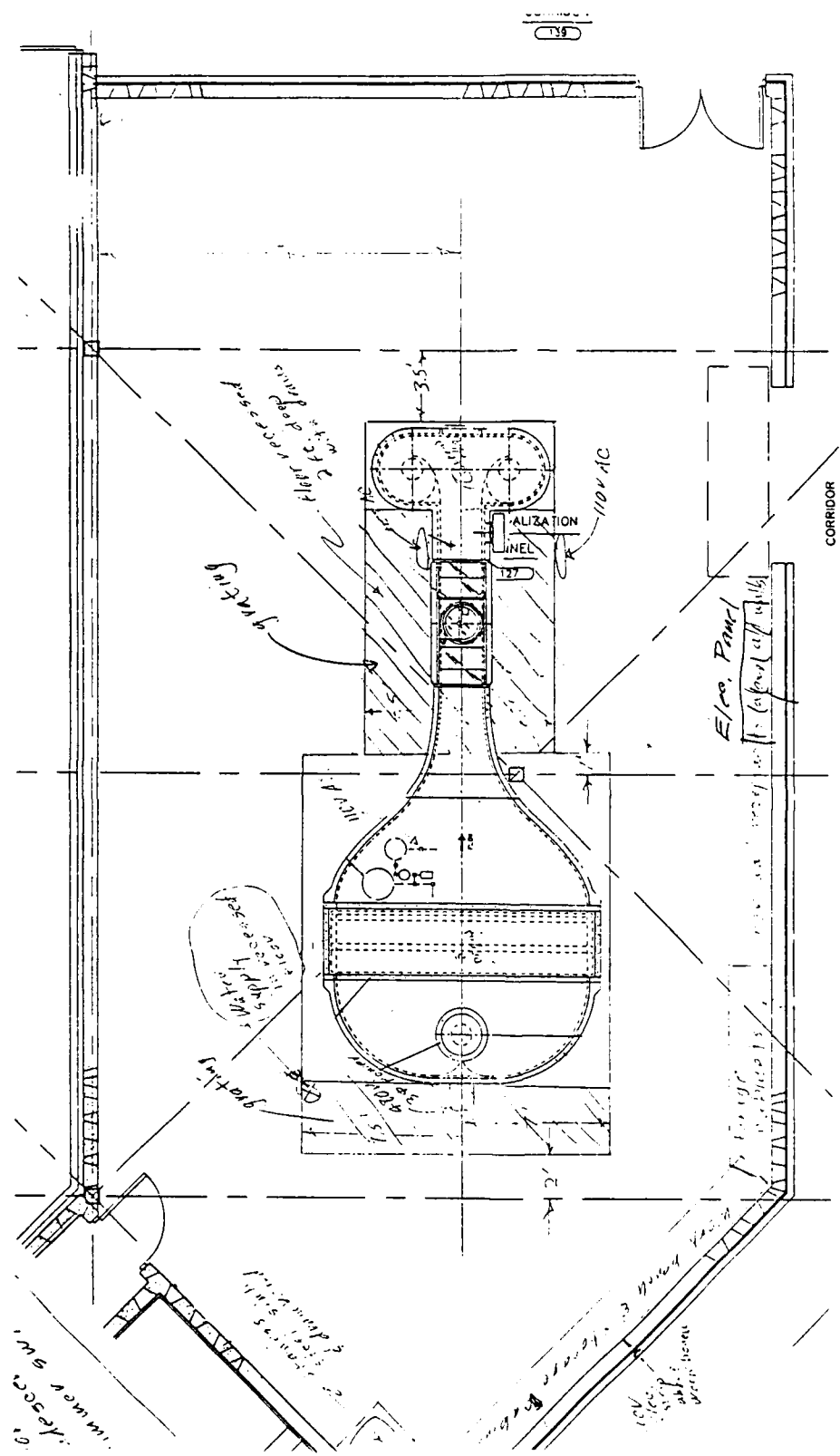


Figure 2b. Sketch of Projected Flow Visualization Laboratory.

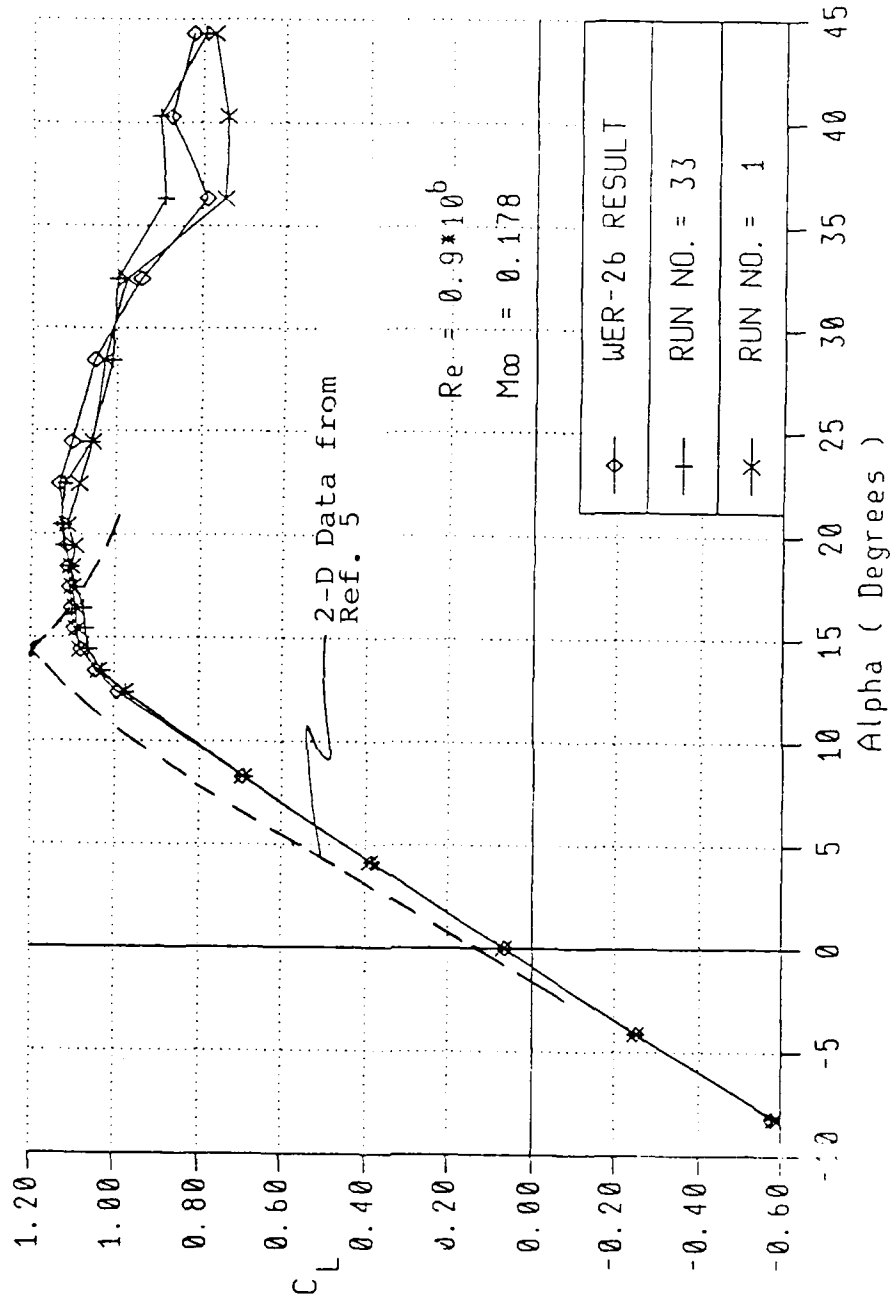


Figure 3. Lift Coefficient, 2-D Compared to 3-D (A.R.=13.3)

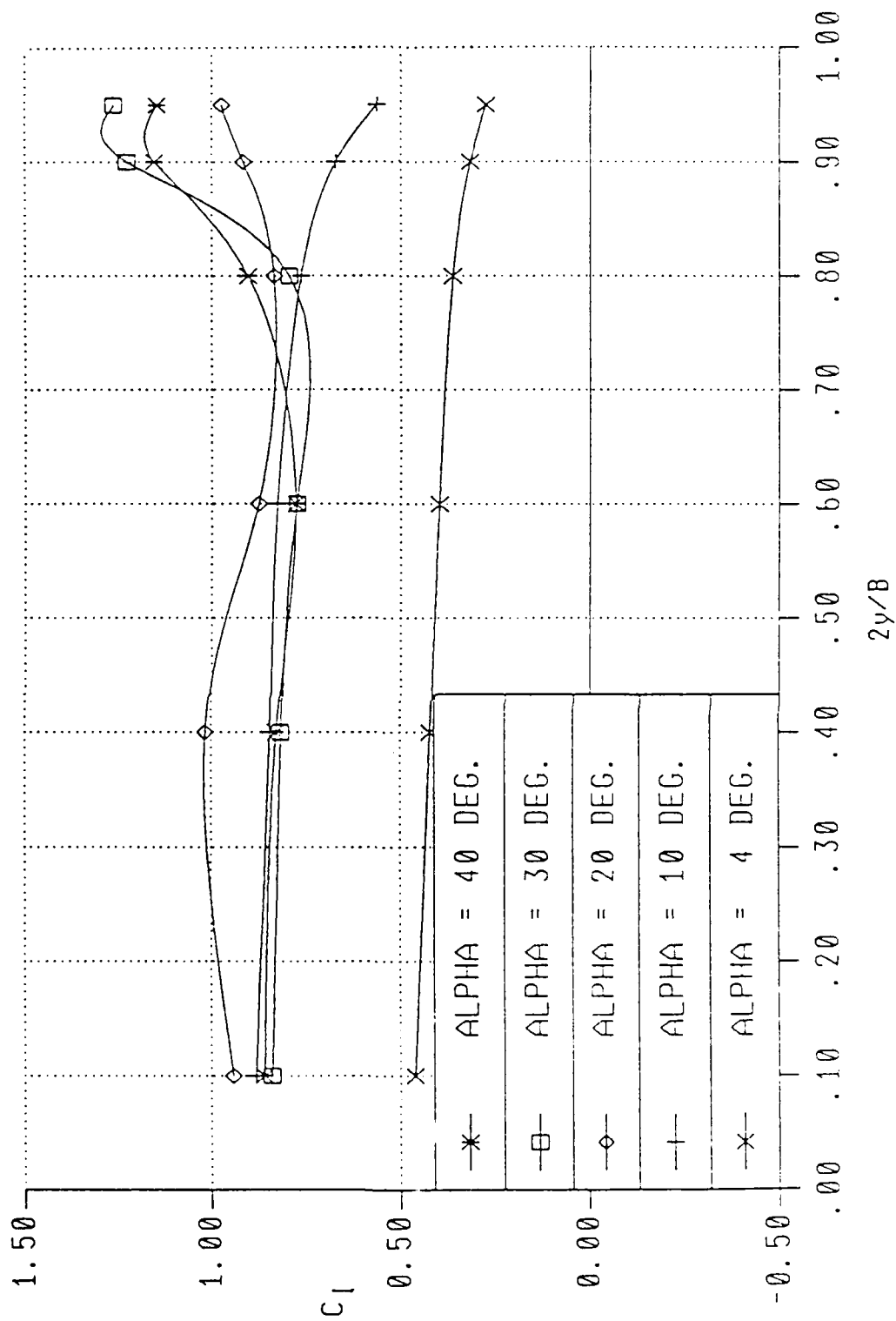


Figure 4. Lift Distribution in Spanwise Direction

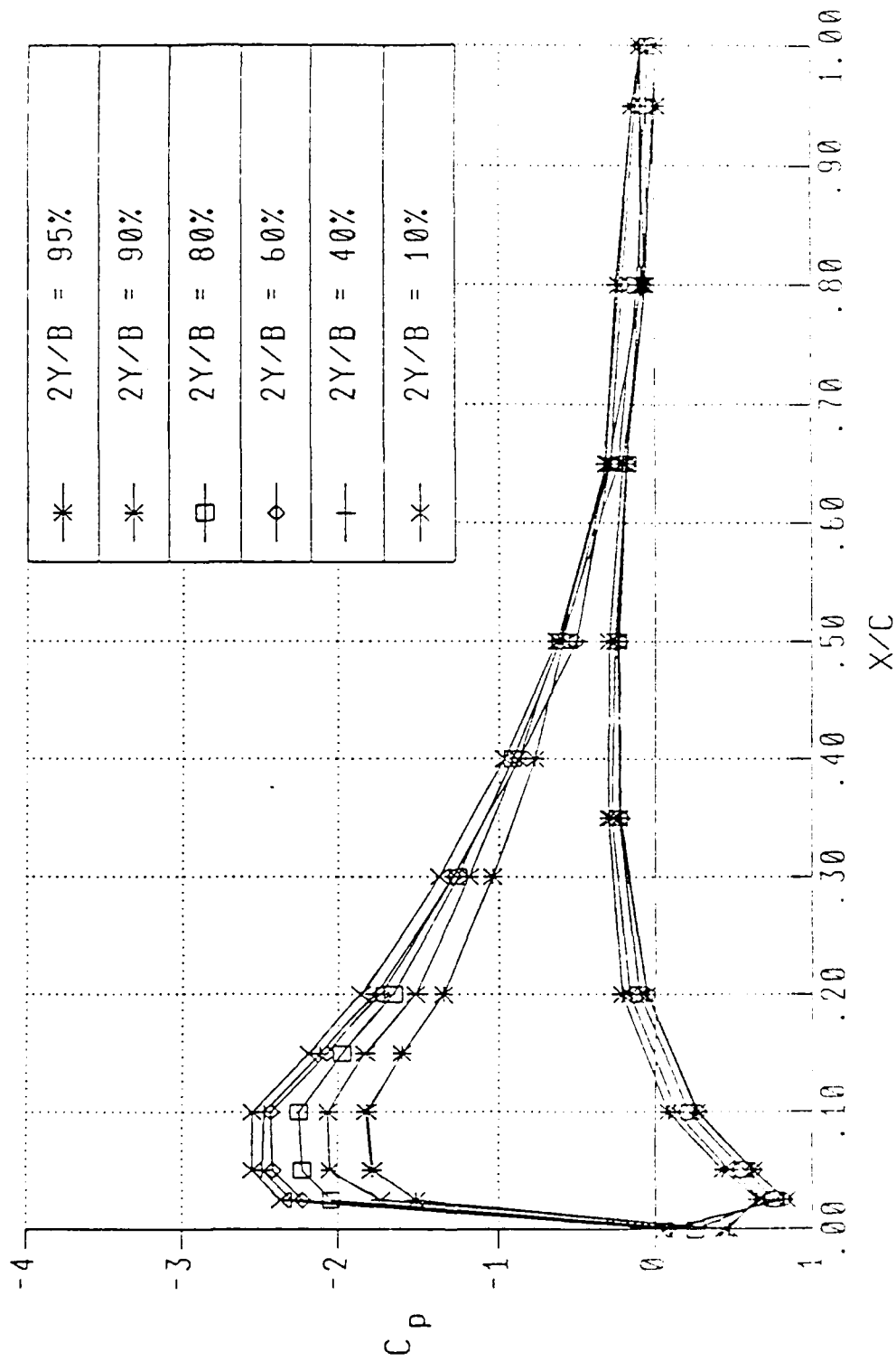


Figure 5. Wing Sections Pressure Distribution $\alpha = 10^\circ$

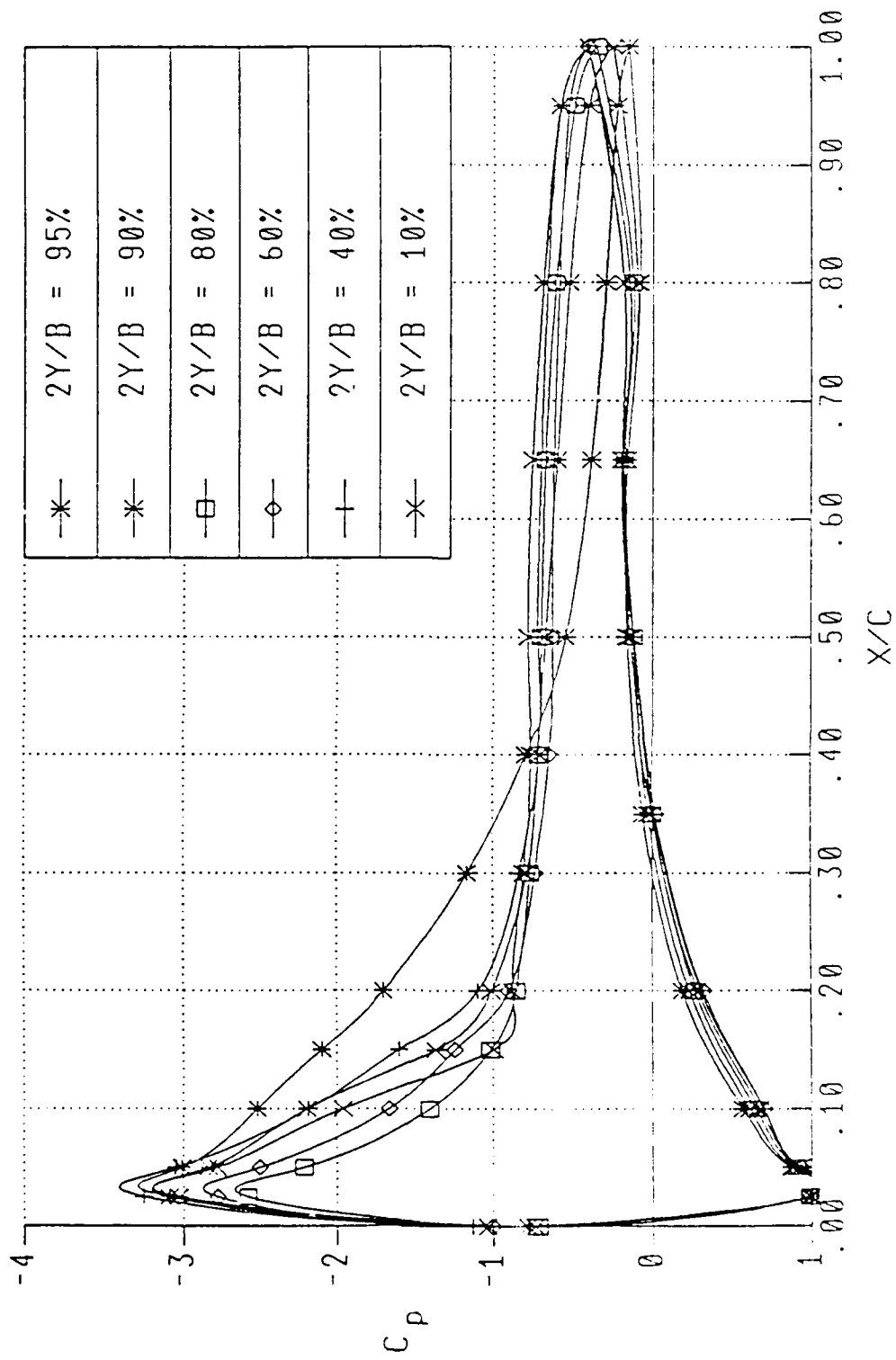


Figure 6. Wing Sections Pressure Distribution $\alpha=20^\circ$

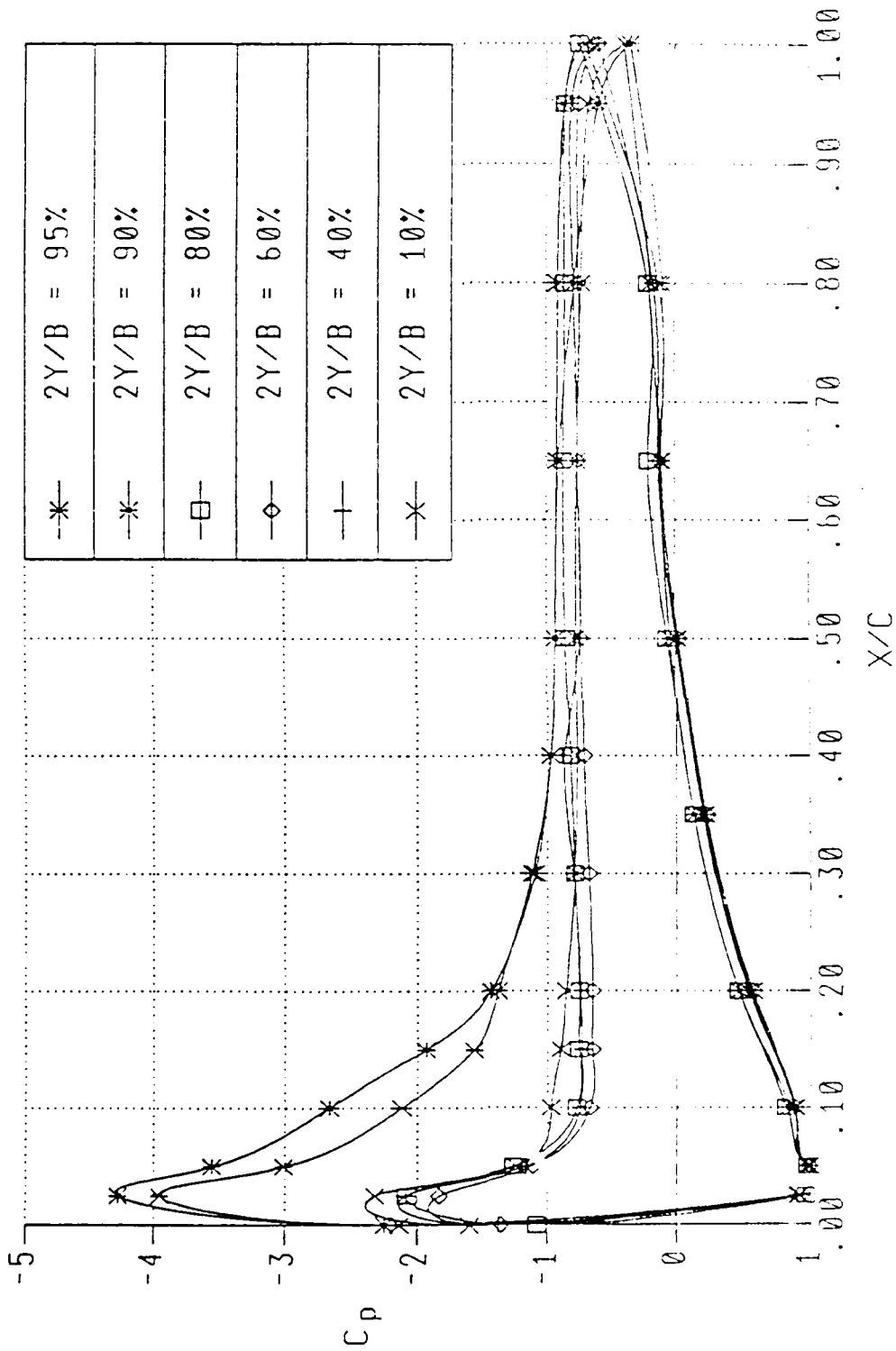


Figure 7. Wing Sections Pressure Distribution $\alpha = 30^\circ$

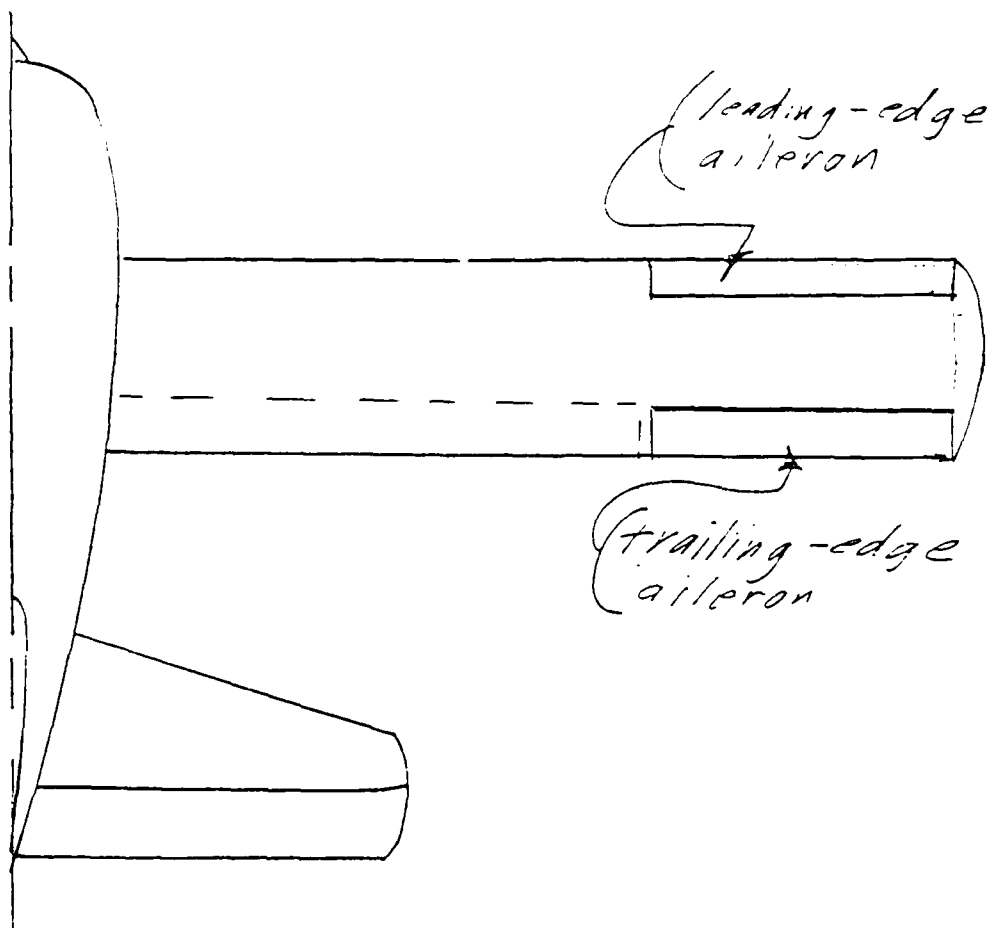
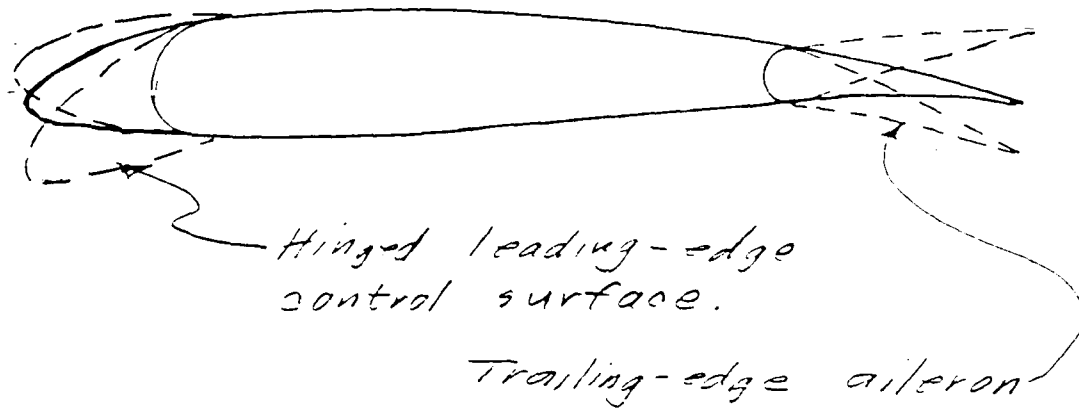


Figure 8. Leading-Edge and Trailing-Edge Ailerons.

Appendix A

IAR 88-110

**COMPILATION OF CHARACTERISTICS
OF AIRFOILS
AT HIGH ANGLES OF ATTACK**

by

Yong Wang

and

Melvin H. Snyder

INSTITUTE FOR AVIATION RESEARCH

THE WICHITA STATE UNIVERSITY

WICHITA, KS 67208

August 1988

INTRODUCTION

A data bank of characteristics of a number of airfoils at high angles of attack has been established at the Institute for Aviation Research at The Wichita State University. This data bank has been established for the use of persons attacking stall and spin problems, wind turbine designers, and those interested in supraaerodynamics (i.e., maneuvering, flight beyond the stall).

The present report presents the characteristics graphically for quick inspection and preliminary design work. Those needing numerical data may apply to the Institute for Aviation Research.

DISCUSSION

The airfoil sections are listed in Table 1 and they are illustrated in figure 1. Note that only the GA(W)-1 and GA(W)-2 airfoils are shown for a full 360 degree range of angles of attack (figures 2 and 3). Characteristics of the other airfoils are shown at angles of attack up to 25 or 45 degrees.

It can be seen from figures 2, 3, and 4 that there are two parts to the lift curve. One type of airfoil flow is attached flow, from negative stall to positive stall (alpha is zero plus or minus 12 to 18 degrees) and attached flow near 180 degrees angle of attack (airfoil flying backwards). At the other angles, the flow is separated (alpha from about 25 degrees to 155 degrees and about 205 degrees to 335 degrees). In this range there are also a positive peak and a negative peak of values of lift coefficient.

The lift curves for separated flow are all nearly the same. It is in the attached region, stall, and just beyond stall that one airfoil differs from another. For example in figure 3, the first peak exceeds the second. In figure 4 the first peak is less than the second. The lift coefficient values up to angle of attack of about 25 degrees are highly dependent on airfoil profile.

Similar observations can be made about the drag coefficient curve. The curve (see figures 2 and 3) appears to be cyclic except for the angles near zero where the flow is attached. Again most of the curve is cyclic (except for alpha = \pm 25 degrees).

It should be noted that the values shown are for steady-state conditions. Actual values of the coefficients for an airfoil with changing angle of attack -- in the region of positive stall and first negative stall -- depend on whether angle of attack is increasing or decreasing, and how rapidly the angle of attack is changing. Examples of hysteresis are shown in reference 2. This characteristic is of great importance to those working on stall/spin problems and on wind turbine problems. Research on aerodynamic hysteresis is continuing at the W.S.U. Institute for Aviation Research.

REFERENCES

1. M. H. Snyder, W. H. Wentz, and A. Ahmed
"Two-Dimensional Tests of Four Airfoils of Attack From 0 to 360 Degrees"
WER-16, Wichita State University, Feb. 1984
2. Dale Satran and Melvin H. Snyder
"Two-Dimensional Tests of GA(W)-1 and GA(W)-2 Airfoils at Angles-of-Attack from 0 to 360 Degrees"
WER-1, Wichita State University, Jan. 1977
3. Robert E. Sheldahl, Paul C. Klimas
"Aerodynamic Characteristics of Seven Symmetrical Airfoil Sections Through 180-Degree Angle of Attack for Use in Aerodynamic Analysis of Vertical Axis Wind Turbines"
SAND80-2114, (Sandia National Laboratories)
4. C. Ostowari and D. Naik
"Post-Stall Wind Tunnel Data for NACA 44XX Series Airfoil Sections"
SERI/STR-217-2559, DE85002948, Jan. 1985
Solar Energy Research Institute
5. Eastman N. Jacobs, Kenneth E. Ward and Robert M. Pinkerton
"The Characteristics of 78 Related Airfoil Sections From Tests In The Variable-Density Wind Tunnel"
NACA Report No. 460
6. Eastman N. Jacobs and Albert Sherman
"Airfoil Section Characteristics as Affected by Variations of The Reynolds Number"
NACA Report No. 586

7. Ira H. Abbott and Albert E. Von Doenhoff
"Theory of Wing Sections"
8. M. H. Snyder, W. H. Wentz, and H. Cao
"Additional Reflection Plane Tests of Control Devices On
An NACA 23024 Airfoil"
WER-26, Wichita State University, February, 1987
9. M. H. Snyder, W. H. Wentz, and A. Ahmed
"Reflection Plane Test of Control Devices On A Thick
Airfoil At High Angles of Attack"
WER-23 rev, Wichita State University, October, 1986
10. W. H. Wentz, M. H. Snyder, and H. V. Cao
"Effects of Spoiler Hingeline Location On The NACA 23024
Airfoil"
WER-27, Wichita State University, August, 1986
11. Laurence K. Loftin, Jr.
"Airfoil Section Characteristics at High Angle of
Attack"
NACA-TN-3341, August, 1954
12. Chris C. Critzos, Harry H. Heyson, and Robert W.
Boswinkle, Jr.
"Aerodynamics Characteristics of NACA 0012 Airfoil
Section at High Angles of Attack From 0 to 180 Degrees"
NACA-TN-3361, January, 1955

TABLE 1
Airfoils Included in Present Report

<u>Figure</u>	<u>Airfoil</u>	<u>Angle of Attack Range (degs.)</u>	<u>Notes</u>
2	GA(W)-1	0 to 360	Ref. 2
3	GA(W)-2	0 to 360	Ref. 2
4	NACA 0012	0 to 180	Ref. 3
5	NACA 0009	0 to 45	Ref. 3
6	NACA 0012	0 to 45	Ref. 3
7	NACA 0012H	0 to 45	Ref. 3
8	NACA 0015	0 to 45	Ref. 3
12	NACA 4409	-10 to 25	NASA TN 3241
13	NACA 4412	-10 to 25	TN 3241
14	NACA 4415	-10 to 25	TN 3241
15	NACA 4418	-10 to 25	TN 3241
19	GA(W)-1	-10 to 47	Ref. 2
20	GA(W)-2	-10 to 47	Ref.
21	NACA 23024	-10 to 45	ailerons 0 to 60°
22	NACA 23024	-10 to 45	ailerons 0 to 60°
23	NACA 23030	-10 to 45	Ref. 1
24	NACA 64-3-618	-10 to 45	Ref. 1

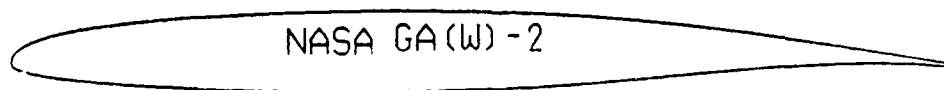
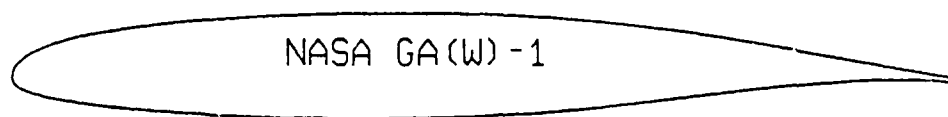


Figure 1. (a) NASA GA(W)-1 and GA(W)-2 airfoil sections

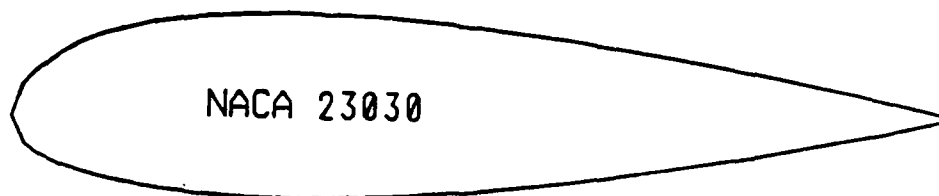
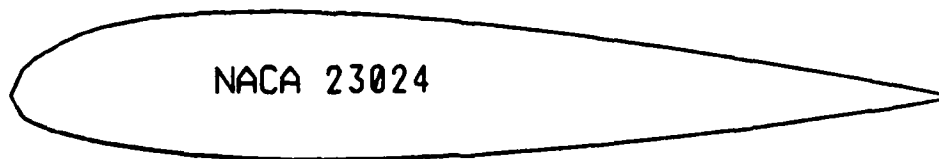
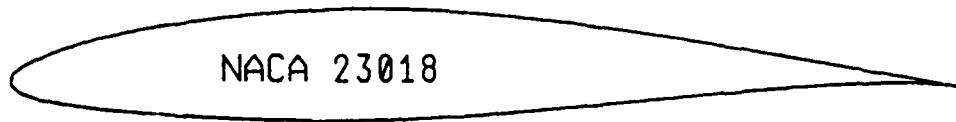


Figure 1. (b) NACA 230-series airfoil sections

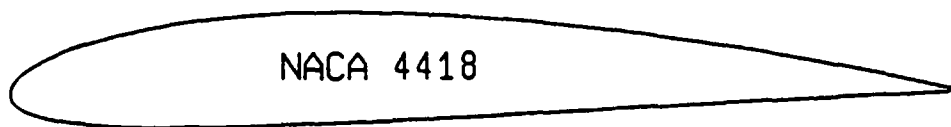
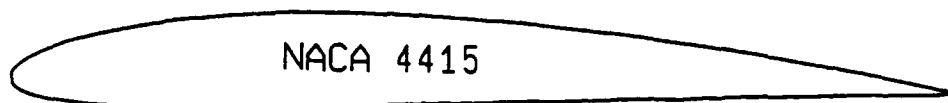
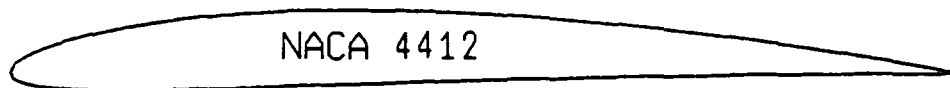
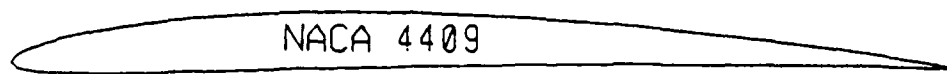


Figure 1. (c) NACA 44-series airfoil sections

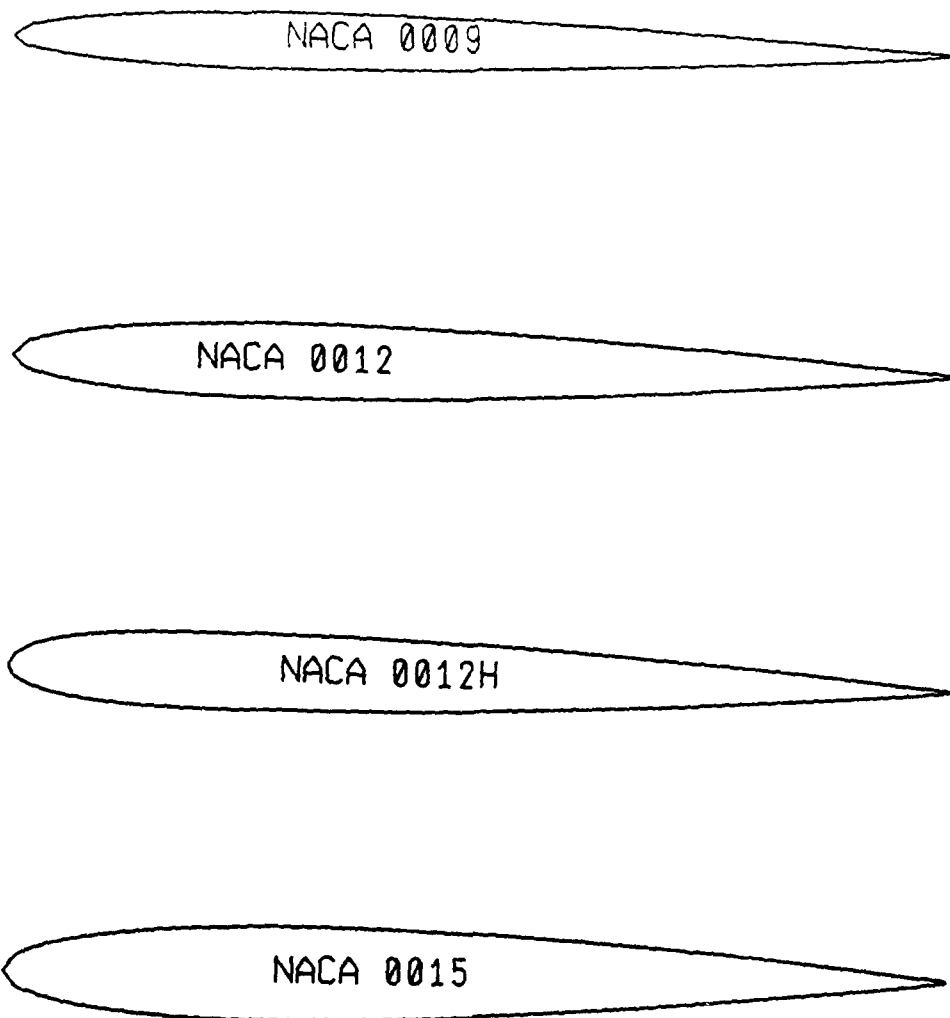


Figure 1. (d) NACA 00-series airfoil sections

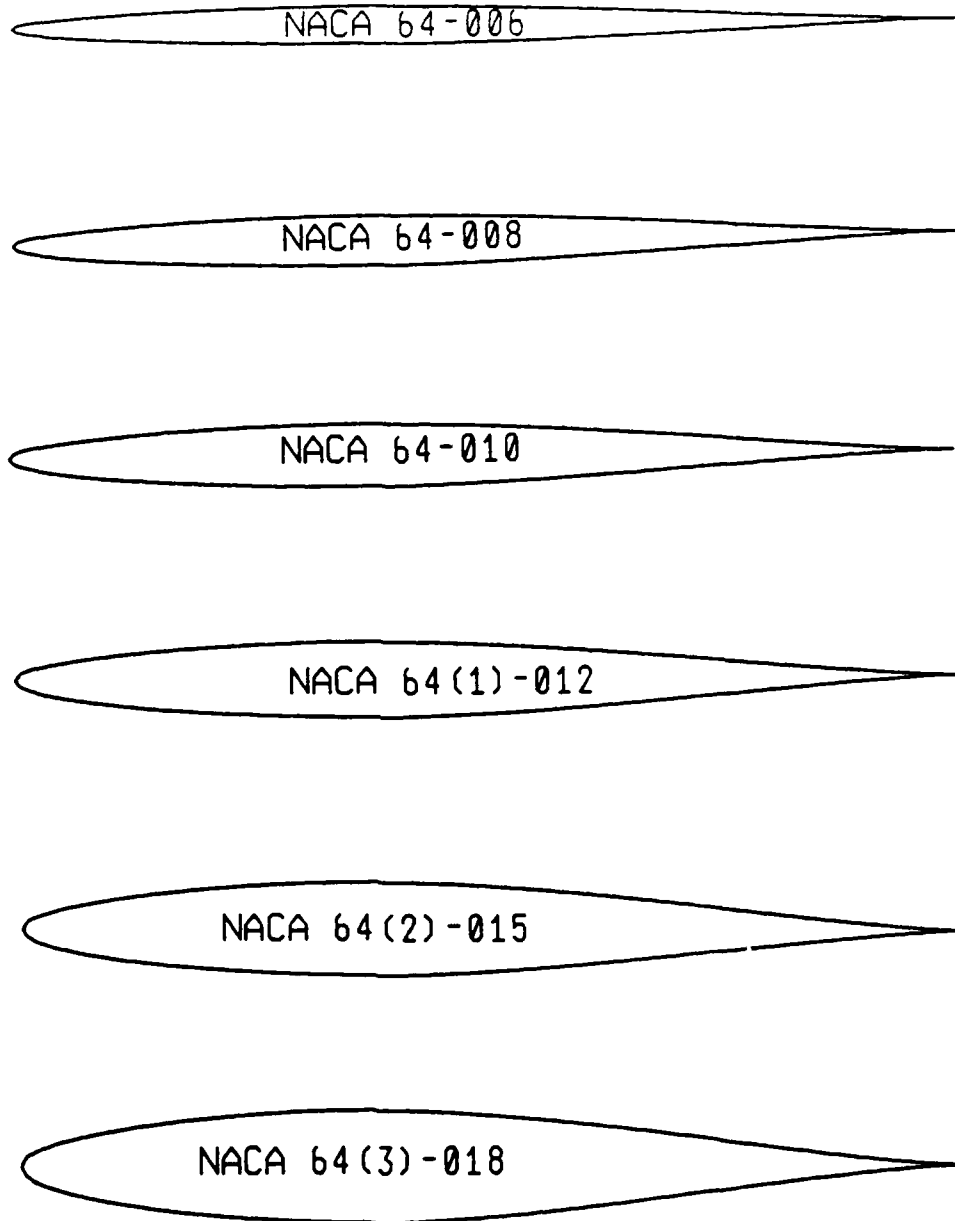


Figure 1. (e) NACA 64-series airfoil sections

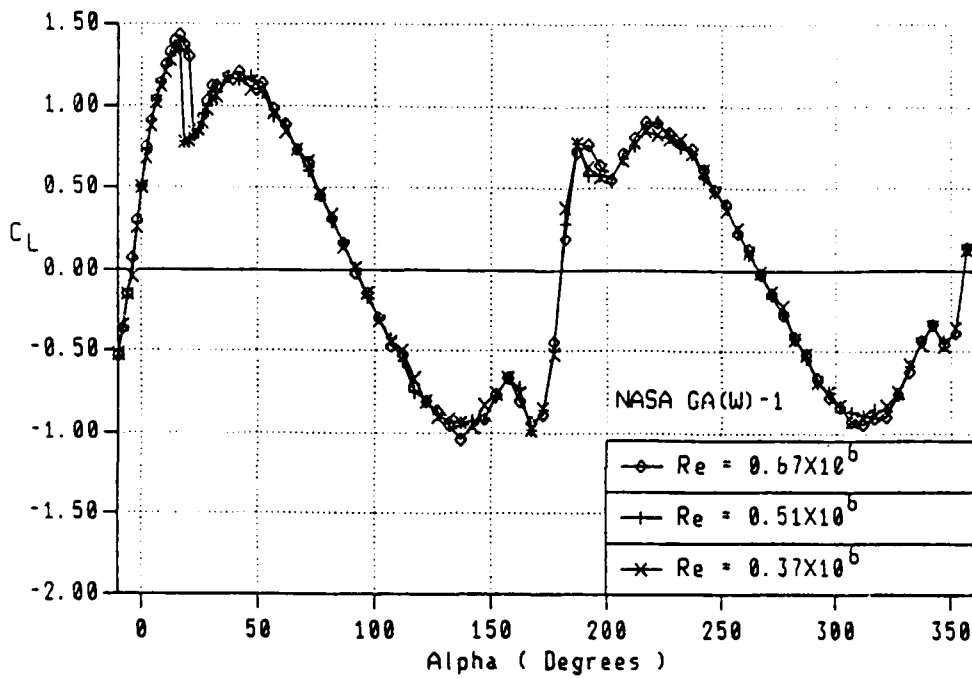


Figure 2. (a) Lift coefficients of NASA GA(W)-1 airfoil

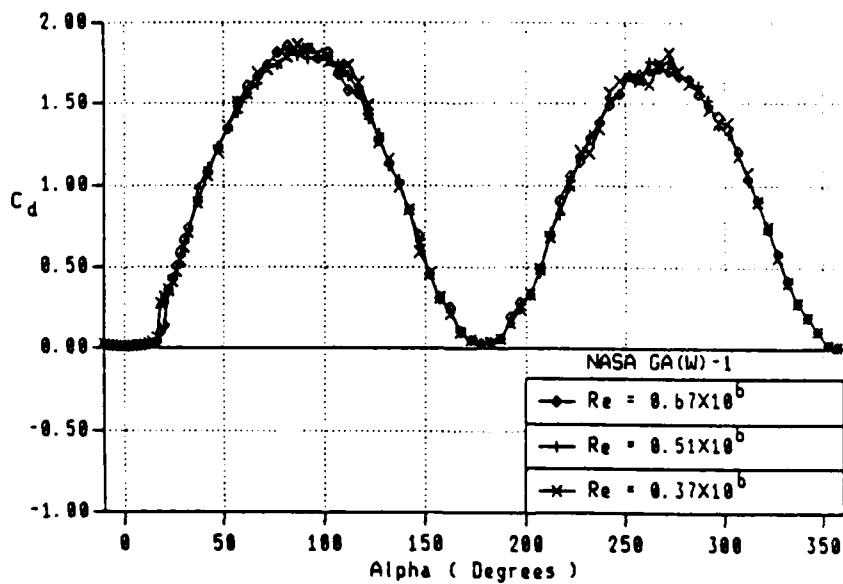


Figure 2. (b) Drag coefficients of NASA GA(W)-1 airfoil

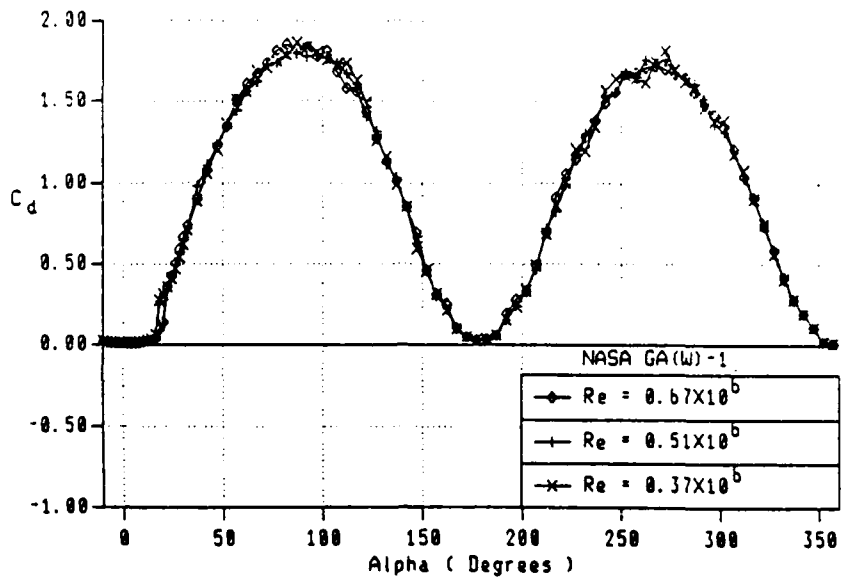


Figure 2. (a) Lift coefficients of NASA GA(W)-1 airfoil

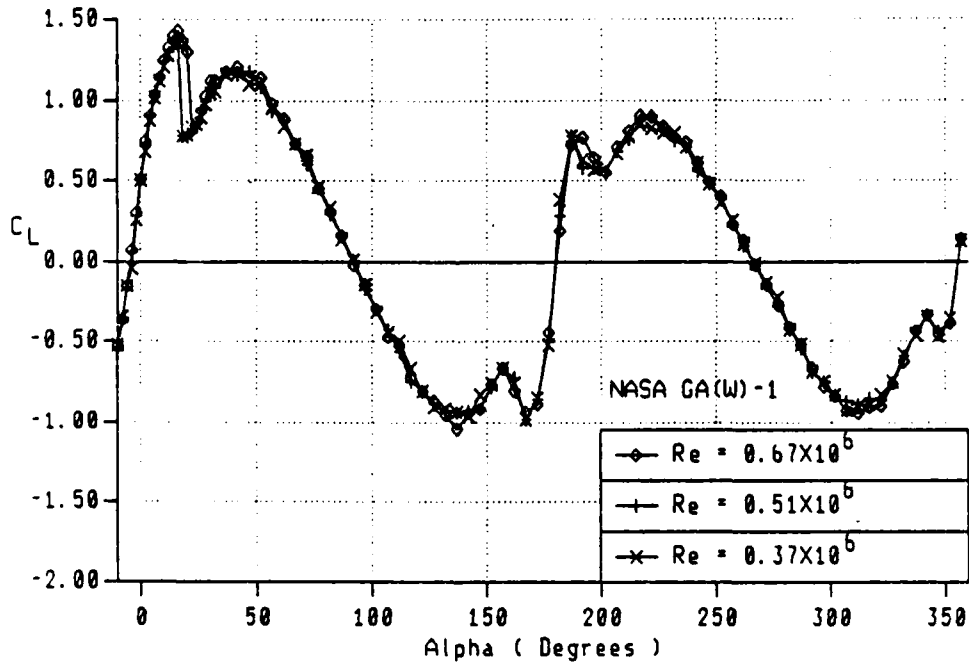


Figure 2. (b) Drag coefficients of NASA GA(W)-1 airfoil

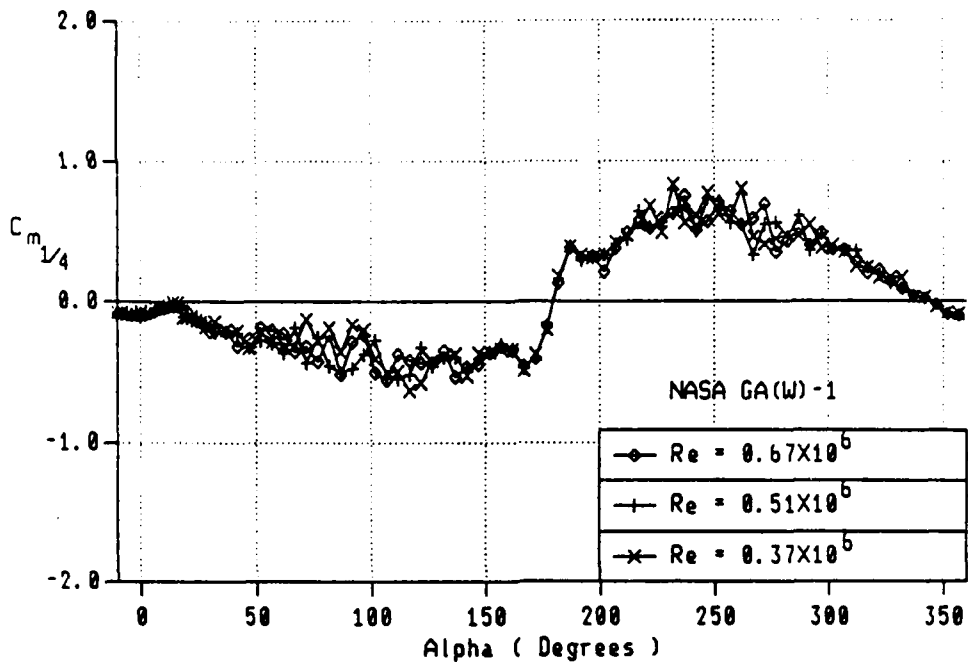


Figure 2. (c) Moment coefficients of NASA GA(W)-1 airfoil

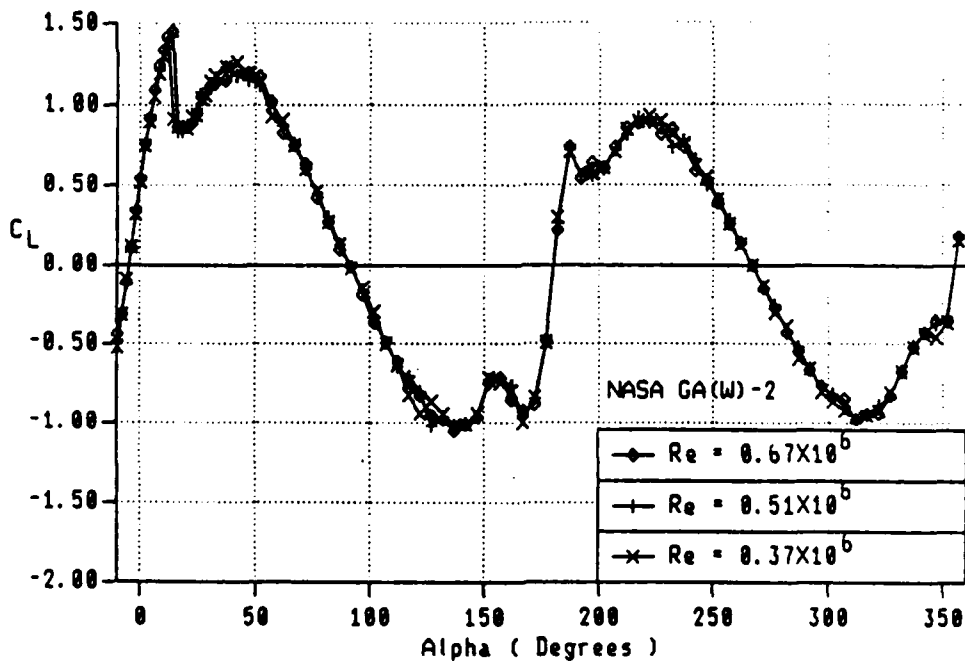


Figure 3. (a) Lift coefficients of NASA GA(W)-2 airfoil

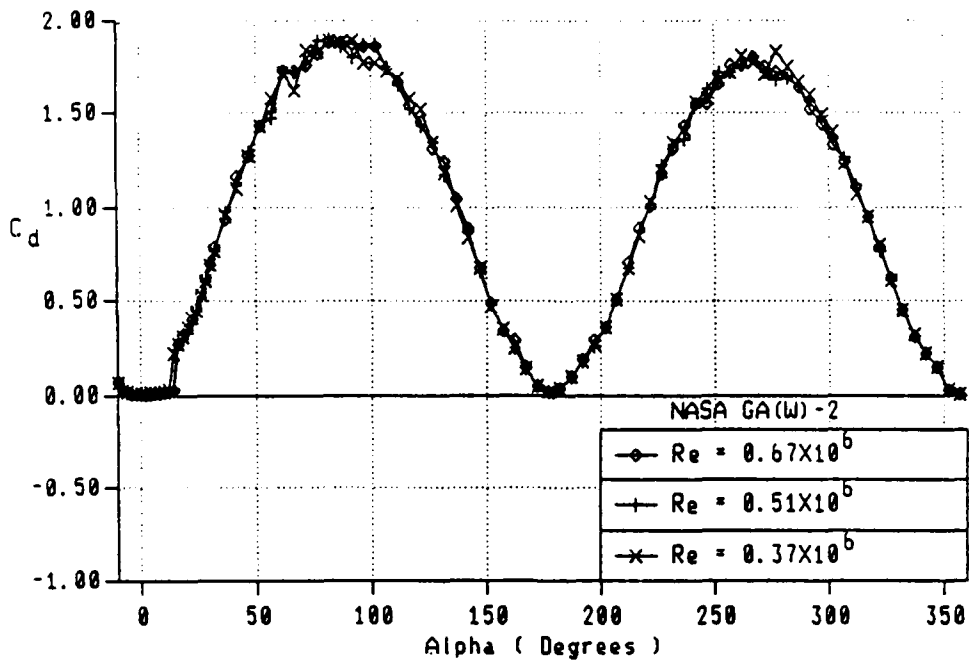


Figure 3. (b) Drag coefficients of NASA GA(W)-2 airfoil

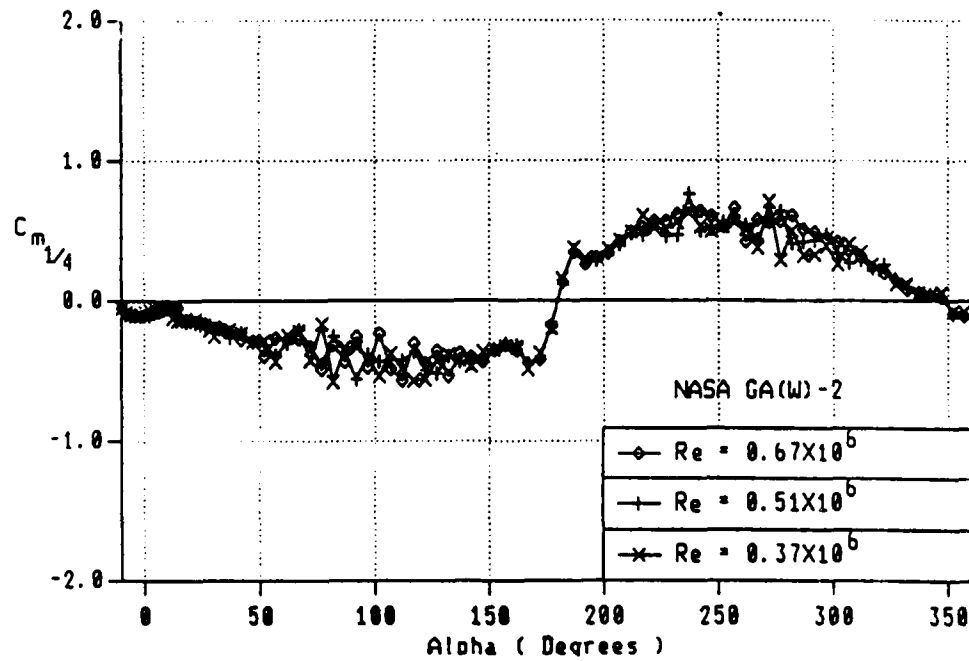


Figure 3. (c) Moment coefficients of NASA GA(W)-2 airfoil

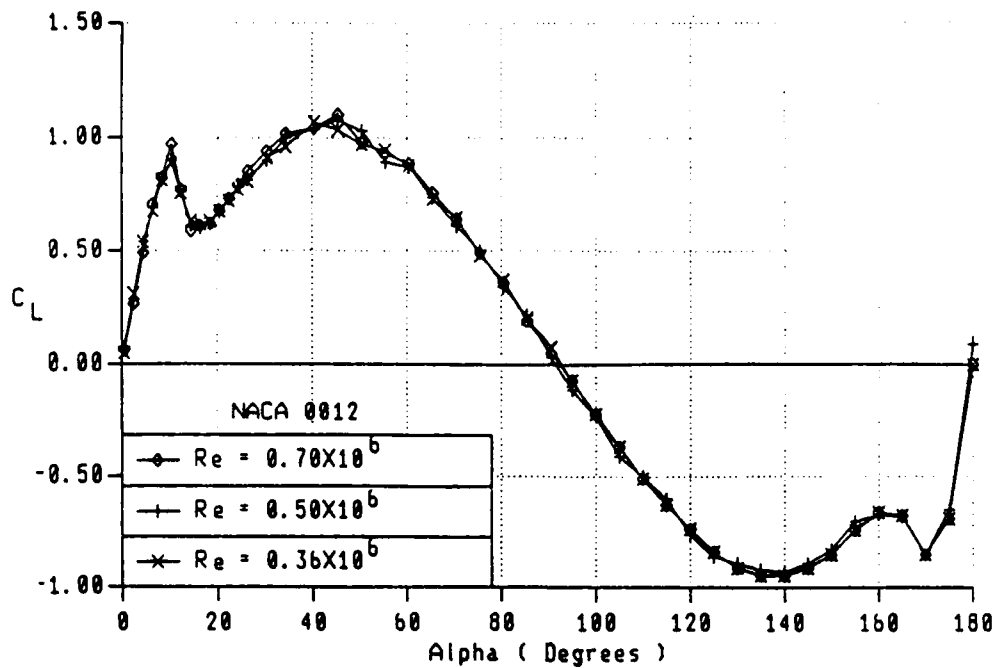


Figure 4. (a) Lift coefficients of NACA 0012 airfoil

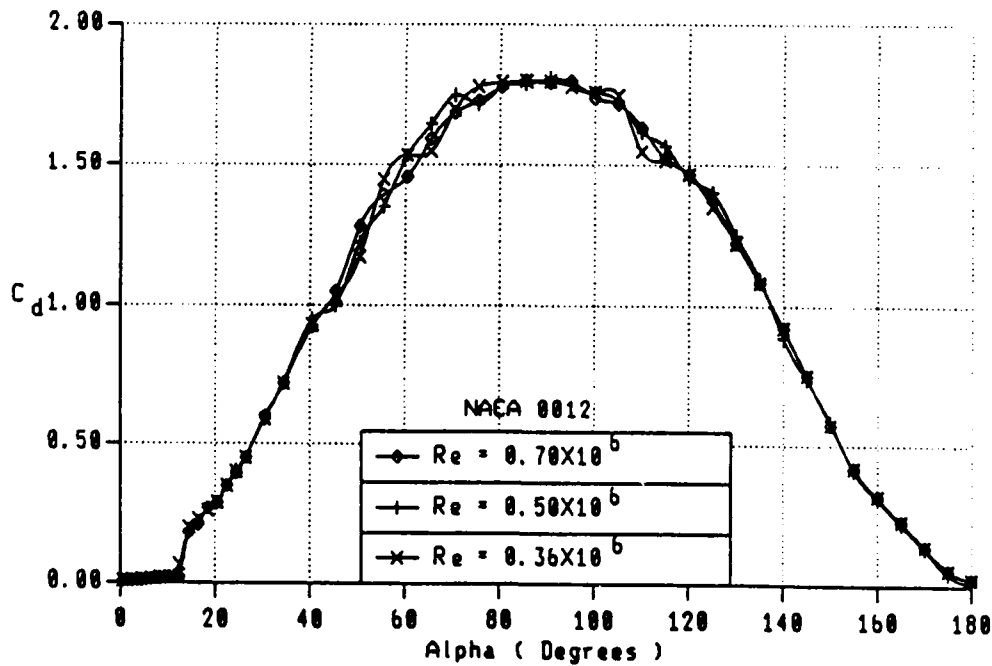


Figure 4. (b) Drag coefficients of NACA 0012 airfoil

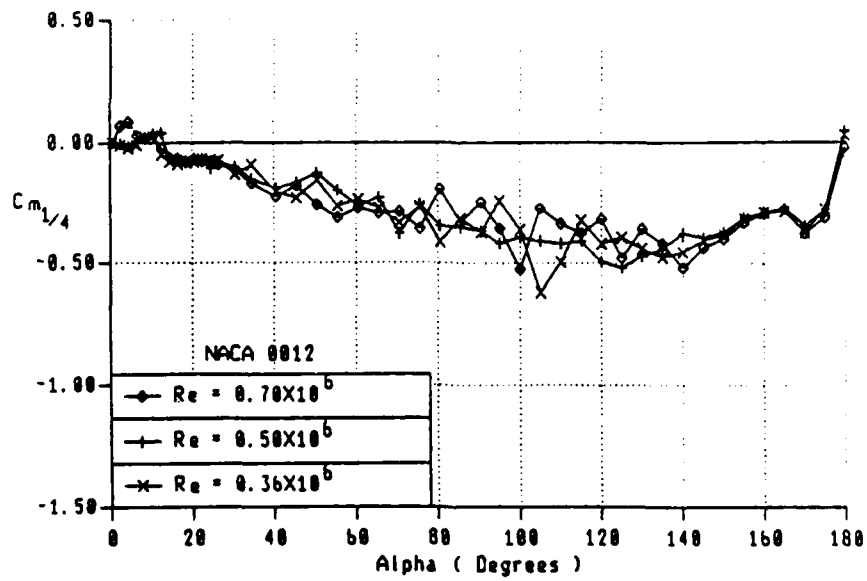


Figure 4. (c) Moment coefficients of NACA 0012 airfoil

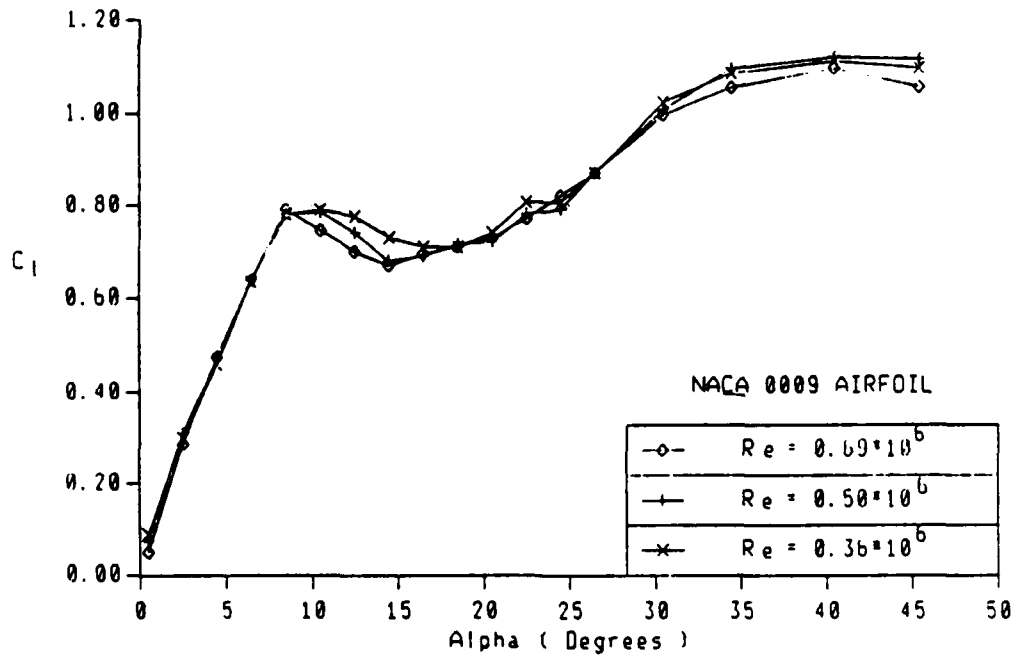


Figure 5. (a) Lift coefficients of NACA 0009 airfoil

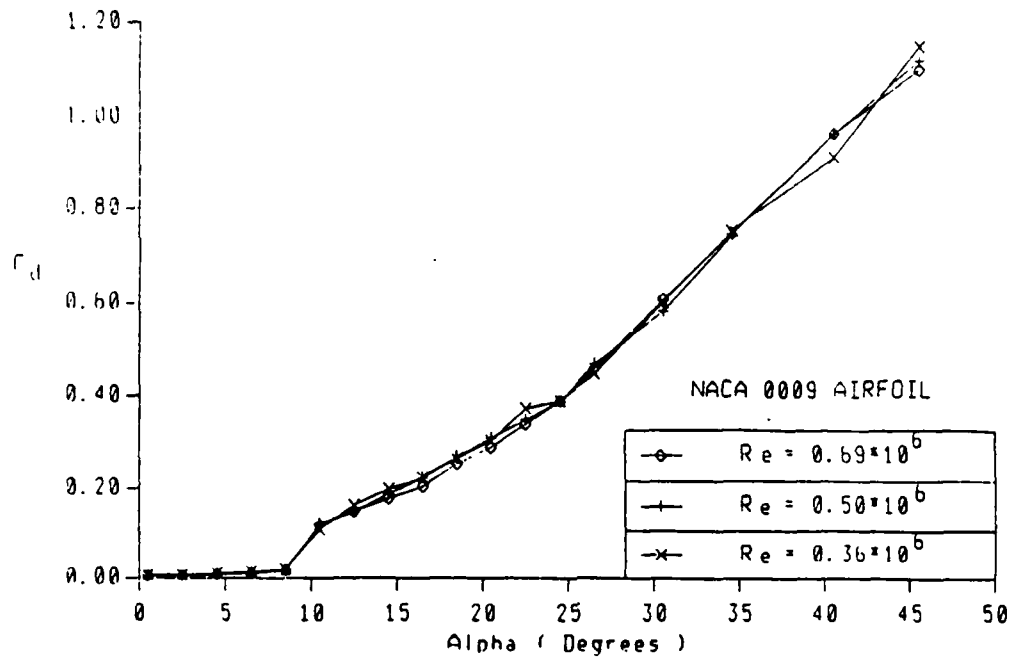


Figure 5. (b) Drag coefficients of NACA 0009 airfoil

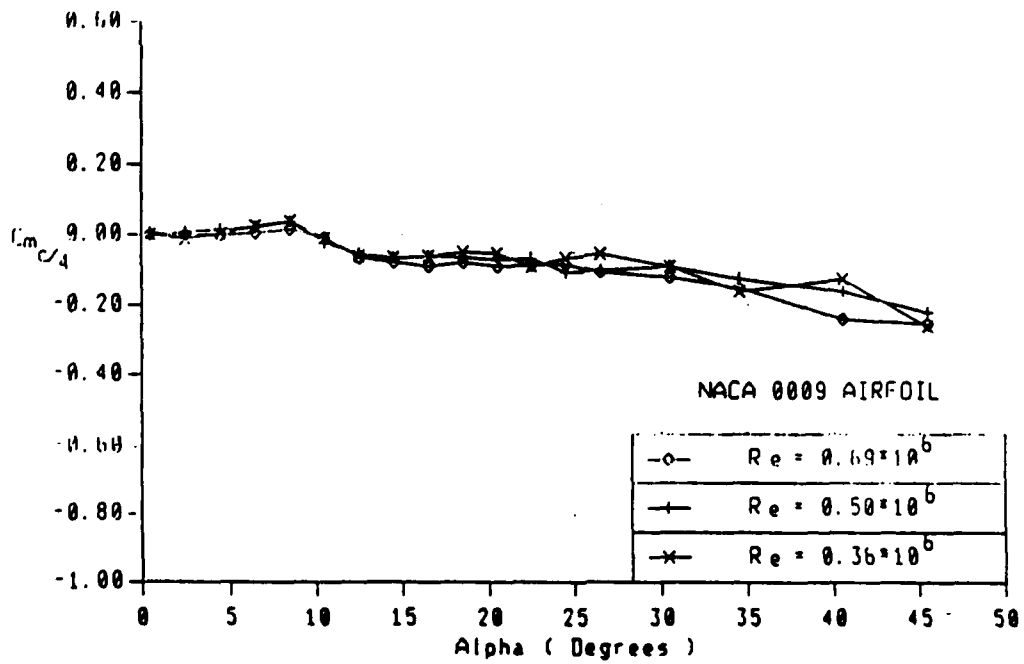


Figure 5. (c) Moment coefficients of NACA 0009 airfoil

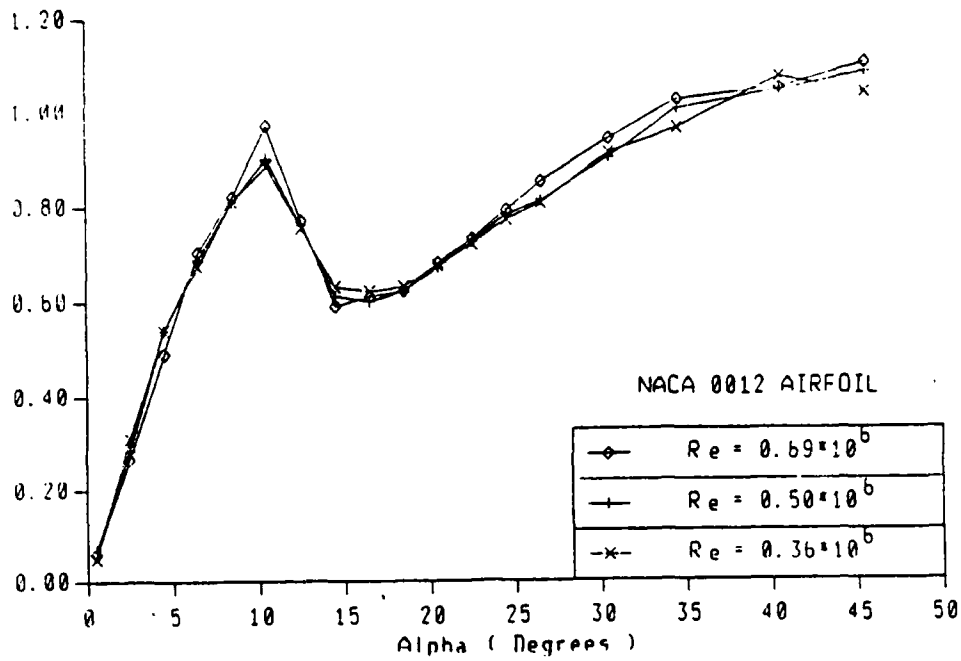


Figure 6. (a) Lift coefficients of NACA 0012 airfoil

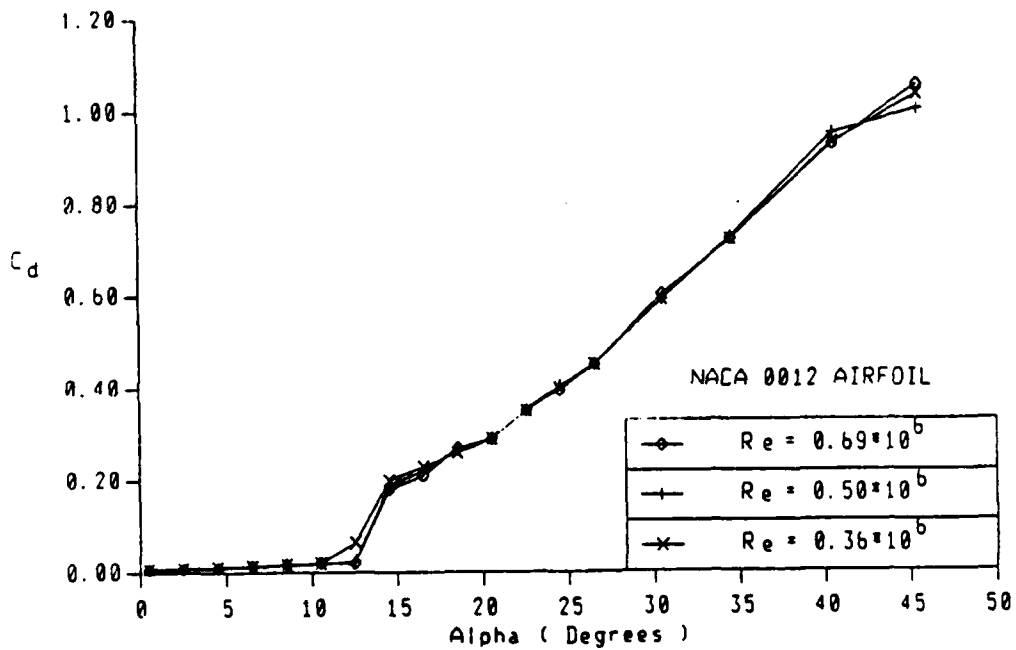


Figure 6. (b) Drag coefficients of NACA 0012 airfoil

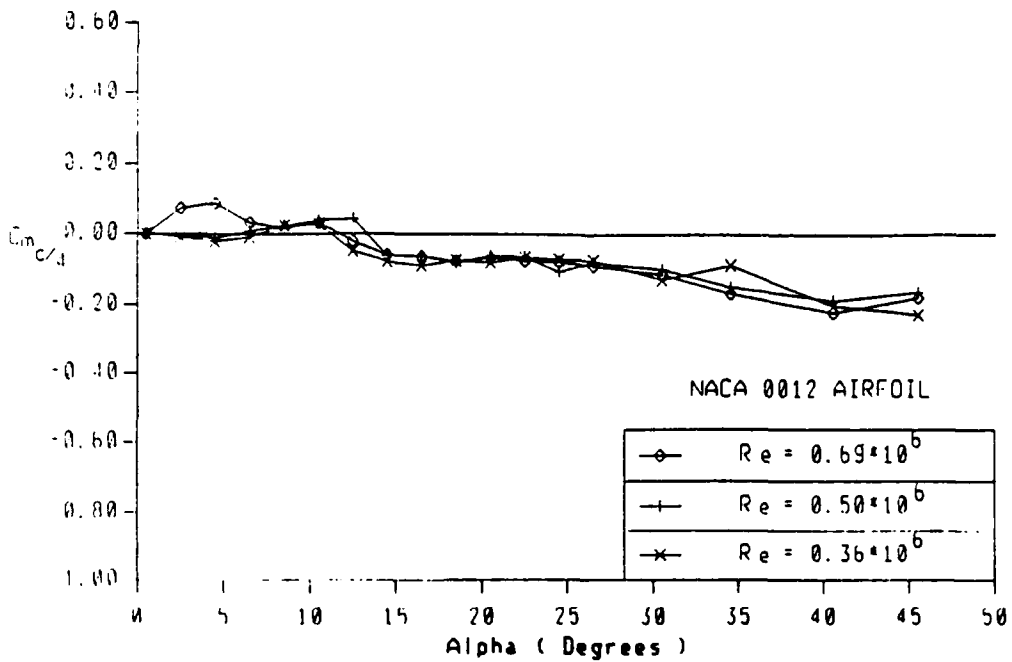


Figure 6. (c) Moment coefficients of NACA 0012 airfoil

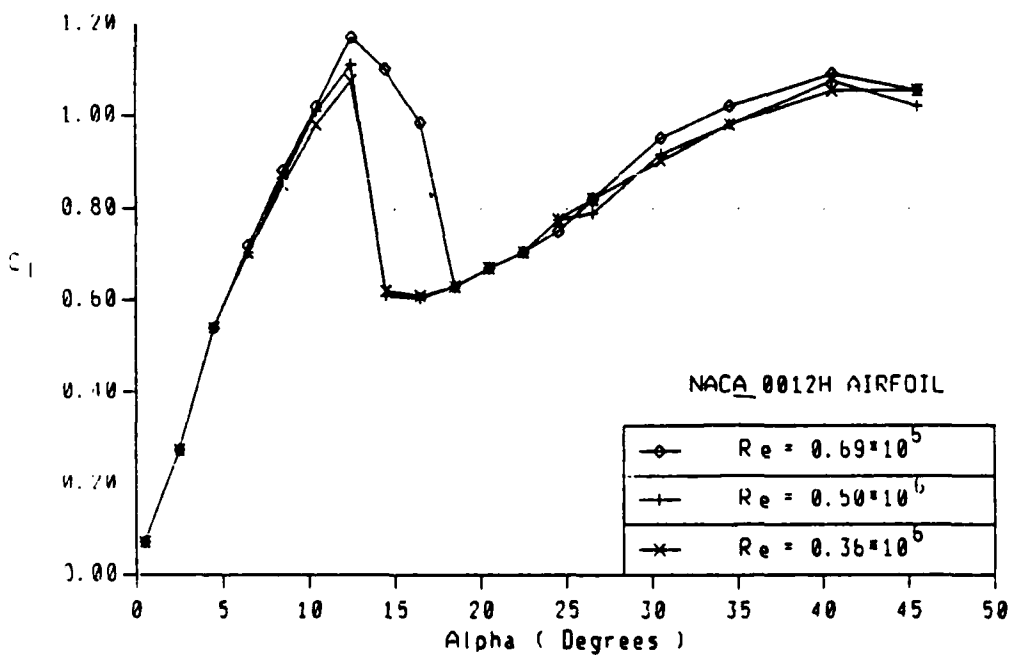


Figure 7. (a) Lift coefficients of NACA 0012H airfoil

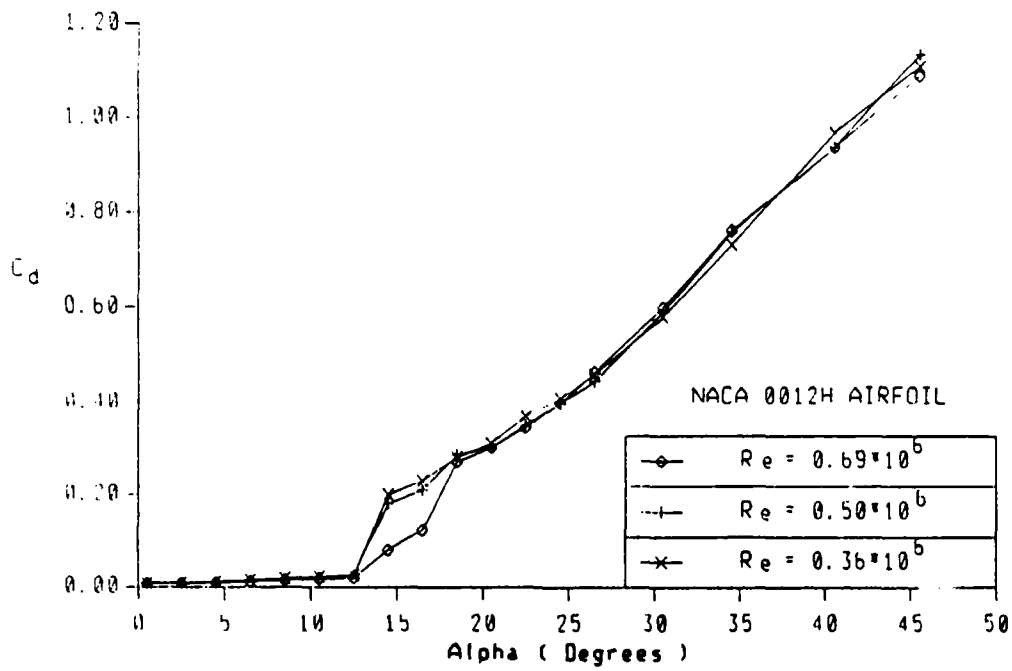


Figure 7. (b) Drag coefficients of NACA 0012H airfoil

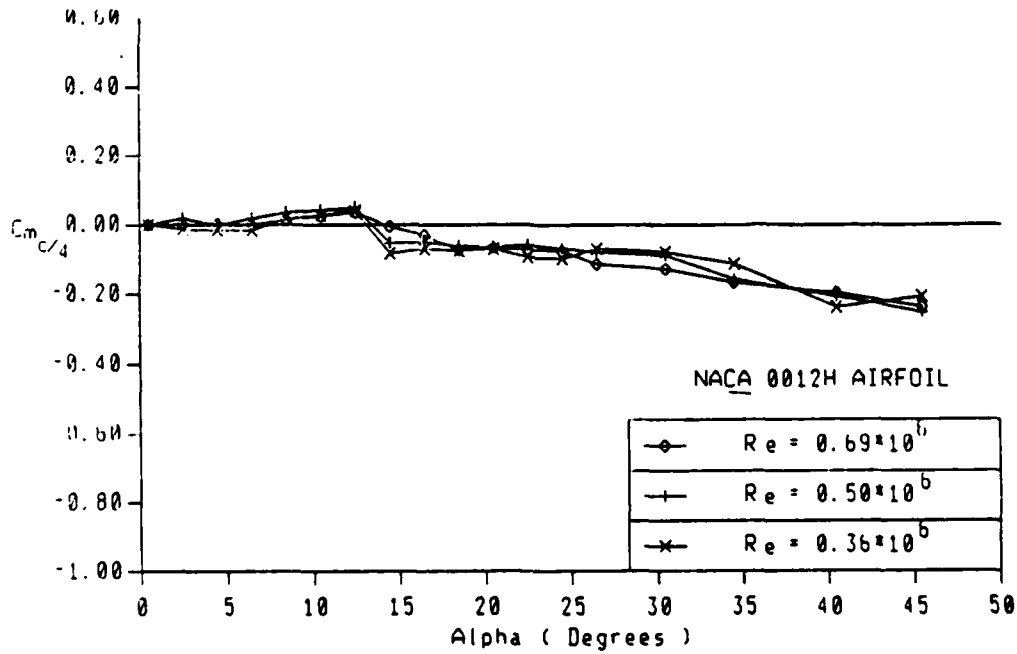


Figure 7. (c) Moment coefficients of NACA 0012H airfoil

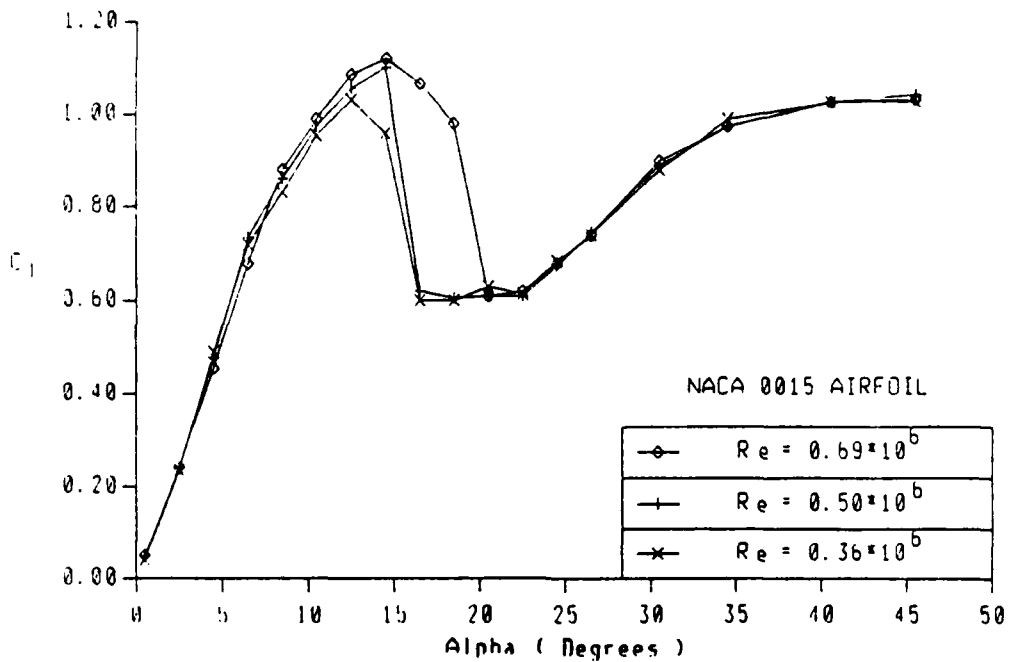


Figure 8. (a) Lift coefficients of NACA 0015 airfoil

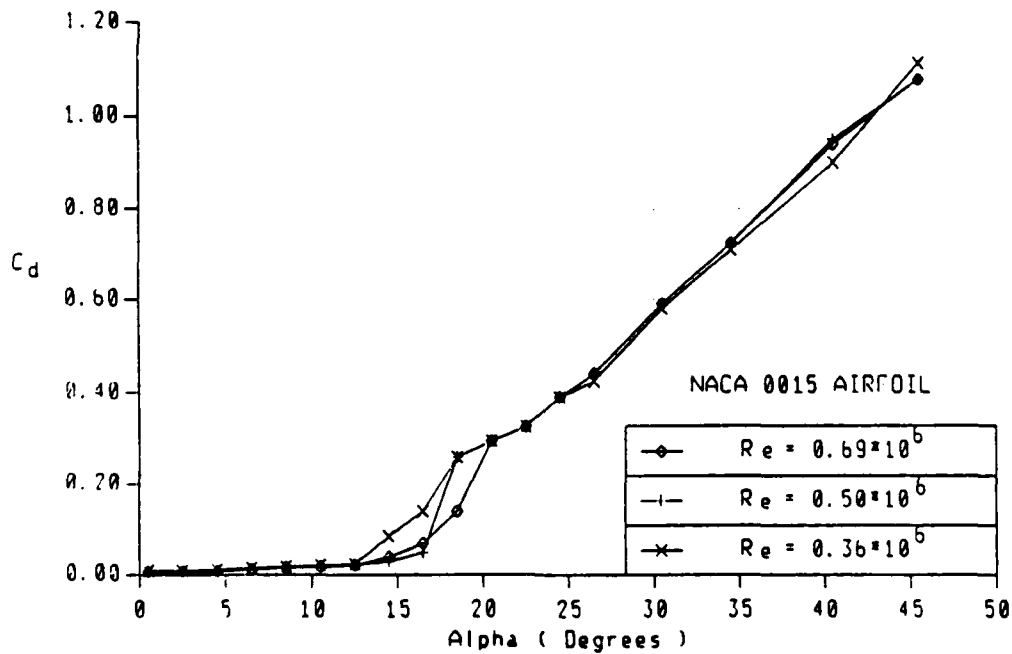


Figure 8. (b) Drag coefficients of NACA 0015 airfoil

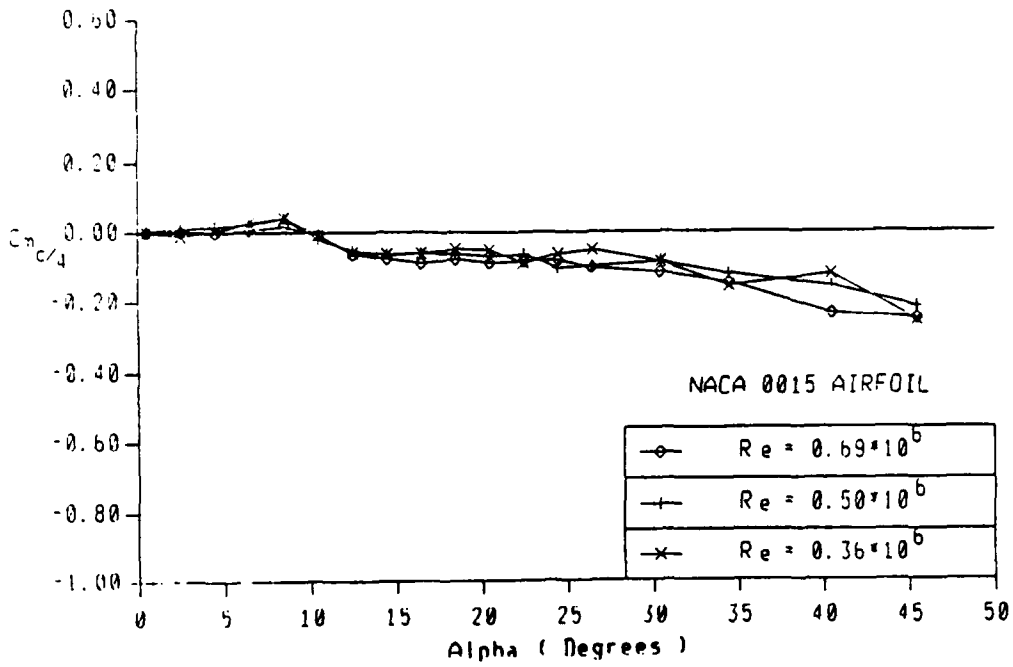


Figure 8. (c) Moment coefficients of NACA 0015 airfoil

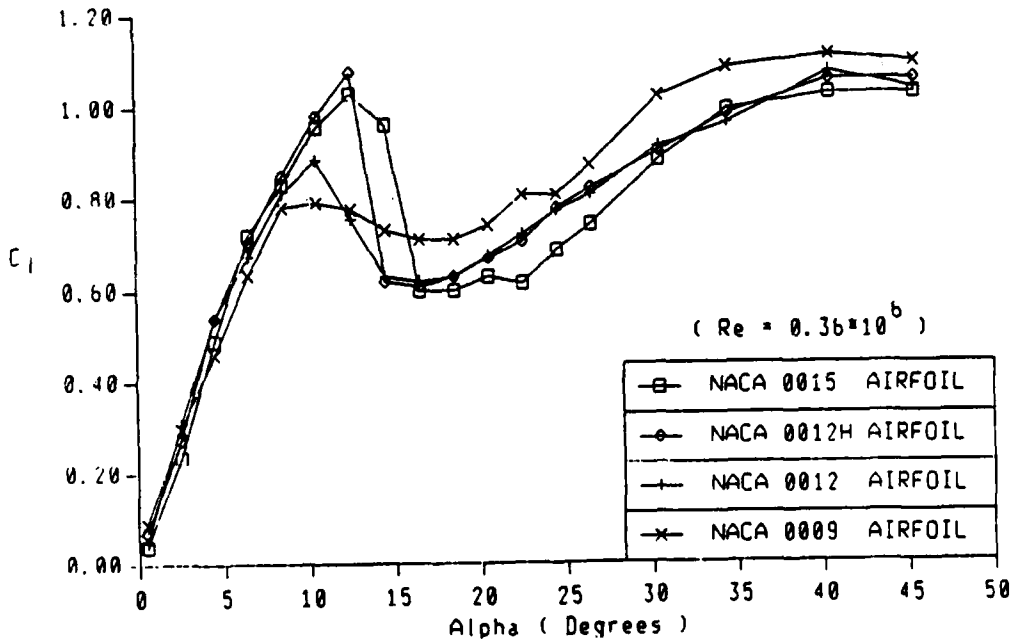


Figure 9. (a) Lift coefficients of NACA 00-series airfoils

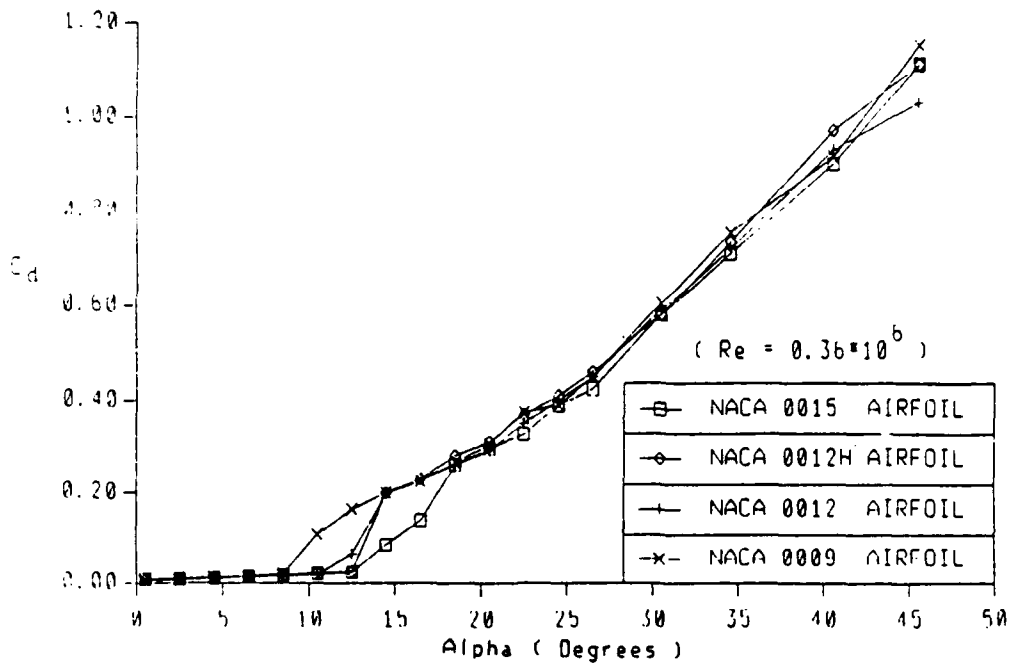


Figure 9. (b) Drag coefficients of NACA 00-series airfoils

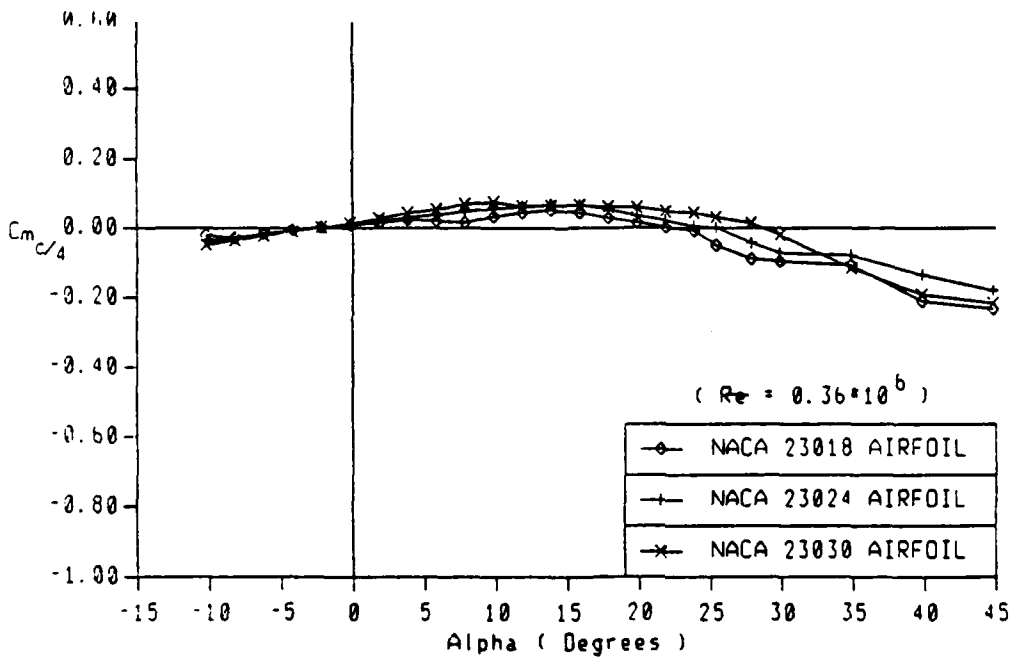


Figure 9. (c) Moment coefficients of NACA 00-series airfoils

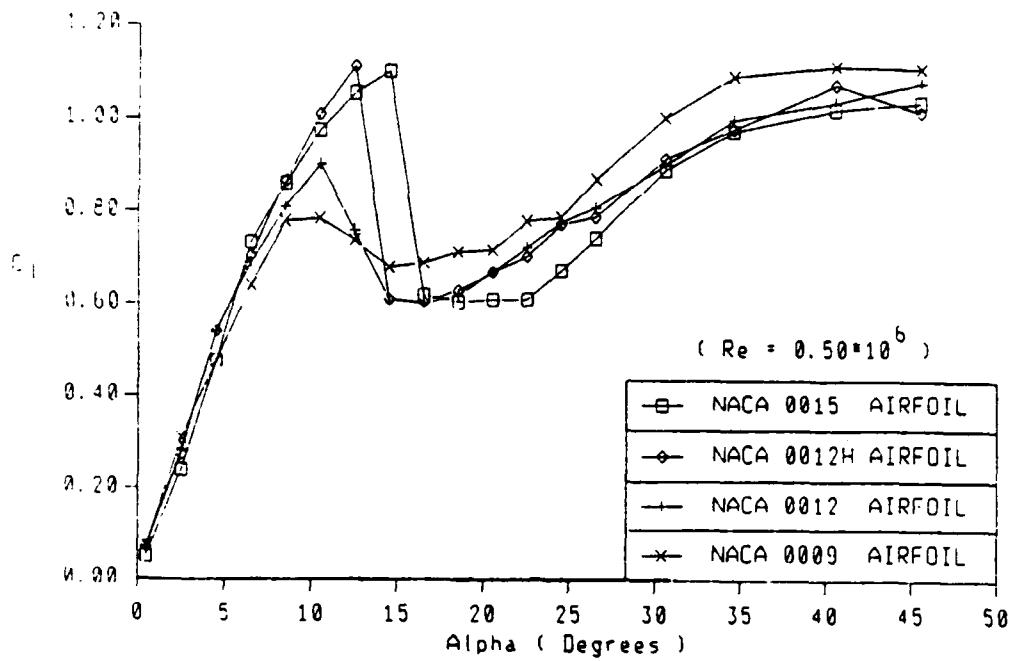


Figure 10. (a) Lift coefficients of NACA 00-series airfoils

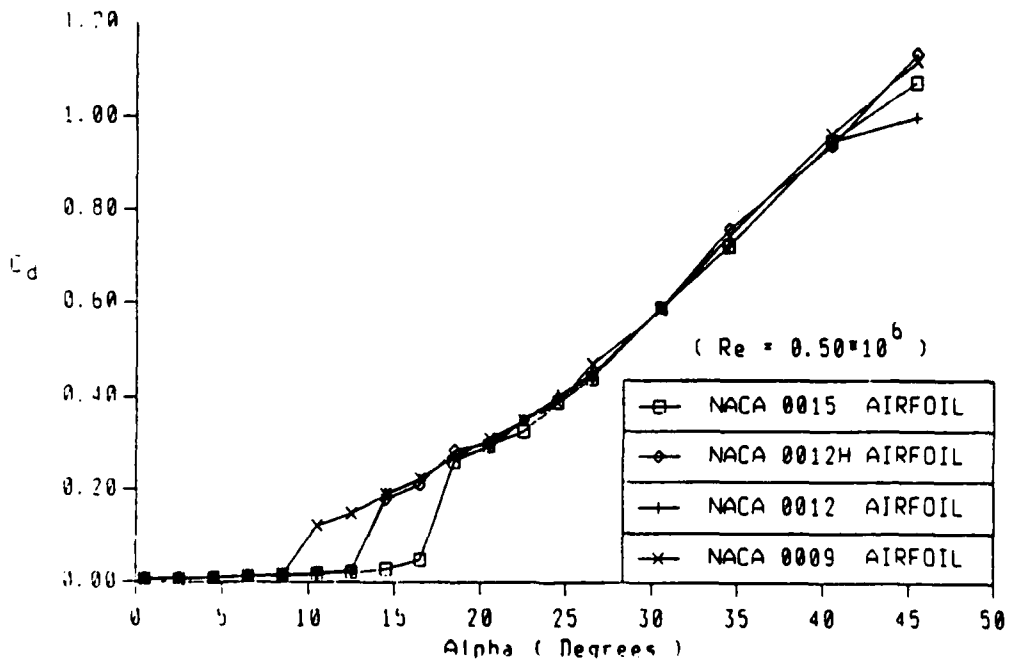


Figure 10. (b) Drag coefficients of NACA 00-series airfoils

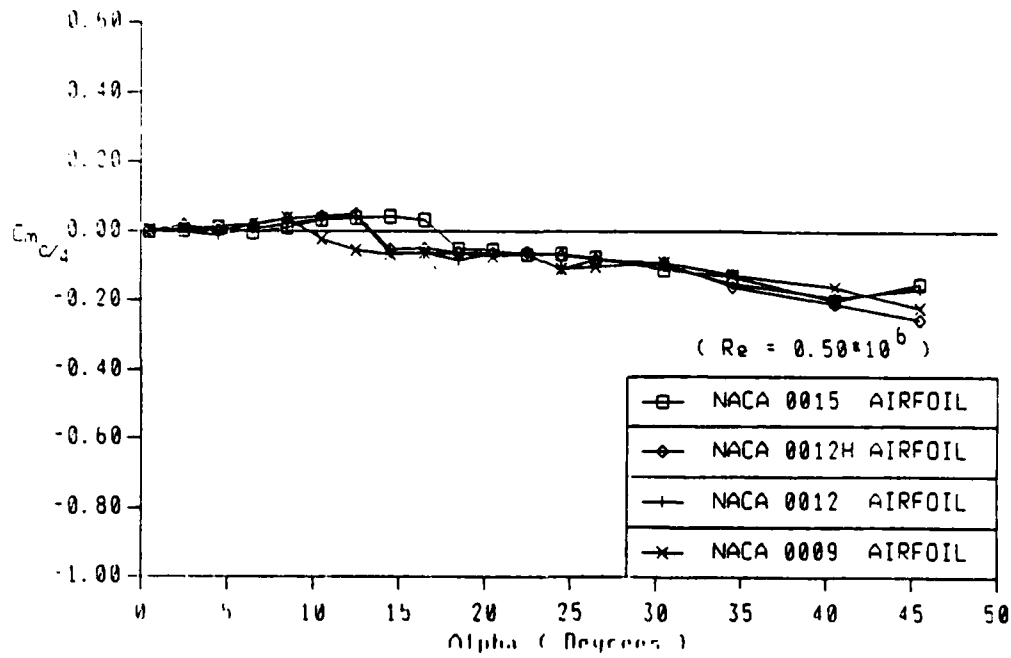


Figure 10. (c) Moment coefficients of NACA 00-series airfoils

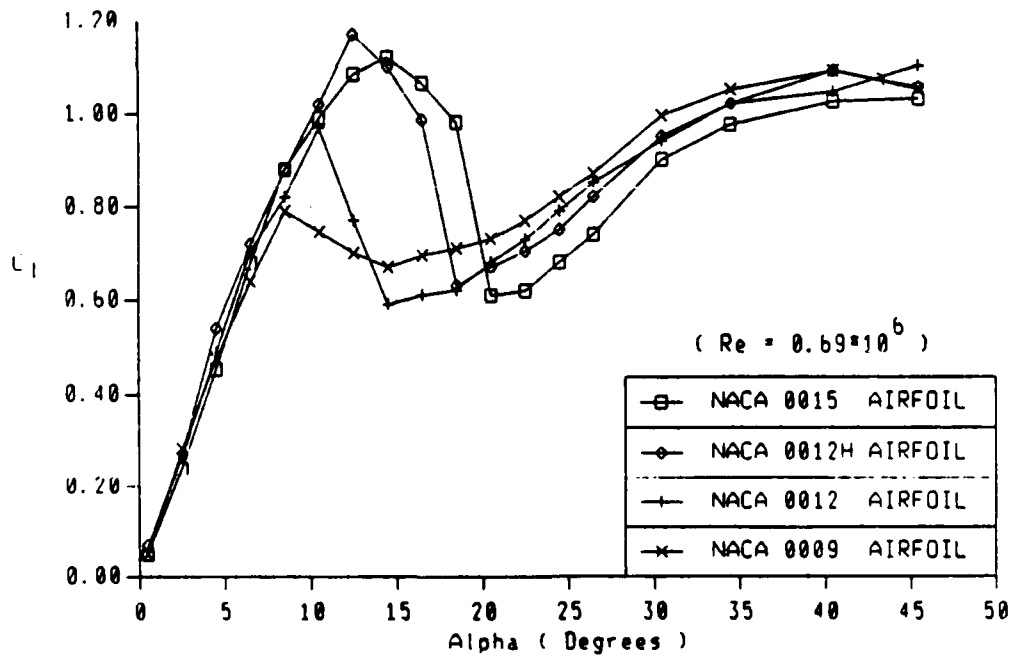


Figure 11. (a) Lift coefficients of NACA 00-series airfoils

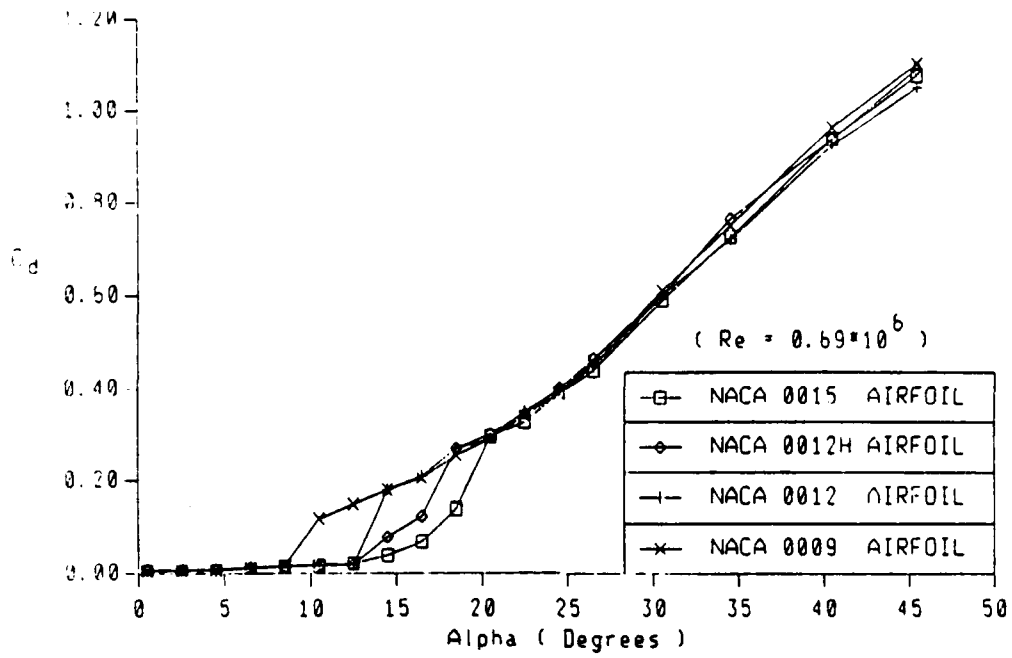


Figure 11. (b) Drag coefficients of NACA 00-series airfoils

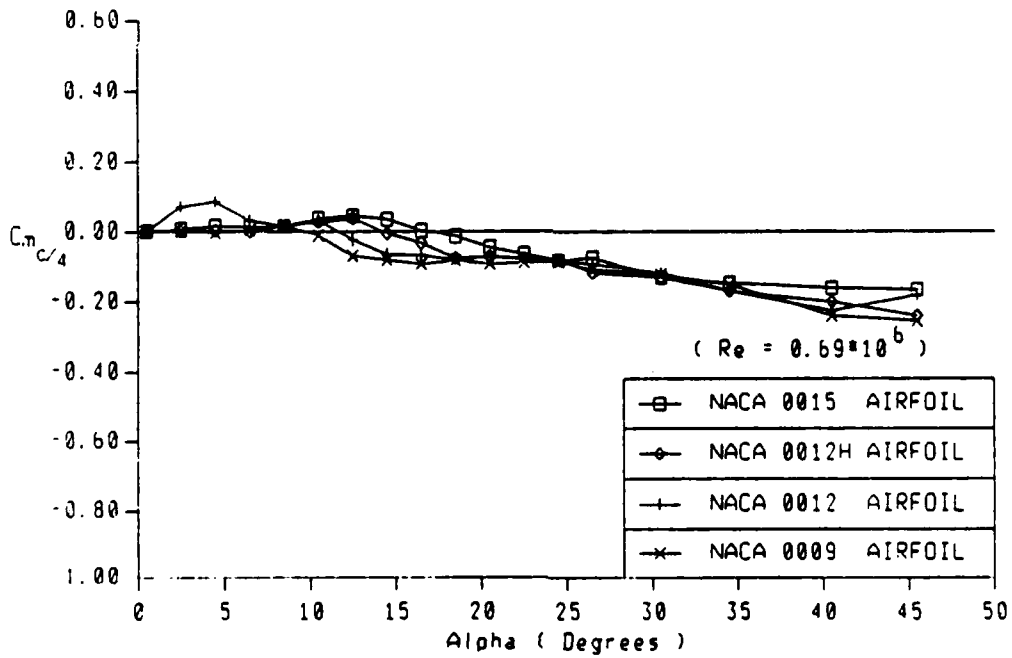


Figure 11. (c) Moment coefficients of NACA 00-series airfoils

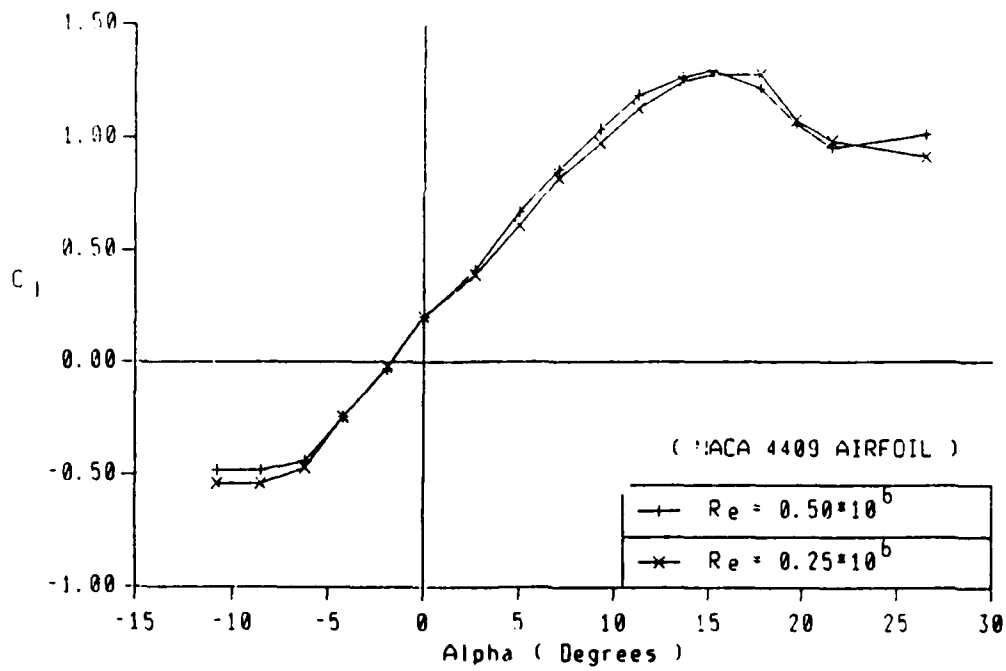


Figure 12. (a) Lift coefficients of NACA 4409 airfoil

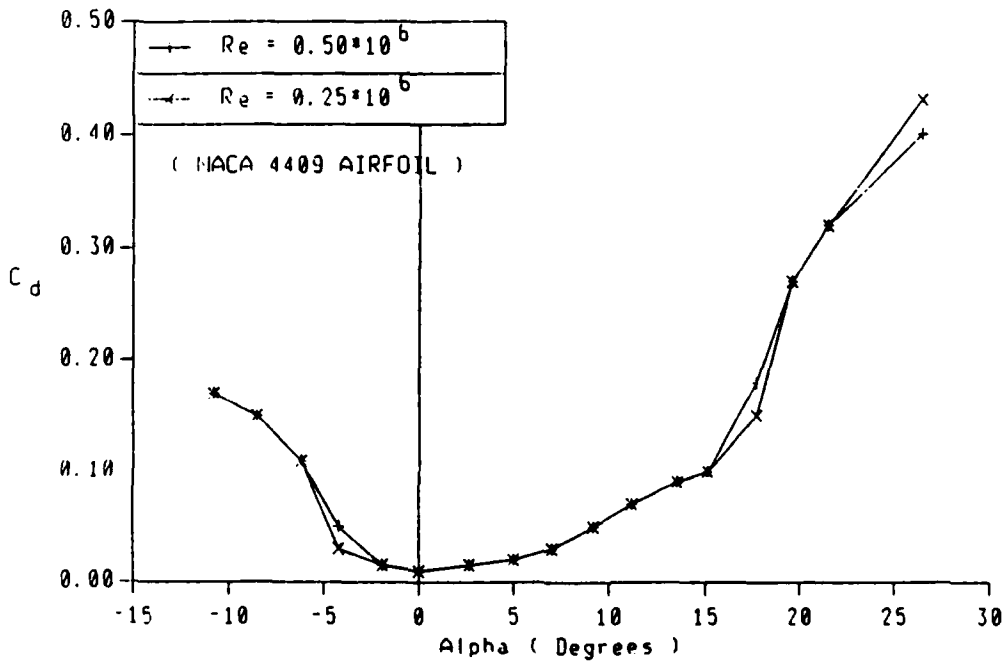


Figure 12. (b) Drag coefficients of NACA 4409 airfoil

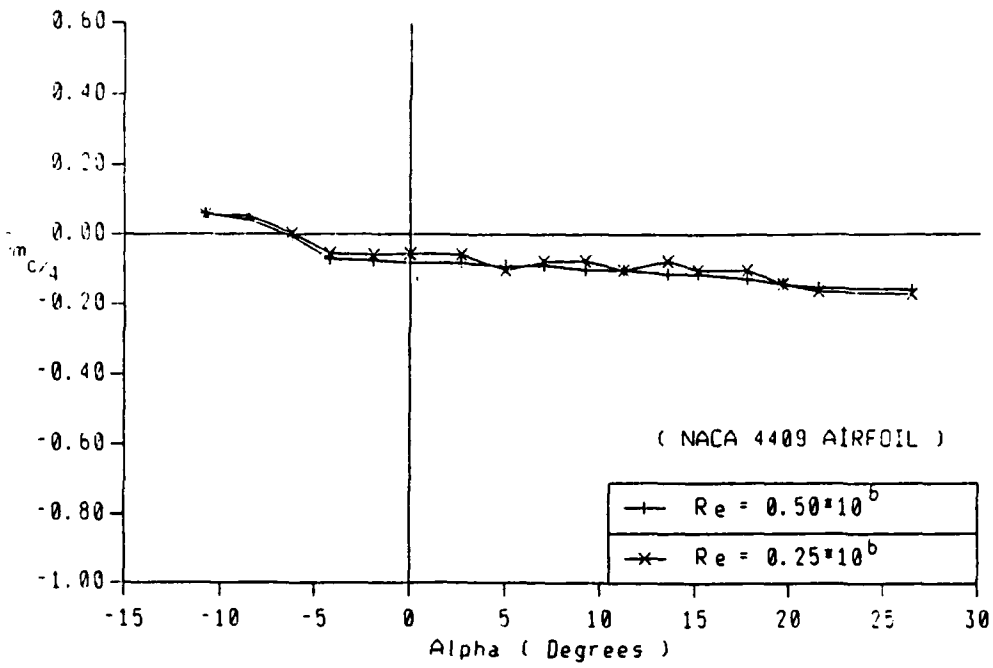


Figure 12. (c) Moment coefficients of NACA 4409 airfoil

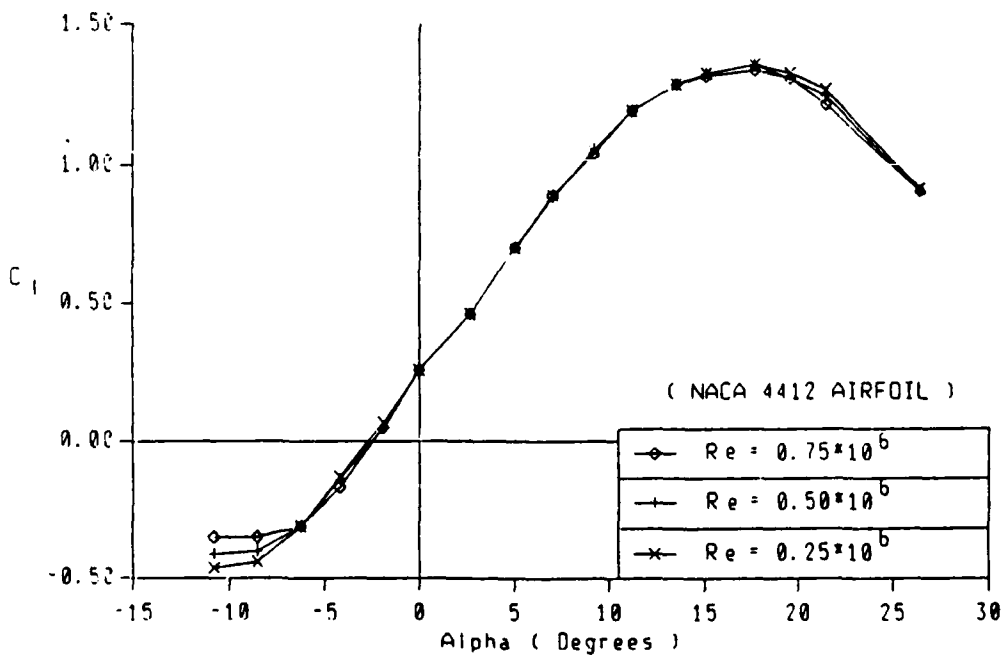


Figure 13. (a) Lift coefficients of NACA 4412 airfoil

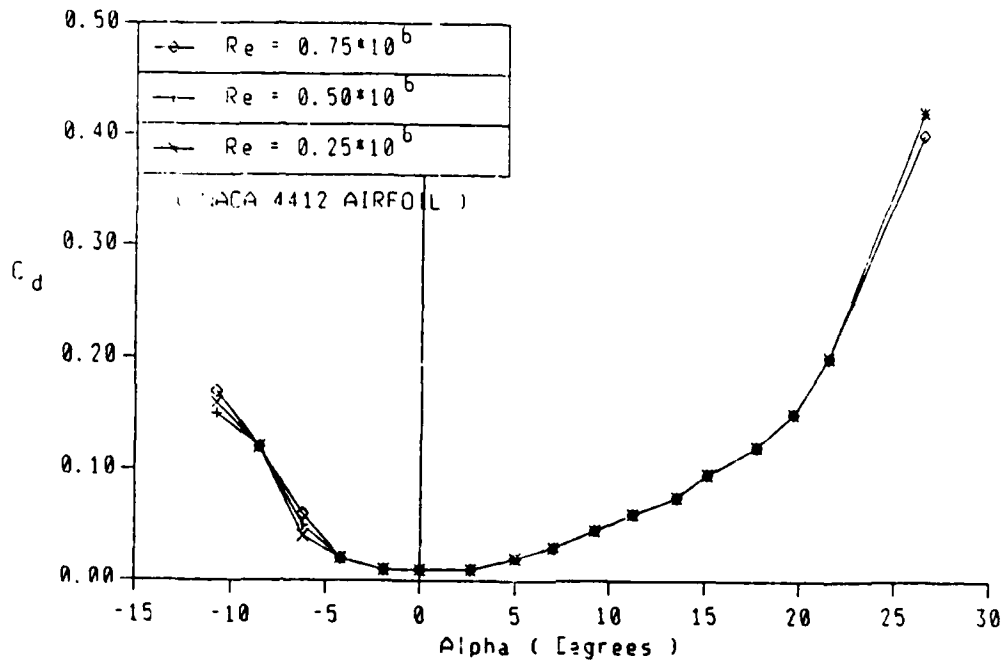


Figure 13. (b) Drag coefficients of NACA 4412 airfoil

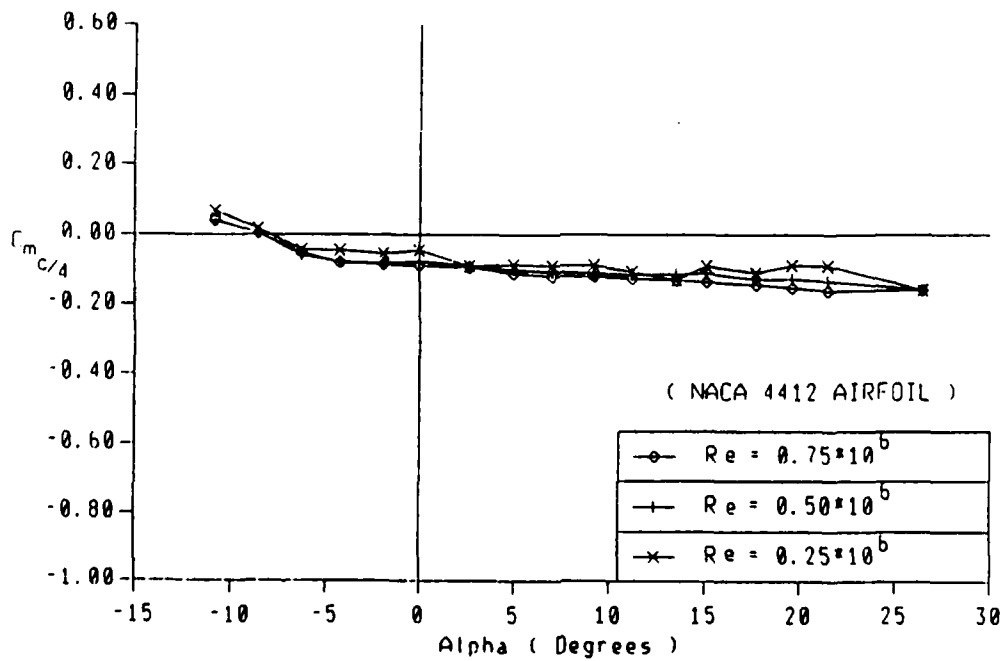


Figure 13. (c) Moment coefficients of NACA 4412 airfoil

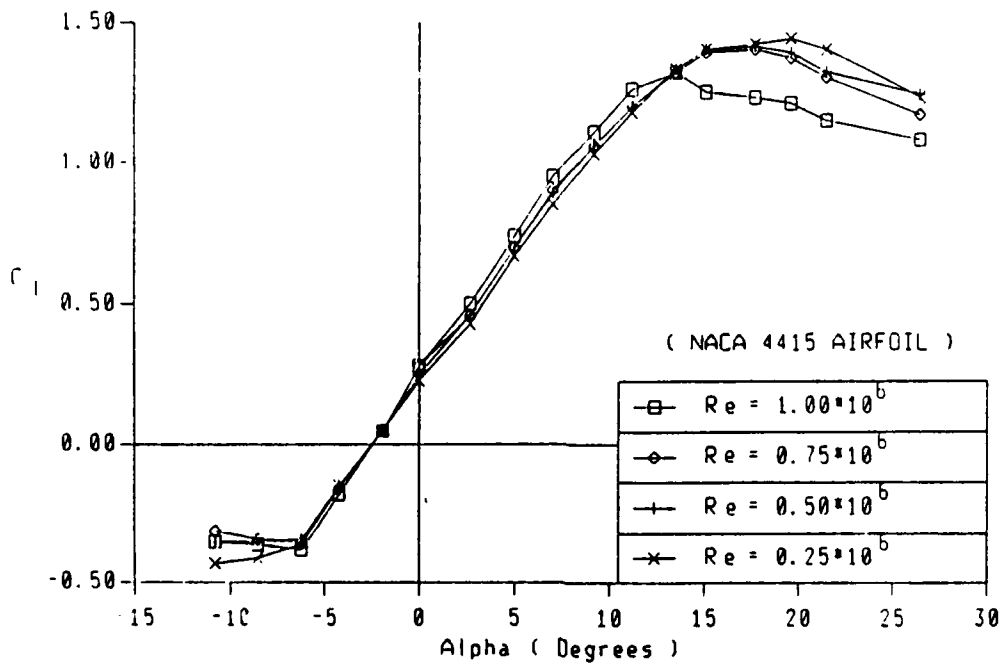


Figure 14. (a) Lift coefficients of NACA 4415 airfoil

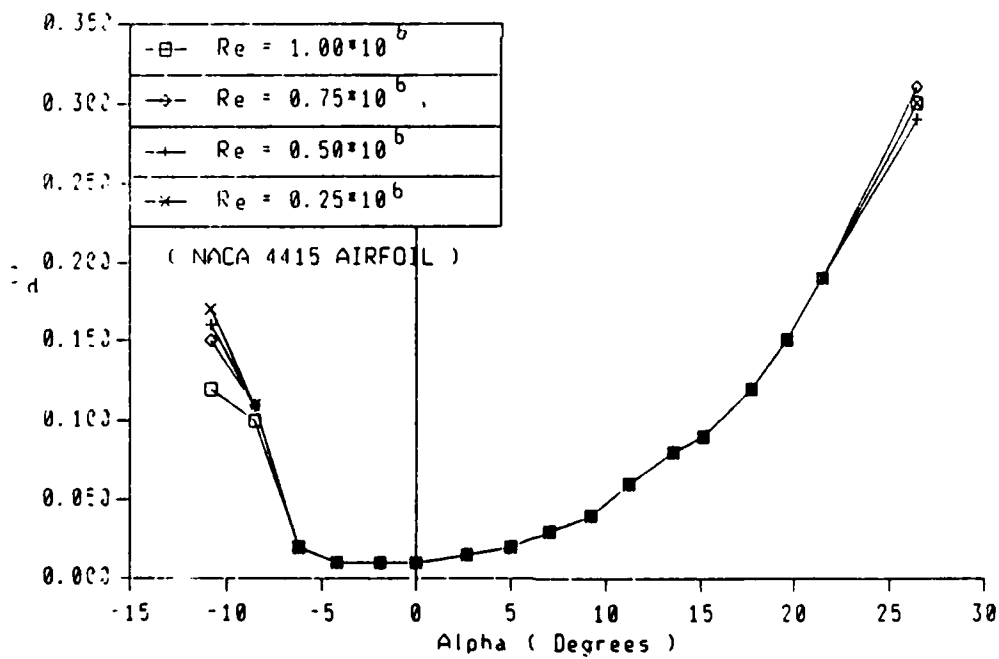


Figure 14. (b) Drag coefficients of NACA 4415 airfoil

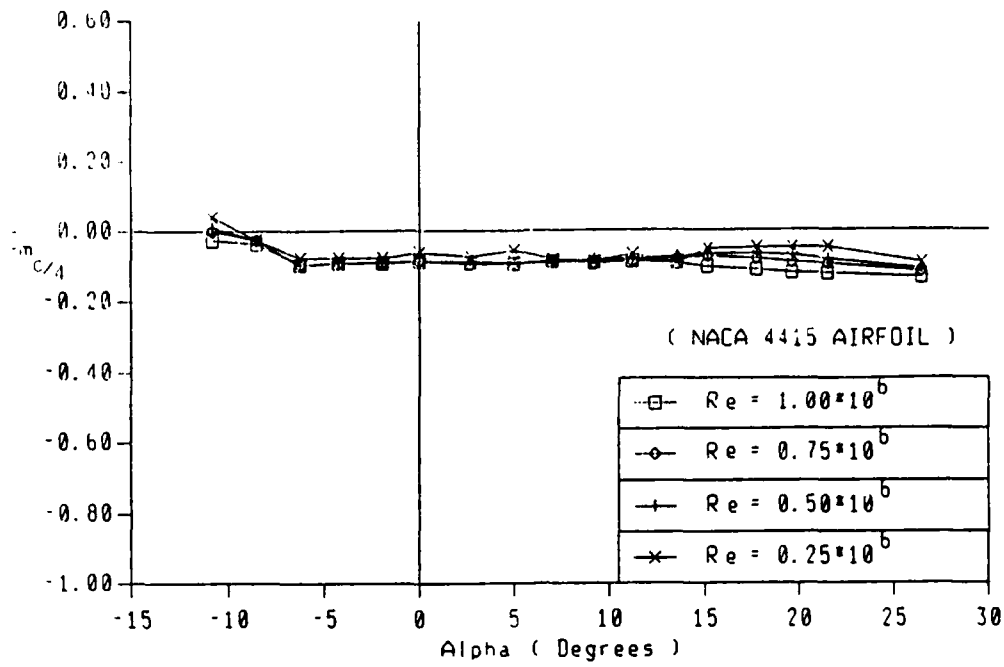


Figure 14. (c) Moment coefficients of NACA 4415 airfoil

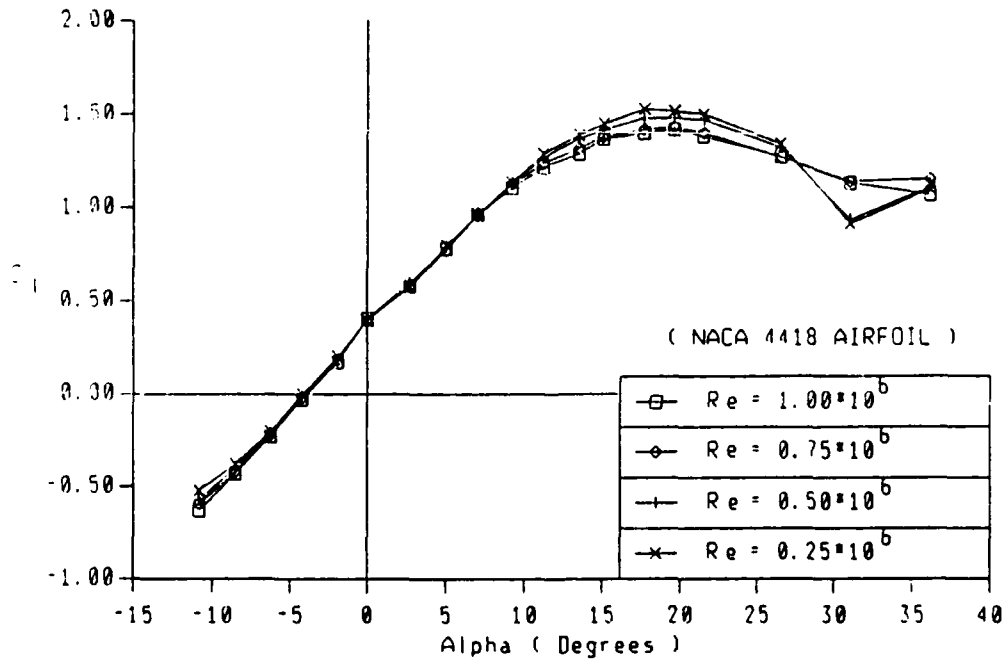


Figure 15. (a) Lift coefficients of NACA 4418 airfoil

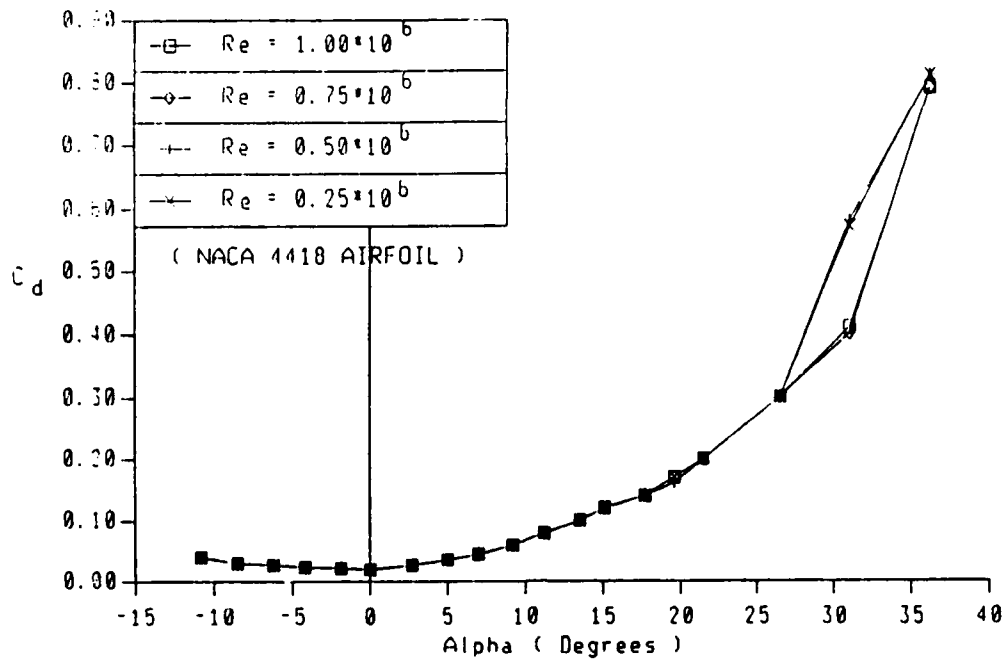


Figure 15. (b) Drag coefficients of NACA 4418 airfoil

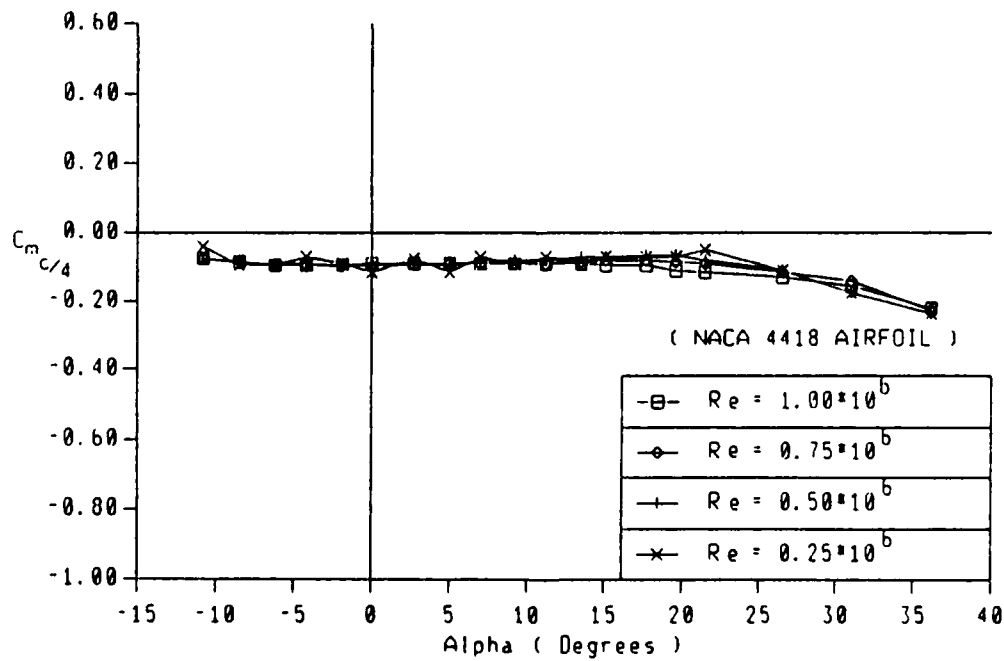


Figure 15. (c) Moment coefficients of NACA 4418 airfoil

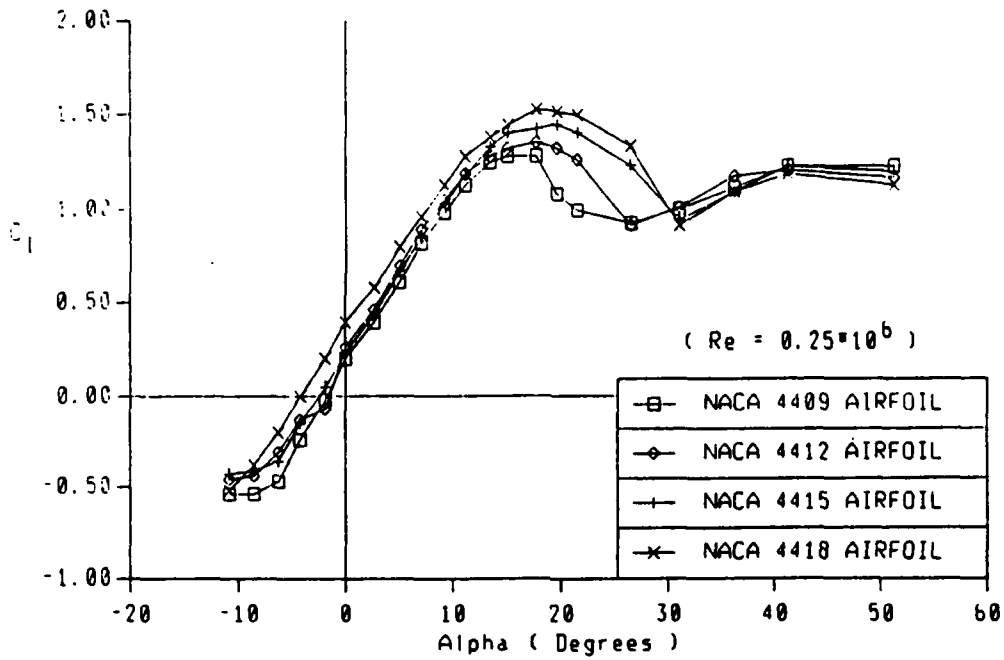


Figure 16. (a) Lift coefficients of NACA 44-series airfoils

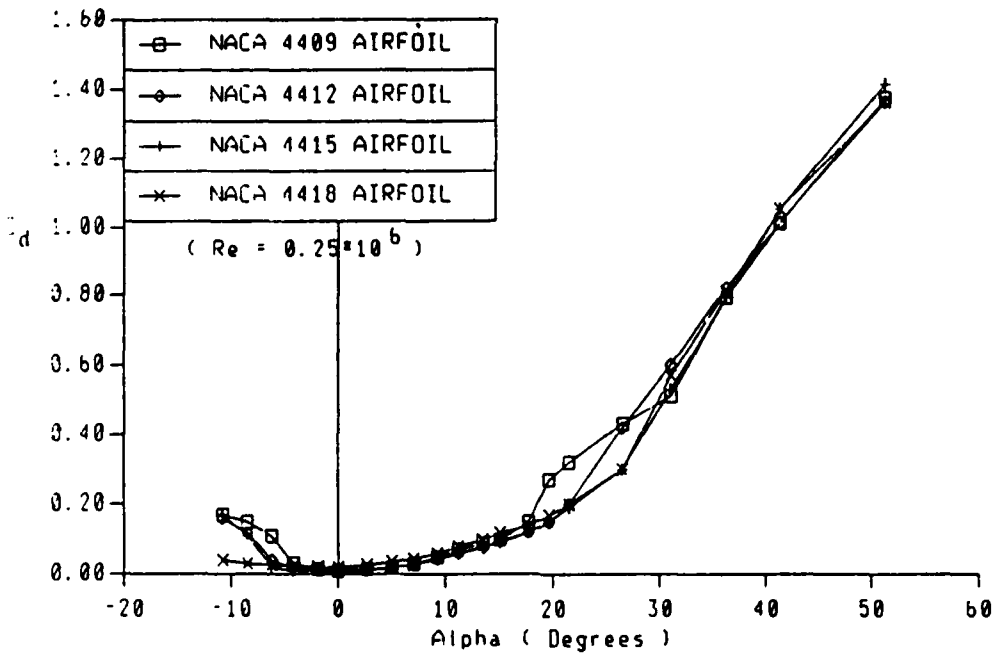


Figure 16. (b) Drag coefficients of NACA 44-series airfoils

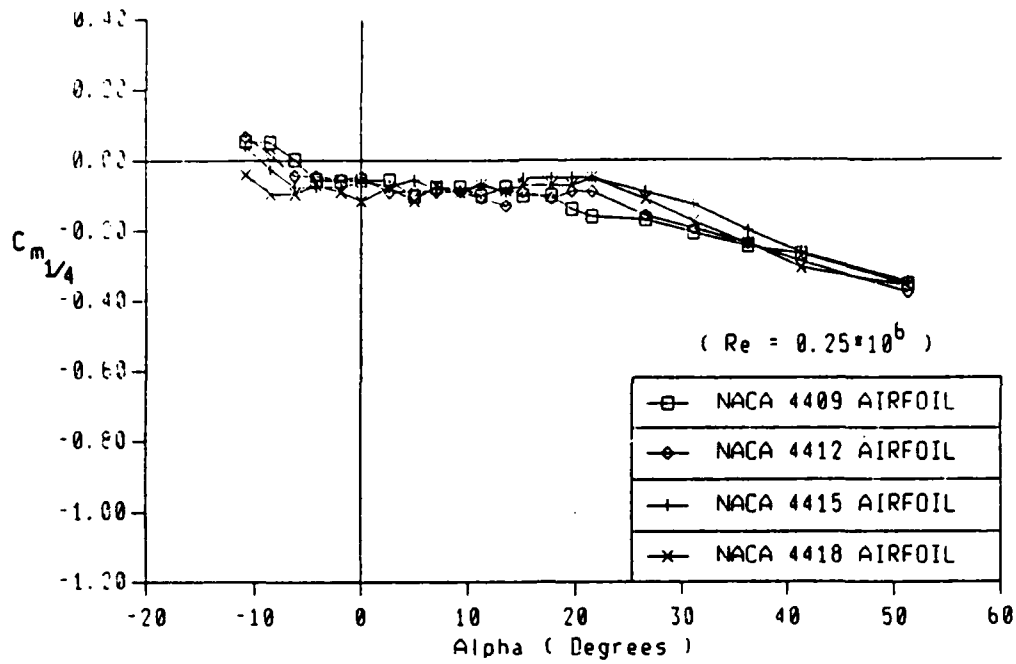


Figure 16. (c) Moment coefficients of NACA 44-series airfoils

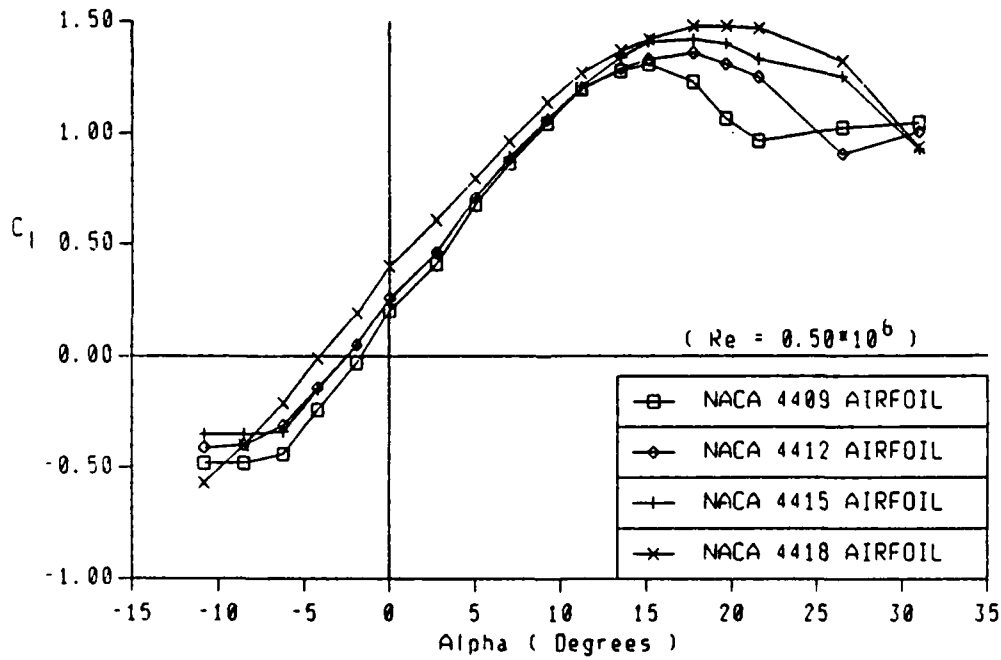


Figure 17. (a) Lift coefficients of NACA 44-series airfoils

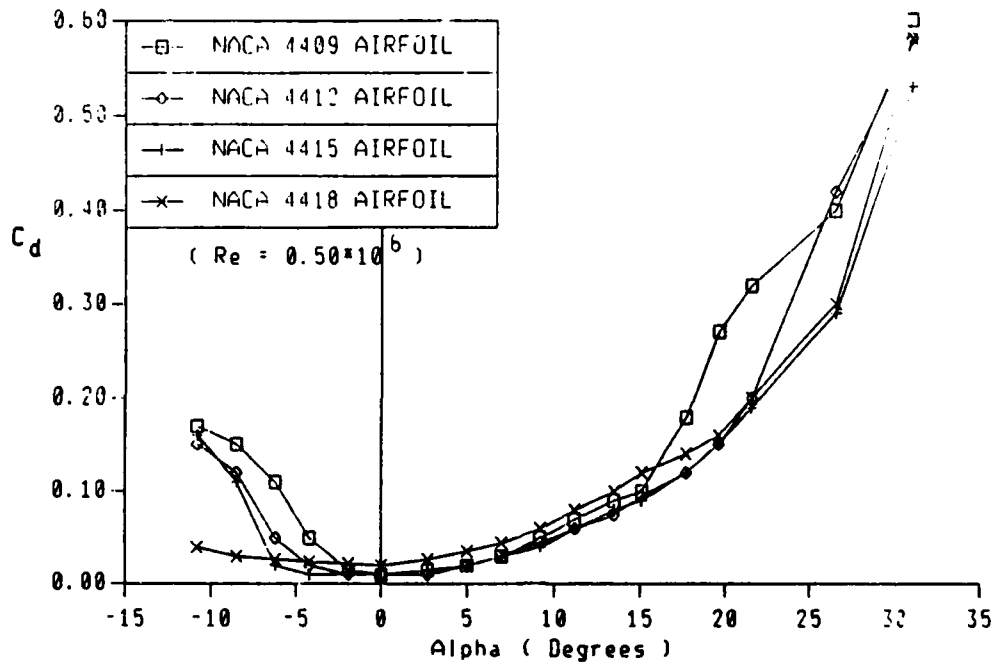


Figure 17. (b) Drag coefficients of NACA 44-series airfoils

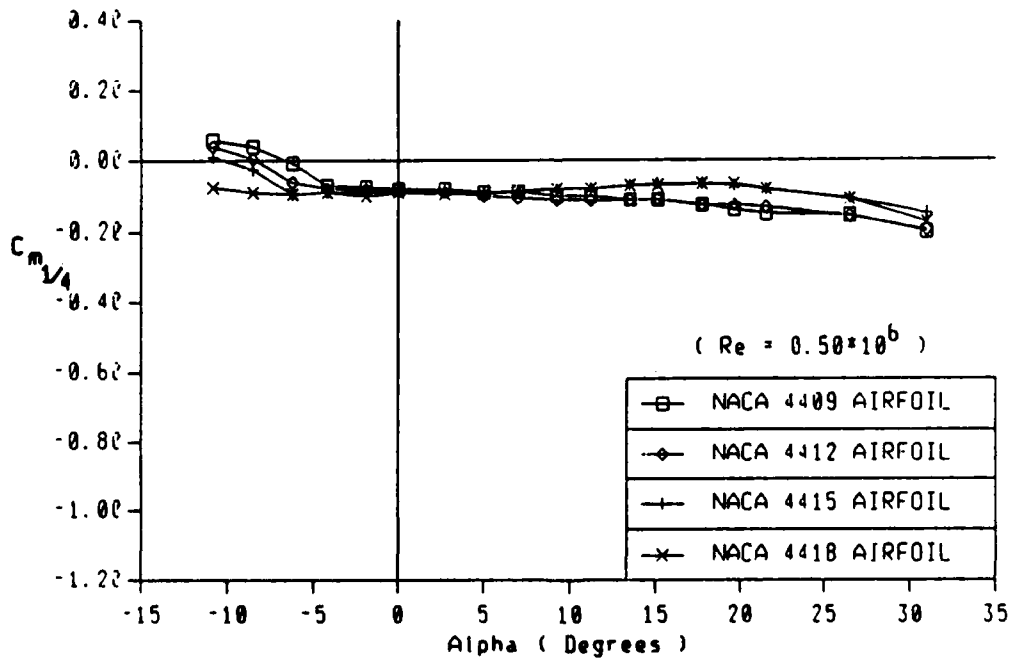


Figure 17. (c) Moment coefficients of NACA 44-series airfoils

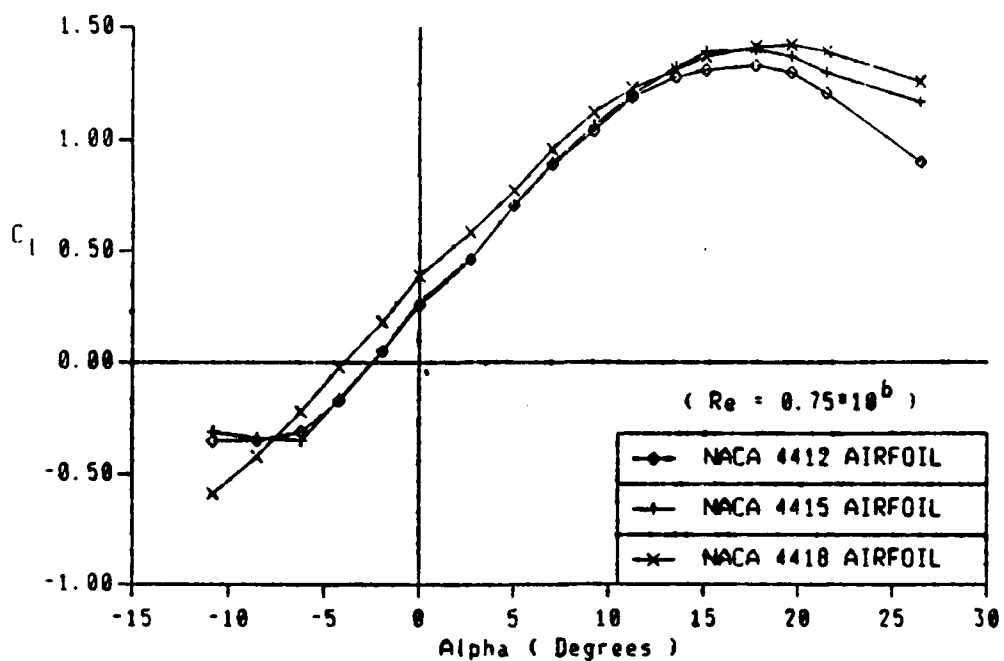


Figure 18. (a) Lift coefficients of NACA 44-series airfoils

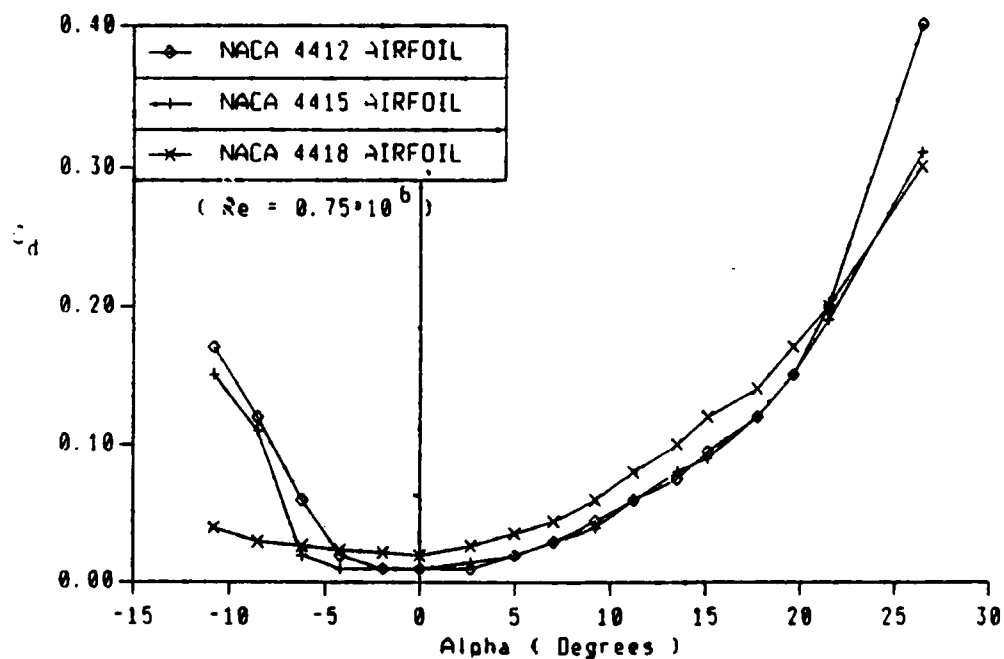


Figure 18. (b) Drag coefficients of NACA 44-series airfoils

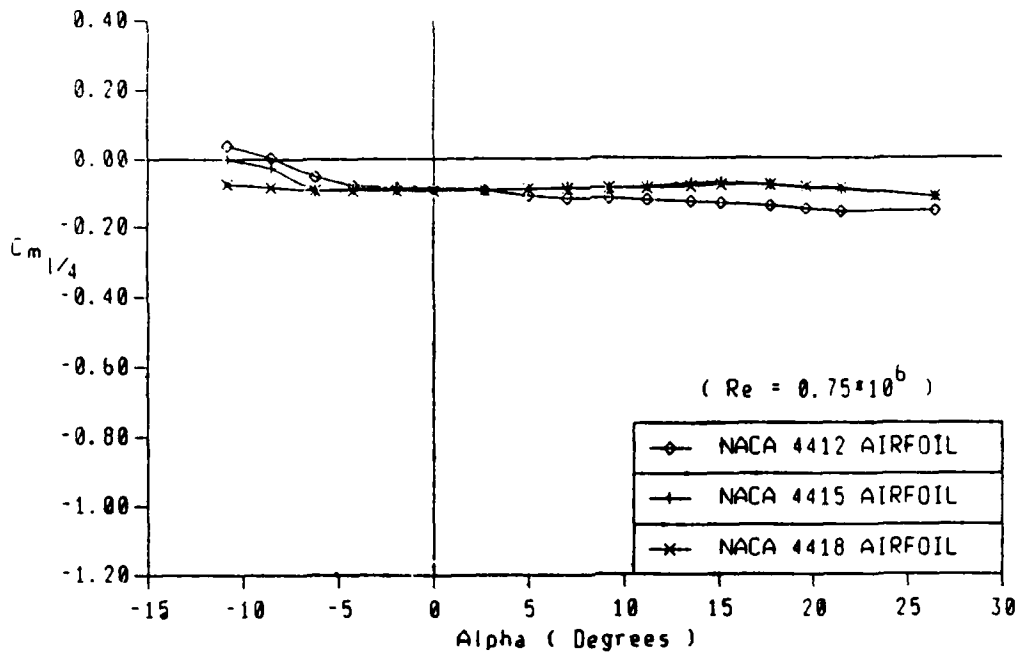


Figure 18. (c) Moment coefficients of NACA 44-series airfoils

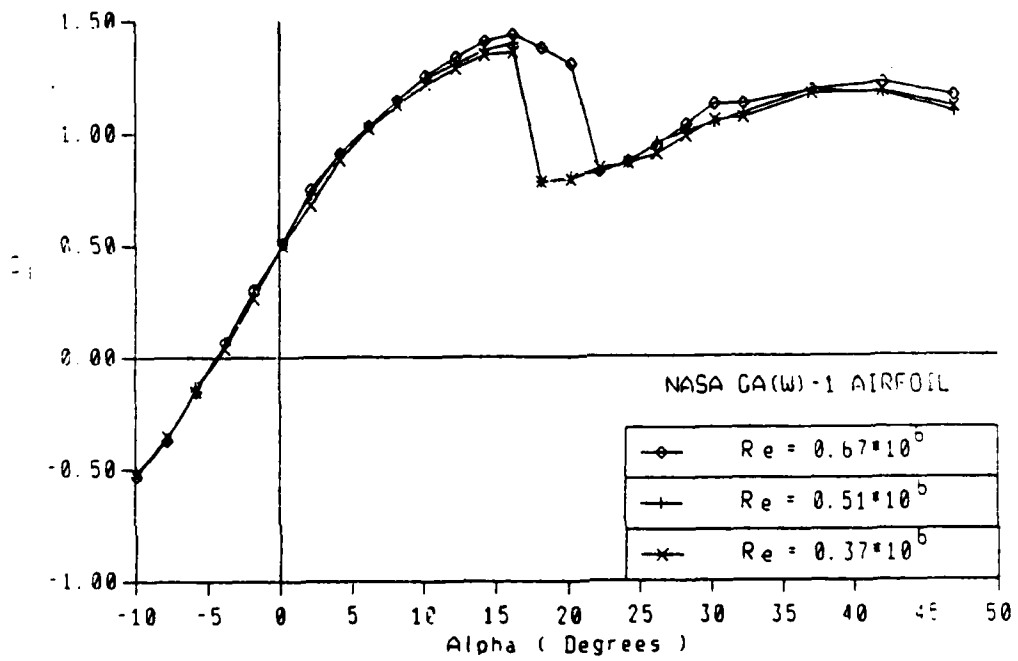


Figure 19. (a) Lift coefficients of NASA GA(W)-1 airfoil

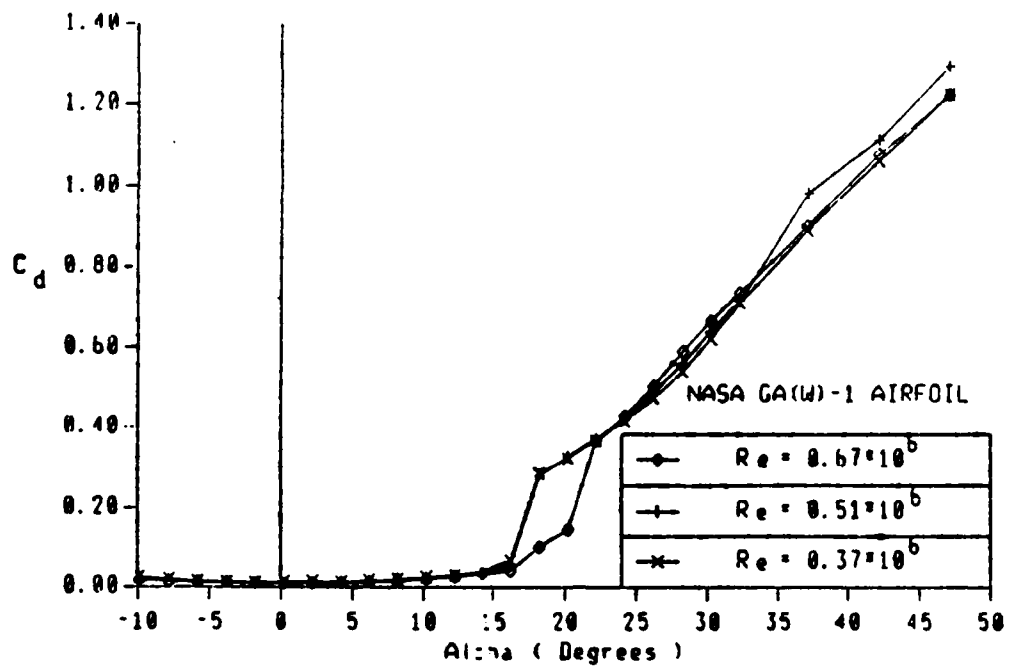


Figure 19. (b) Drag coefficients of NASA GA(W)-1 airfoil

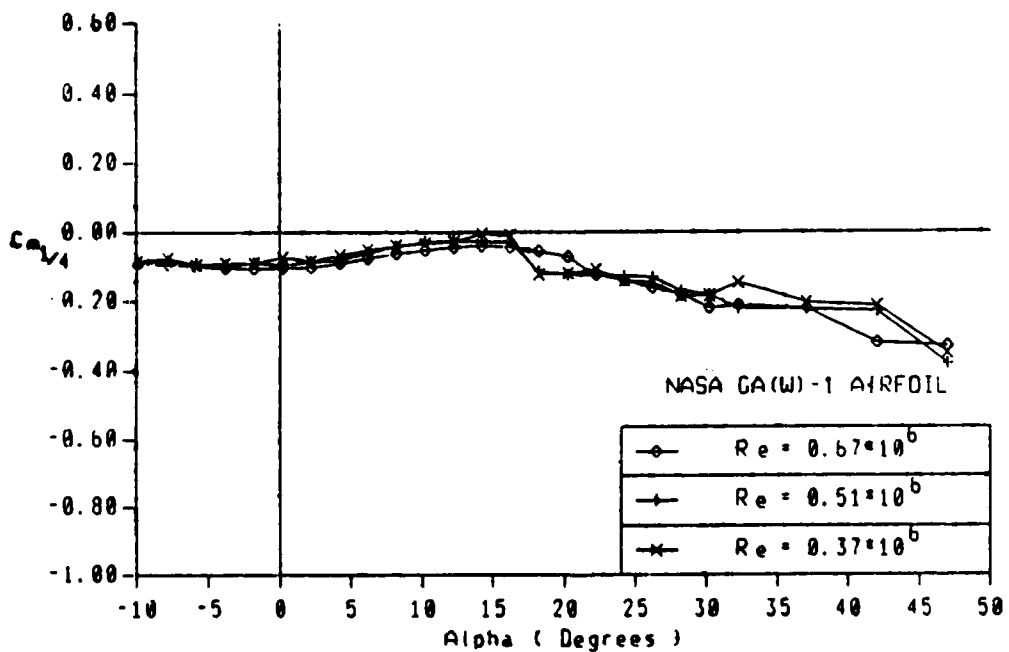


Figure 19. (c) Moment coefficients of NASA GA(W)-1 airfoil

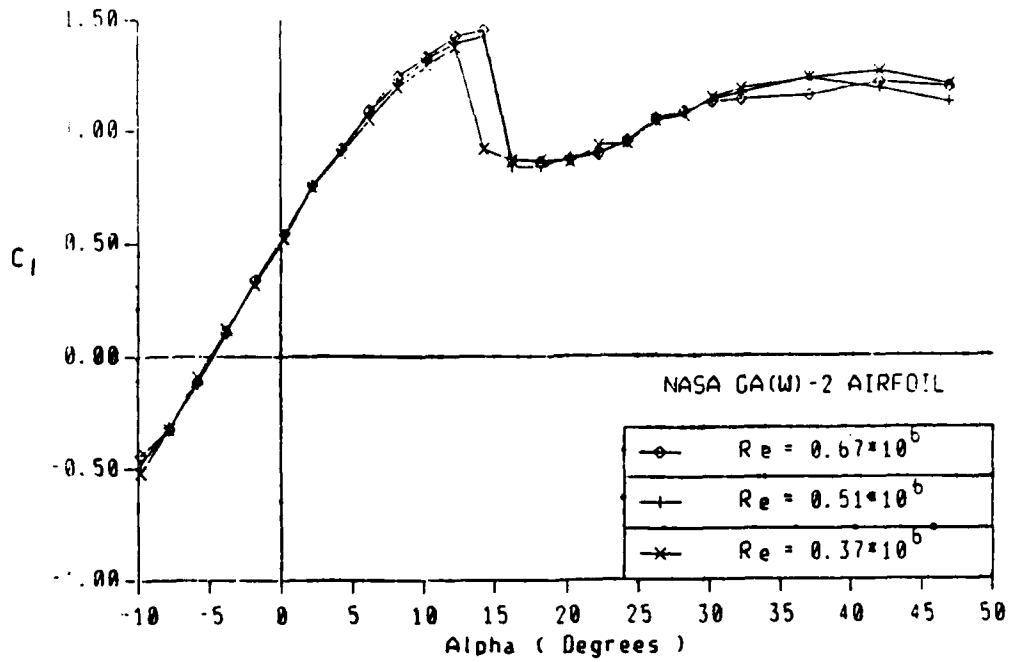


Figure 20. (a) Lift coefficients of NASA GA(W)-2 airfoil

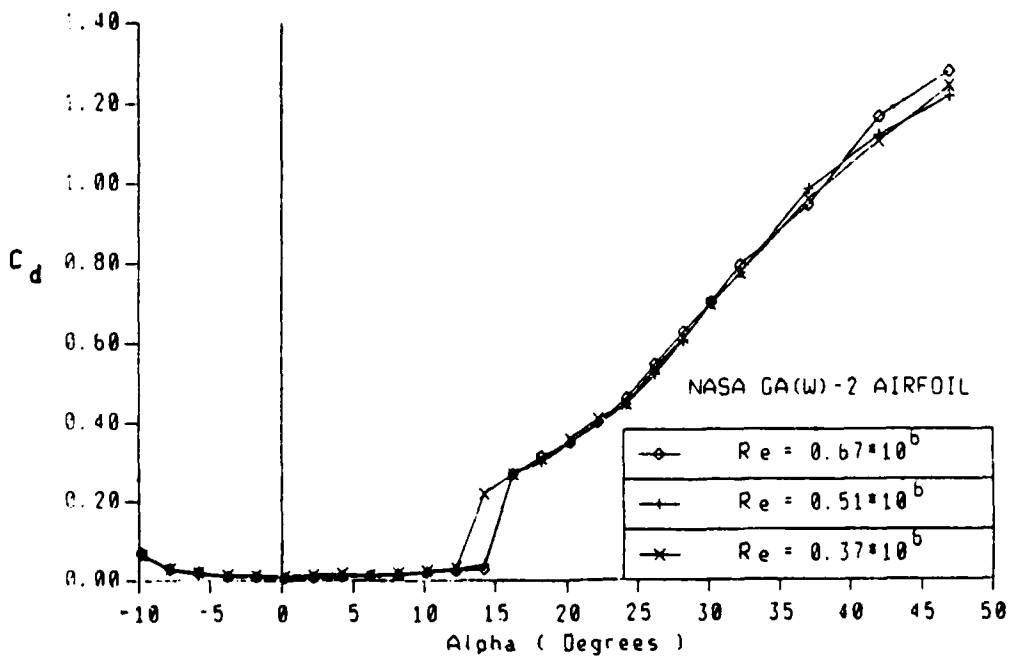


Figure 20. (b) Drag coefficients of NASA GA(W)-2 airfoil

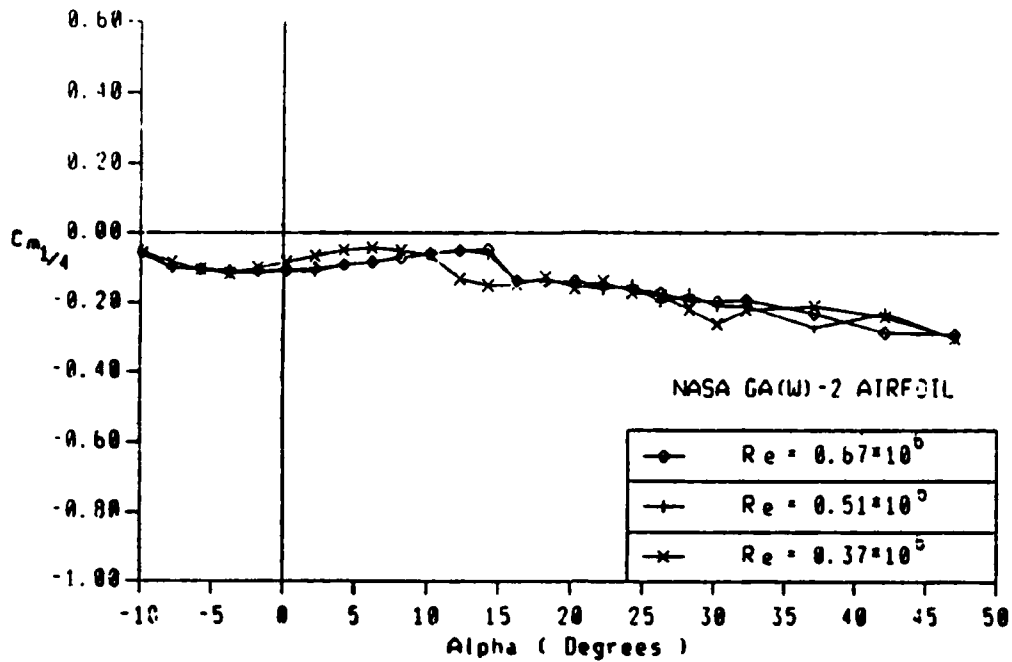


Figure 20. (c) Moment coefficients of NASA GA(W)-2 airfoil

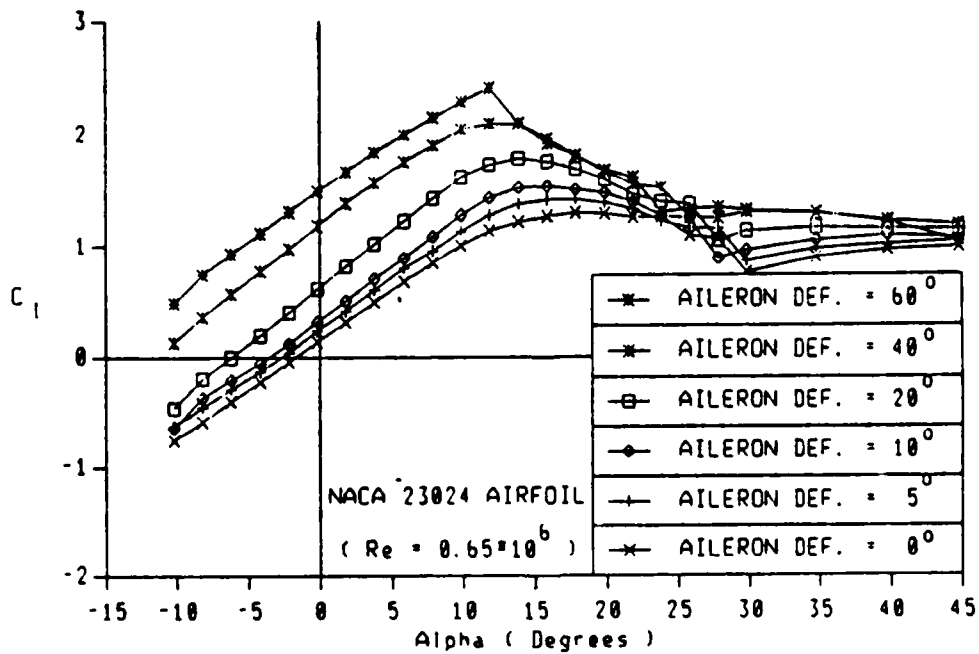


Figure 21. (a) Lift coefficients of NACA 23024 airfoil

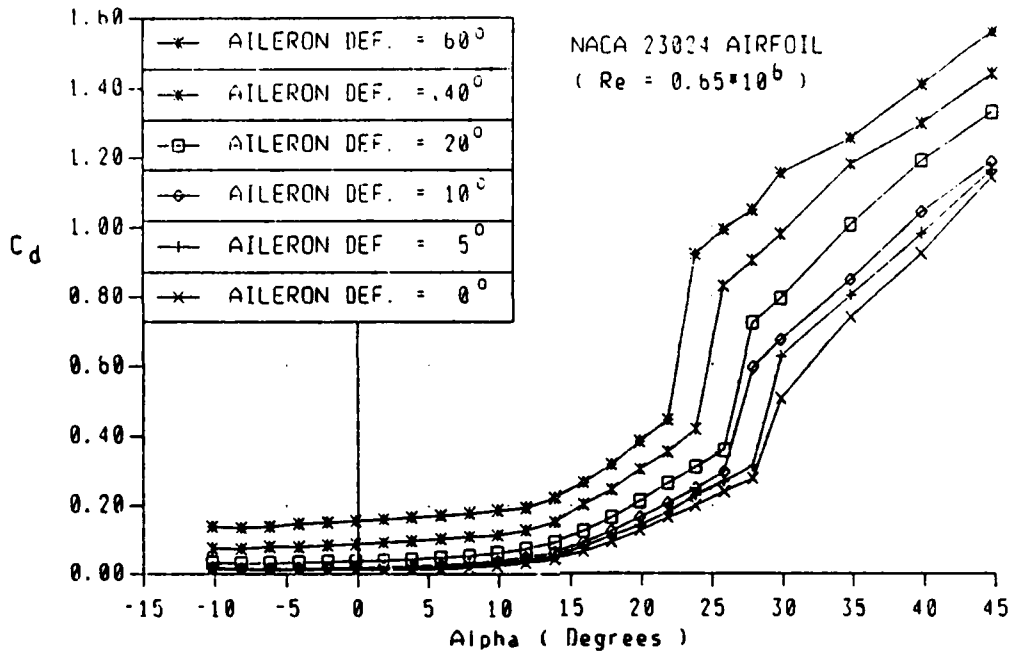


Figure 21. (b) Drag coefficients of NACA 23024 airfoil

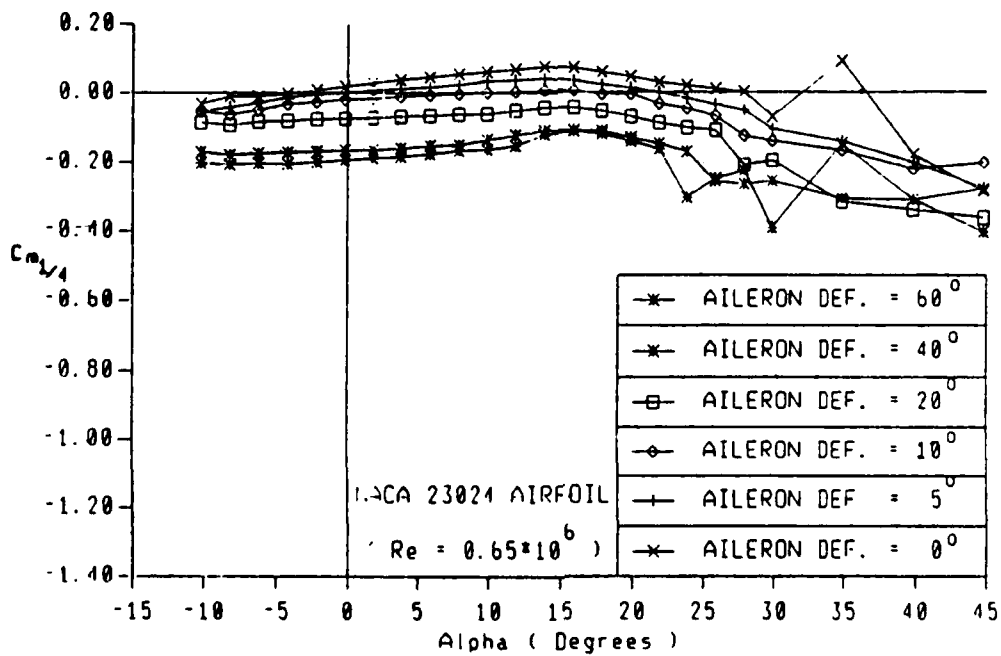


Figure 21. (c) Moment coefficients of NACA 23024 airfoil

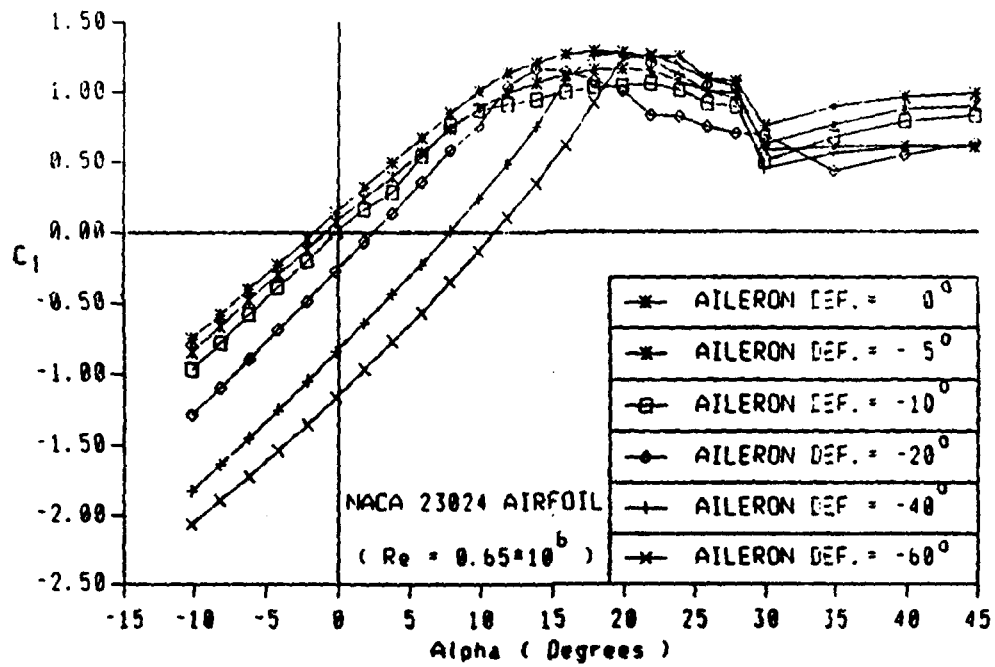


Figure 22. (a) Lift coefficients of NACA 23024 airfoil

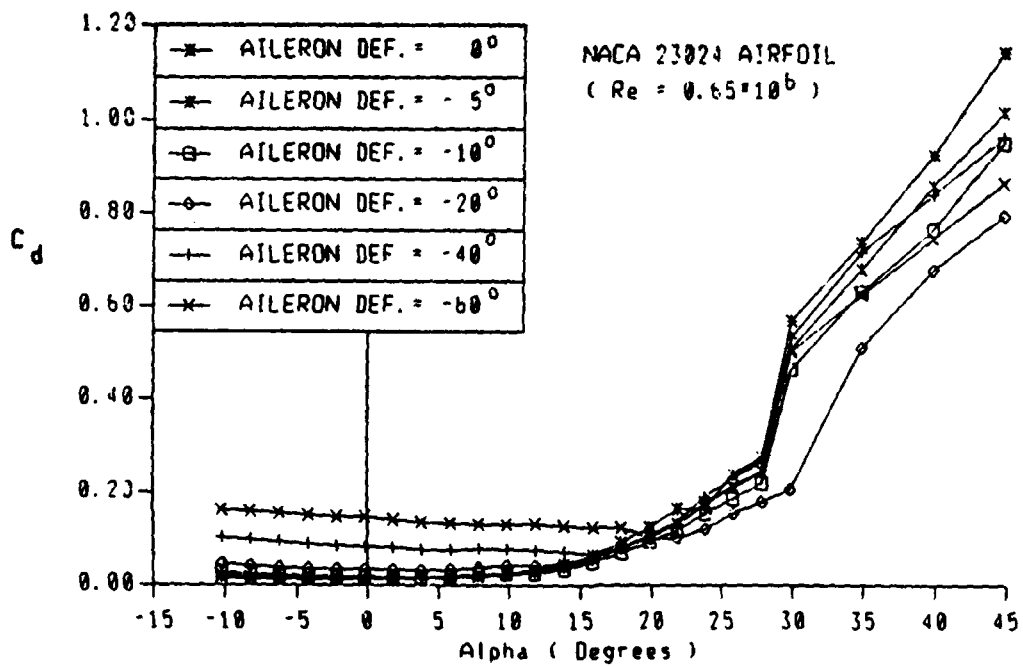


Figure 22. (b) Drag coefficients of NACA 23024 airfoil

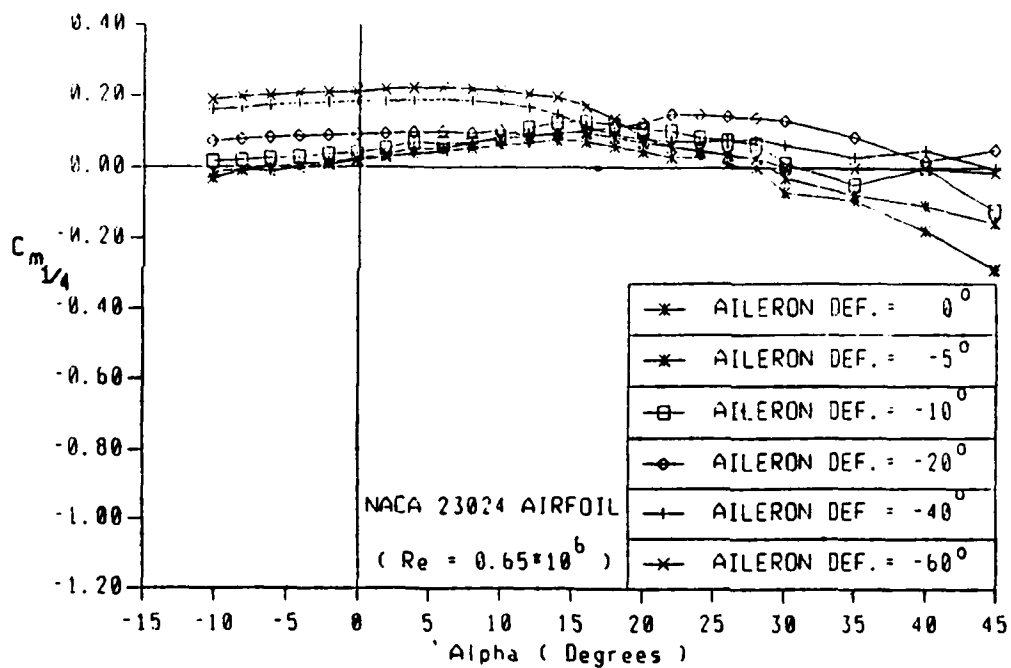


Figure 22. (c) Moment coefficients of NACA 23024 airfoil

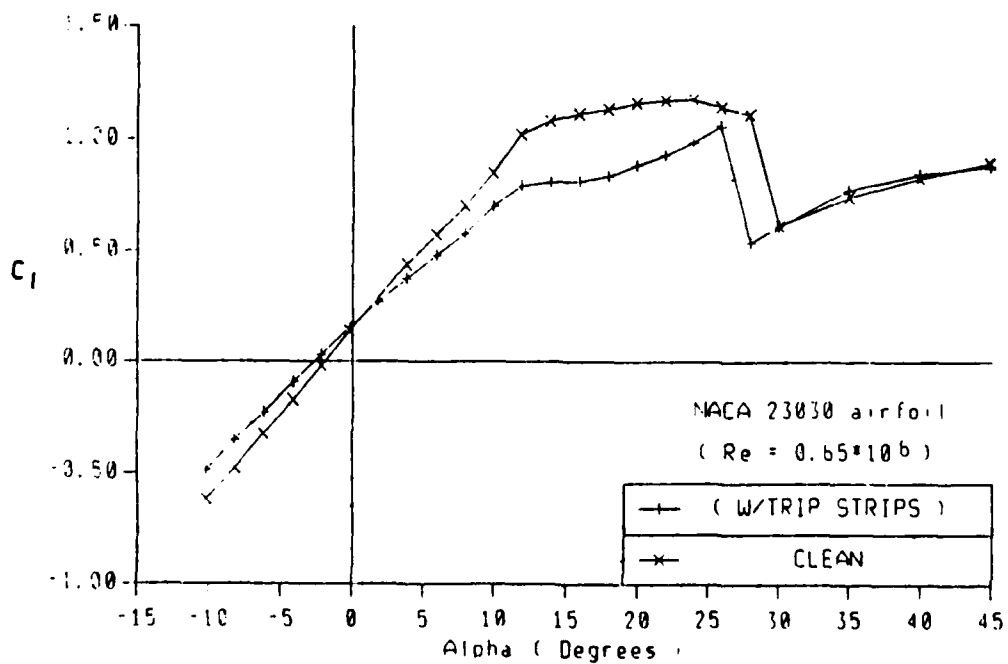


Figure 23. (a) Lift coefficients of NACA 23024 airfoil

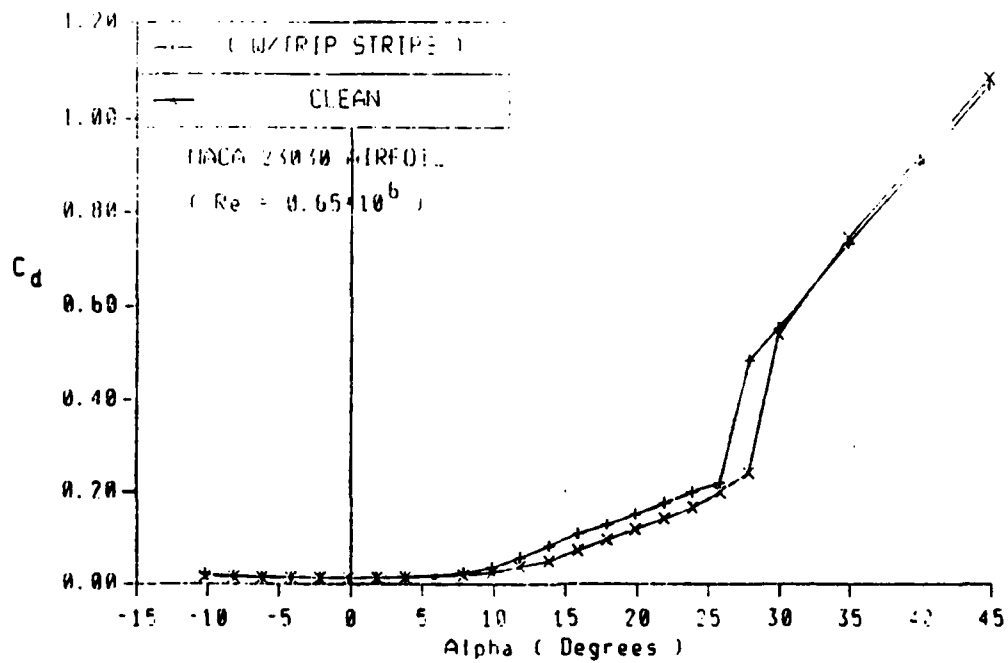


Figure 23. (b) Drag coefficients of NACA 23024 airfoil

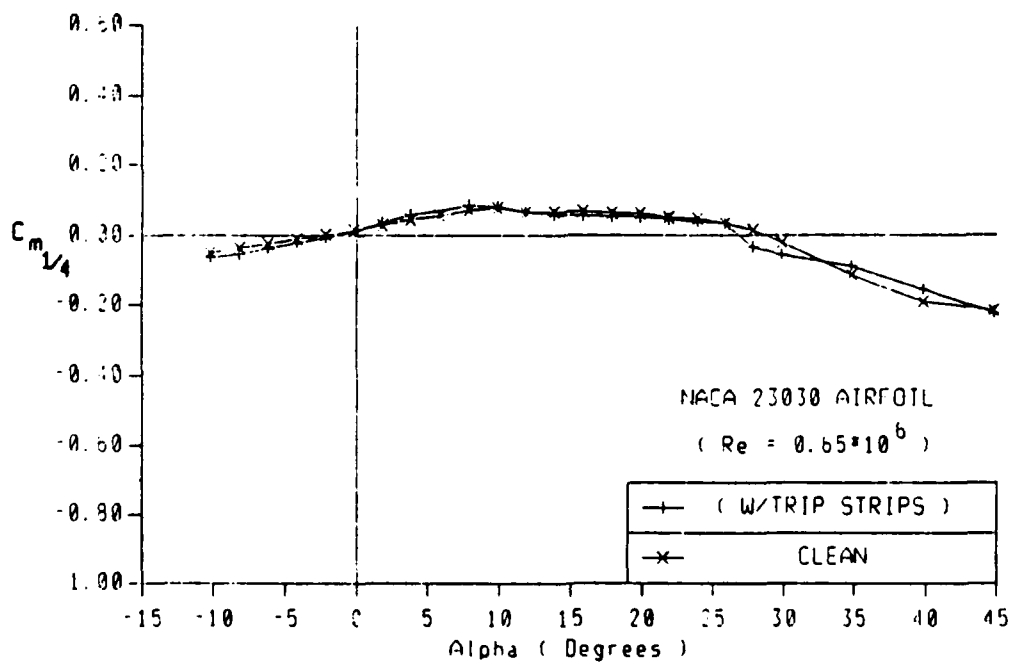


Figure 23. (c) Moment coefficients of NACA 23024 airfoil

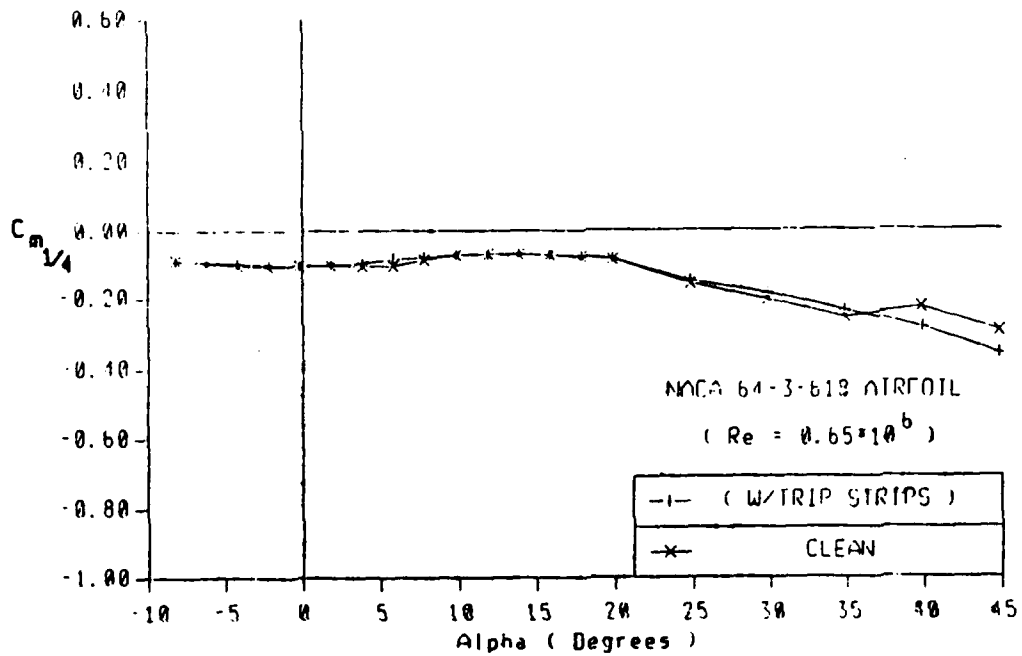


Figure 24. (a) Lift coefficients of NACA 64-3-618 airfoil

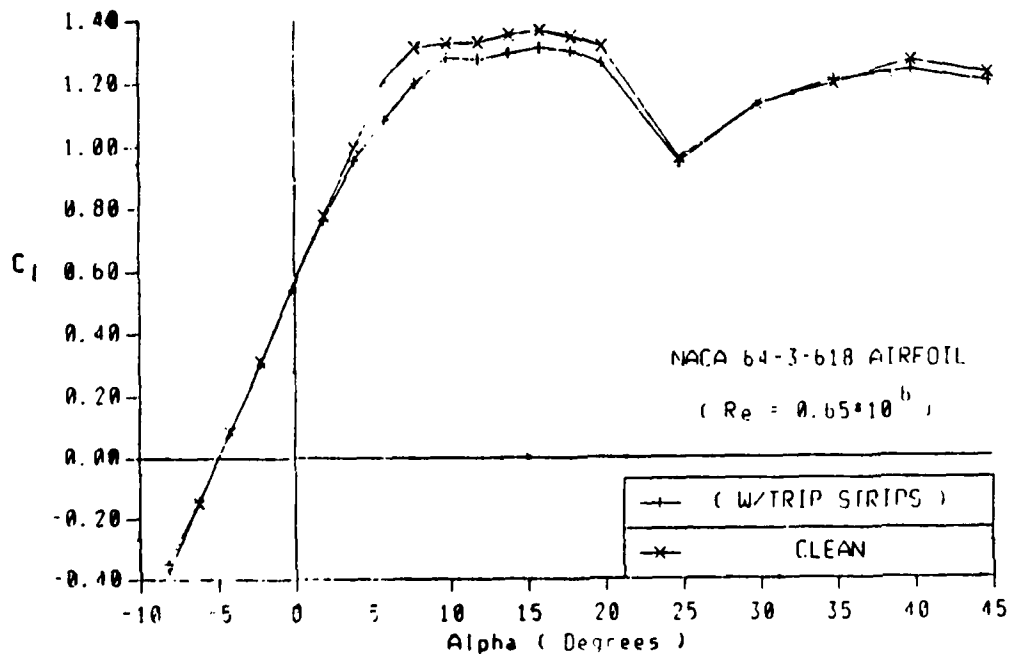


Figure 24. (b) Drag coefficients of NACA 64-3-618 airfoil

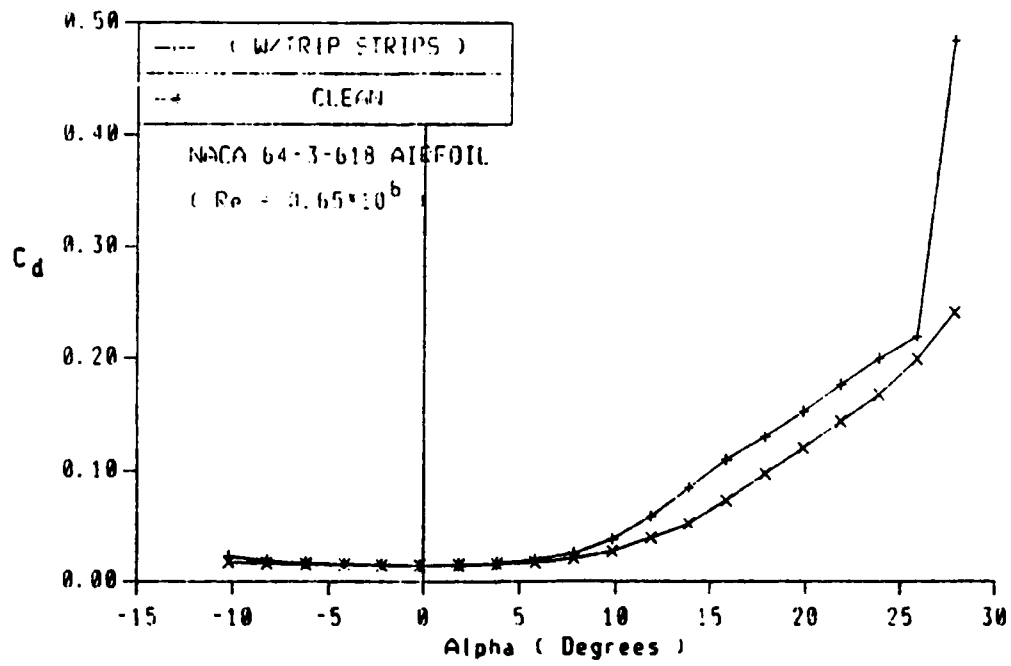


Figure 24. (c) Moment coefficients of NACA 64-3-618 airfoil

Appendix B

IAR 88-111

PREDICTING OPTIMAL DROOPED LEADING-EDGE EXTENSION LENGTH FOR AN NACA 0015 WING THROUGH FLOW VISUALIZATION

by

August A. Asay

and

Melvin H. Snyder

INSTITUTE FOR AVIATION RESEARCH

THE WICHITA STATE UNIVERSITY

WICHITA, KS 67208

May 1988

ABSTRACT

Investigation into the optimal length drooped leading-edge extension for an untapered, aspect ratio 7.4, NACA 0015 wing was performed in The Wichita State University 2 X 3 foot water tunnel. The data were obtained using flow visualization techniques; force data was not taken. A reflection plane model was used for this study. Three different leading-edge drooped extensions were tested and compared to the basic wing. Leading-edge drooped extension lengths were investigated by applying leading-edge cuffs to the experimental model at the 60-100% half-span, 70-100% half-span, and 70-95% half-span positions on the wing. The tests were conducted at angles of attack from 0 deg. to 30 deg., with increments of 5 deg., at a Reynolds number of 14,200. At high angles of attack, a vortex developed at the inboard edge of the drooped leading-edge extension. This vortex divided the stalled inboard wing from the apparently unstalled outboard portion of the wing. From visual observations it appeared that the inboard edge location of 60% half-span protected more wing area than the other inboard locations tested. The best location for the outboard edge of the leading-edge droop extension was observed to be at 95% half-span.

LIST OF SYMBOLS

<u>Symbol</u>	<u>Definition</u>
b	Wing Span
c	Wing chord
C	Coefficient of lift = L / qS
C_L	Local or section lift coefficient
C_{l1}	
DLEE	Drooped Leading-Edge Extension
L	Lift
Re	Reynolds Number = $\rho V c / \mu$
S	Wing Planform Area
v	Water Velocity
y	Coordinate in spanwise direction
α	Angle of Attack
ρ	Density
μ	Dynamic Viscosity
Γ	Circulation

INTRODUCTION

Over one-fourth of general aviation fatalities are due to stall and uncontrollable spin (Ref. 1). Since a pilot is no longer required to demonstrate stall/spin recovery, greater emphasis has been placed on improving and delaying stall departure and the subsequent spin.

The NASA-Langley Research Center has developed many leading edge extensions to overcome the stall/spin problem (Ref. 2). One device which shows much promise is the drooped leading-edge extension (DLEE). NASA has tested these devices in the spin tunnel and in flight test and has found them to increase the stall angle and to deter stall departure without having detrimental effects (Ref. 3).

The purpose of this project was to find the optimum DLEE length on an untapered wing through flow visualization. The wing aspect ratio was 7.4 and the airfoil section was NACA 0015 with no twist. The facility used was The Wichita State University 2 X 3 foot water tunnel. The flow patterns over the airfoil were made visible by injecting dyes into the stream from the model. The modification done on the basic wing consisted of applying three different leading-edge cuffs providing three DLEEs on the leading-edge of the wing from 60-100% half-span, 70-100% half-span, and 70-95% half-span.

MODEL CONFIGURATION

The model used was of the reflection-plane type which allowed a larger wing span and chord to be tested. The airfoil section of the model is an NACA 0015. This model is shown in figure 1. The DLEE first tested extended from 60% to 100% of semispan. This length was decided upon from previous studies (Ref. 2). The DLEE were shortened to see if a smaller DLEE would show the same visual effect as the 60% to 100% of semi-span length. The model with the leading-edge cuffs is shown in figure 2.

WING AND LEADING EDGE EXTENSION

wing span (simulated)	44.5 in.
half-span	22.25 in.
wing chord	6.0 in.
wing max. thickness	0.9 in.
DLEE extension	5% of chord
DLEE droop	2% of chord
DLEE lengths	60-100% (8.90 in.), 70-100% (6.67 in.), 70-95% (5.67 in.) of half-span

EXPERIMENTAL PROCEDURE

Water flow velocity was set at 0.35 ft./sec.; higher velocity caused the dye filaments to break up too soon after leaving the dye ports. Reynolds number was 14,200, based on the unmodified chord of 6 inches. The first tests were done on the wing using seven different dye colors to observe the different flow patterns. Angle of attack was varied from 0 deg. to 30 deg. to 5 deg. increments. At each angle the flow patterns were recorded using still pictures and video tape. However, it was found that still pictures did not supply as accurate a record as did video taping. This procedure was repeated for each DLEE tested.

When the leading-edge extension cuffs were attached to the wing, three dye tubes were placed on the upper surface just downstream of the inboard DLEE edge. As shown in figure 3, these tubes were placed where they would not interfere with the flow, but were positioned to show the flow patterns. It is desirable to place the tube outlets at the stagnation point of the wing. Since the stagnation point of the wing changes with angle of attack, the tubes were placed at the stagnation point for an angle of attack of five degrees.

RESULTS

When the wing was tested without the DLEE, it was noticed that, at zero angle of attack, the wing experienced laminar separation at approximately 60% c. This laminar separation is due to the low test Reynolds number of 14,200.

At low angles of attack ($\alpha < 5$ deg.) the DLEE had very little effect on the flow over the wing. At an angle of attack close to 5 deg., the separation line behind the DLEE did not advance as far forward as on the rest of the wing. This change is apparently due to turbulence induced by the edge discontinuity of the DLEE/wing combination.

At 8 deg. angle of attack, a vortex formed on the inboard DLEE edge. This vortex formed on both the 60-100% half-span and 70-100% half-span DLEE wings and turned in the opposite sense to the wingtip vortex. Vortex bursting occurred at approximately 50% c when an angle of attack of 10 deg. was encountered. This bursting is attributed to the adverse pressure gradient on the wing.

At about 15 deg. angle of attack, it appeared that a second vortex developed on the 60-100% half-span and 70-100% half-span DLEE wing. This vortex started on the DLEE inboard edge and ran diagonally along the wing toward the outboard section. This vortex can be seen in figure 4. It appeared that this vortex rotated in the same direction as the wingtip vortex.

Both the 60-100% half-span and 70-100% half-span DLEEs produced vortices at the same angle of attack. These vortices appeared to be approximately the same size. However, the 60-100% half-span DLEE protected more wing area than the 70-100% half-span DLEE. Through observation, the area difference was approximated at 10%. This difference is shown in figures 5 and 6.

When the 70-100% half-span DLEE was modified to 70-95% half-span the wing tip vortex increased in size. After the modification was made, the diagonal vortex encountered with the

70-100% half-span DLEE no longer existed. The flow over the wing appeared to improve with this modification.

Some analysts have described this vortex as an aerodynamic fence which prevents the stall from progressing to the outboard section of the wing. This fanciful description of the observed phenomenon is an over-simplification.

It is true that there is some tendency for the stalled region on a wing to spread spanwise even on an untapered unswept wing. This spread is due to the pressure gradient as shown in figure 7 (This pressure data is from a reflection plane wind tunnel test and is supplied as being typical). However, the spread of the stall is not very great; at a given angle of attack, equilibrium is quickly attained and the stalled region remains constant.

In the case of the use of a drooped leading-edge extension, the part of the wing to which the DLEE is applied has a different airfoil section -- a section which has a greater chord and, which, (because of the shift of the chord line and of the zero-lift line) at a given angle of attack of the basic wing is operating at a higher aerodynamic angle of attack. This part of the wing is developing higher circulation than the adjoining plain wing. The bound vortex strength is greater. This difference may be seen by comparing figures 8a and 8b. This change in the lift generated, and, therefore, the strength of the bound vorticity must produce a region of fairly intense shedding of vorticity at the inboard end of the DLEE -- vorticity of opposite sense to that shed over the rest of the semi-span.

It can be seen, from figures 4, 5, and 6, that this additional counter-rotating trailing vortex has its apparent origin at the leading-edge discontinuity at the inboard end of the DLEE (similar to the way the vortices on a delta wing apparently originate at the apex, but, in fact, are generated all along the leading-edge).

This vortex does not trail downstream parallel to the freestream direction, again for the reason of the spanwise pressure gradient. Figure 9 pictures this spanwise pressure gradient which drives the vortex outboard. This pressure gradient is stronger than that illustrated in figure 7, because the airfoil sections have different camber, chord, and aerodynamic angle of attack.

CONCLUSION

- 1) The wing experienced laminar separation at approximately 60% chord, at an angle of attack of zero degrees. This was caused by the low Reynolds number.
- 2) With an added DLEE, flow visualization patterns on the wing changed very little at low angles of attack ($\alpha < 5$ deg.).
- 3) At approximately $\alpha = 8$ deg., a vortex, rotating opposite to the tip vortex, formed on the inboard DLEE edge.
- 4) At about 15 deg. α , a second vortex developed. This vortex appears to be rotating in the same direction as the tip vortex and is diagonal on the wing surface.
- 5) Vortex bursting occurred at $\alpha = 10$ deg., at 40% chord, and then moved forward at higher angles of attack.

6) When the outboard edge of DLEE was brought in from 100% of the semispan to 95% of the semispan, the tip vortex increased in size. This caused the flow behind the DLEE to improve.

7) From the inboard cuff locations tested, the best cuff position is with the inboard end at 60% half-span. The 60% location was chosen because more wing area remained unstalled than with the other cuffs.

8) The best procedure for recording this flow visualization data is the use of motion pictures. Still pictures were found to be unreliable.

9) Wind tunnel force and pressure distribution tests are being run at W.S.U. and will be reported in the near future.

REFERENCES

1. DeMeis, Richard, "Taming the Deadly Spin," Aerospace America, Volume 23, June 1985.
2. Staff of NASA-Langley Research Center, "Exploratory Study of Effects of Wing Leading Edge Modifications on the Stall Spin Behaviors of a Light General Aviation Aircraft," NASA TP 1589, 1979.
3. Yip, Long, "Stall/Departure Resistance of a Personal Owner Trainer Type Aircraft," Oral presentation, AIAA Techfest XIV, November 13-14, 1987, Wichita, KS.
4. Phutlek, Pornchai, "Experimental Investigation of Separated Flow Fields on a Wing with a Sharp Discontinuous Leading-Edge to Improve Stall/Spin Resistance," Phd Dissertation, The Wichita State University, Wichita, KS, 1988.

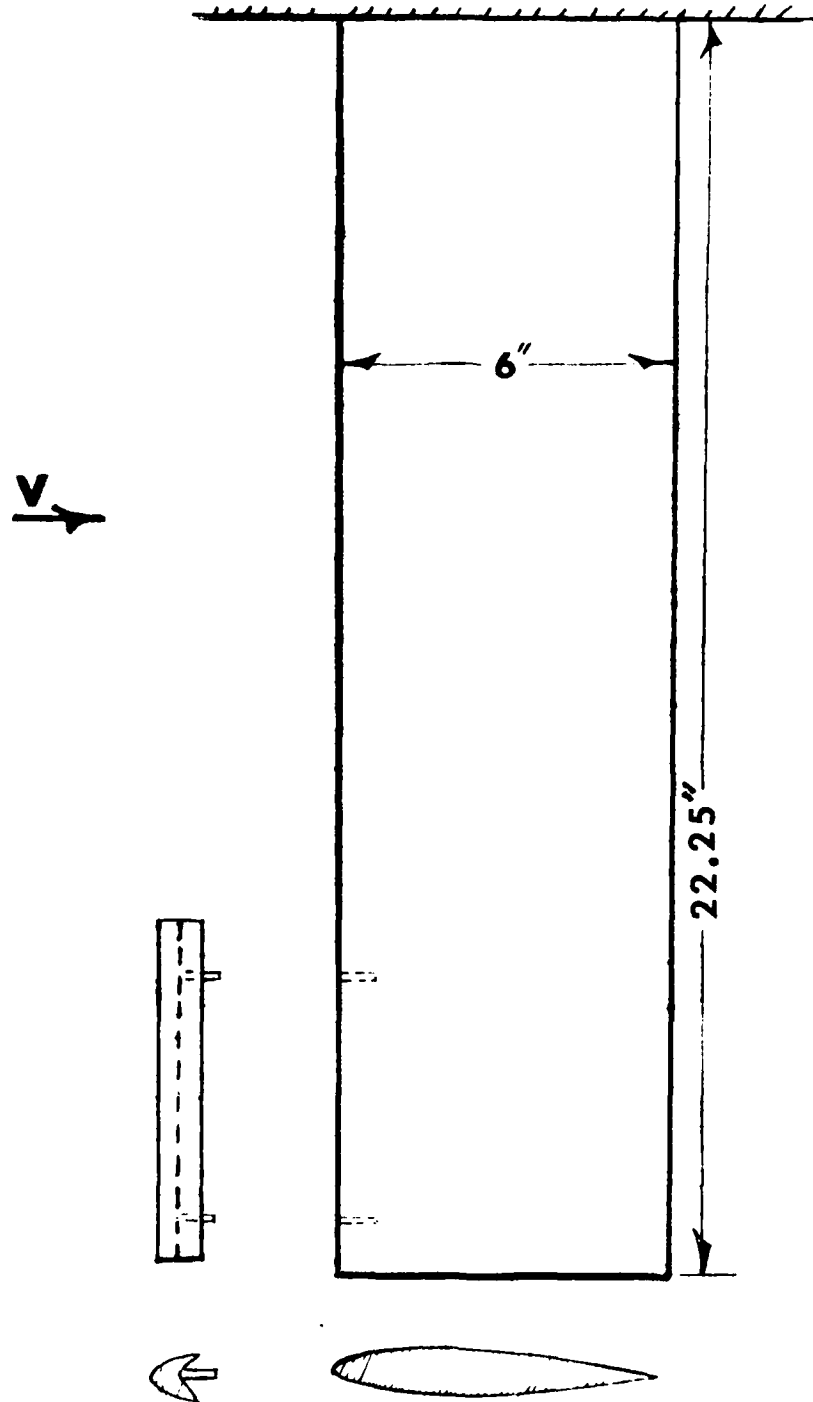
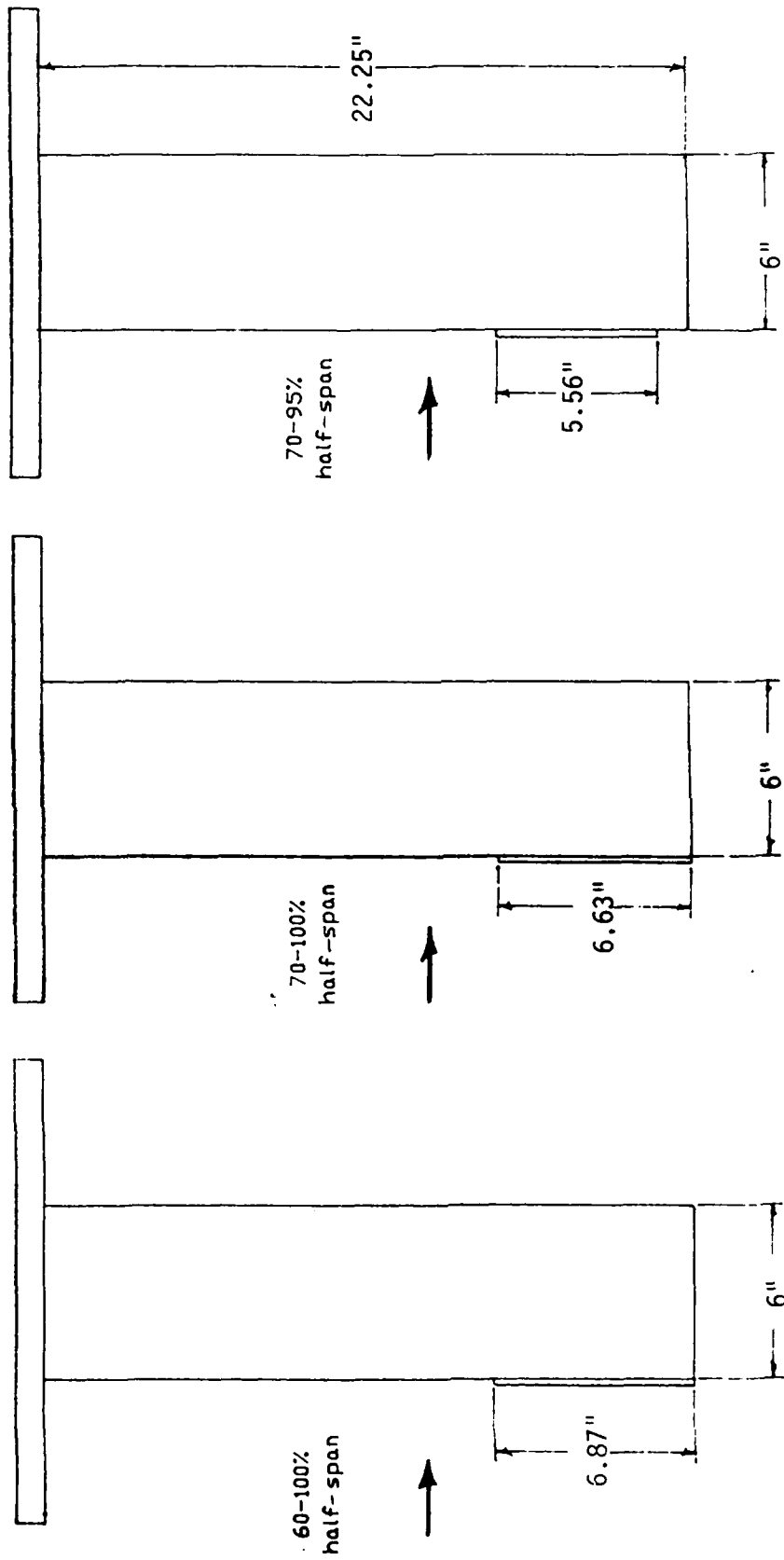


Figure 1. Plan and Airfoil Section View of Water Tunnel Model.



B-10

Figure 2. Configurations of DLEE Mounted on Wing Semi-Span.

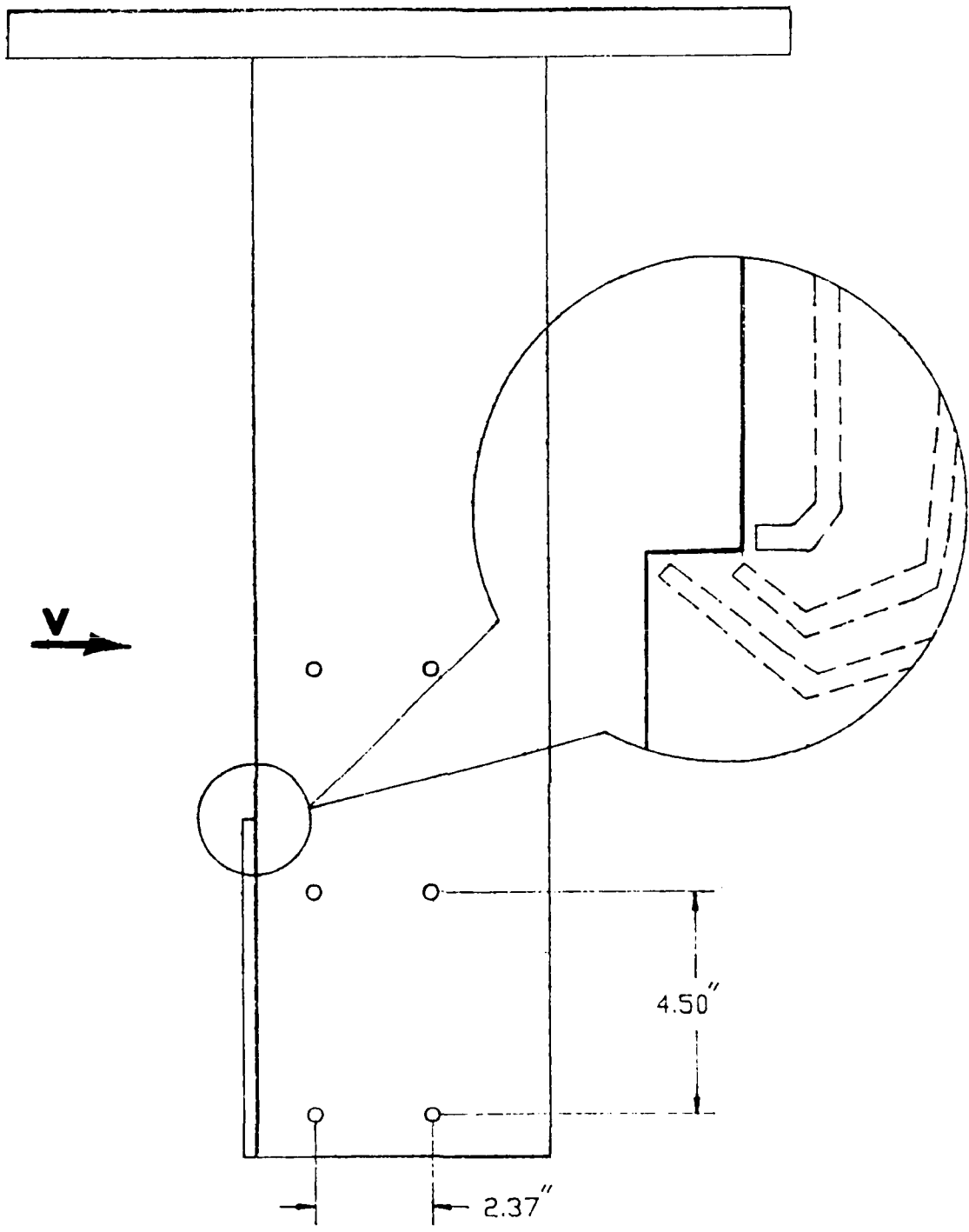


Figure 3. Dye Tube Placement

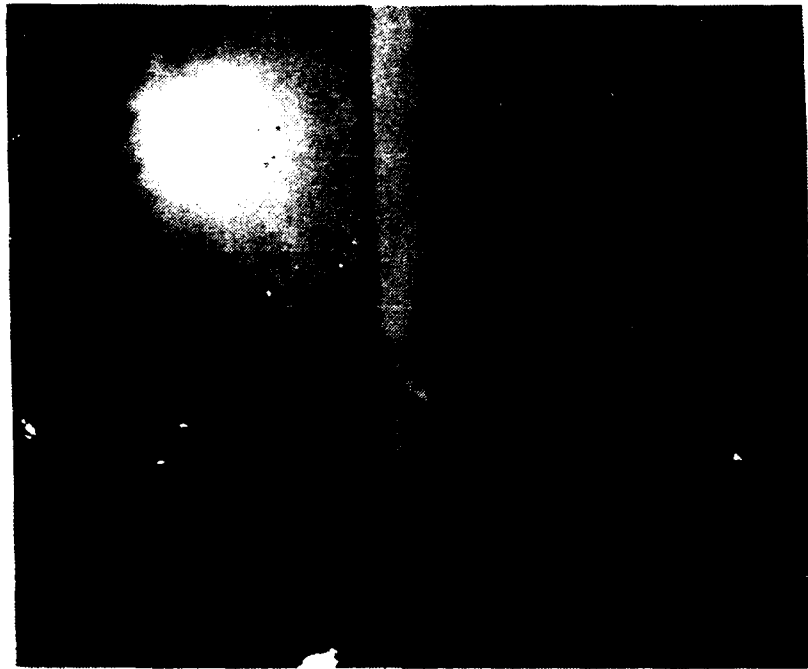


Figure 4. DLEE Extends from 70 to 100 Percent of Semi-Span.
 $\alpha = 15^\circ$

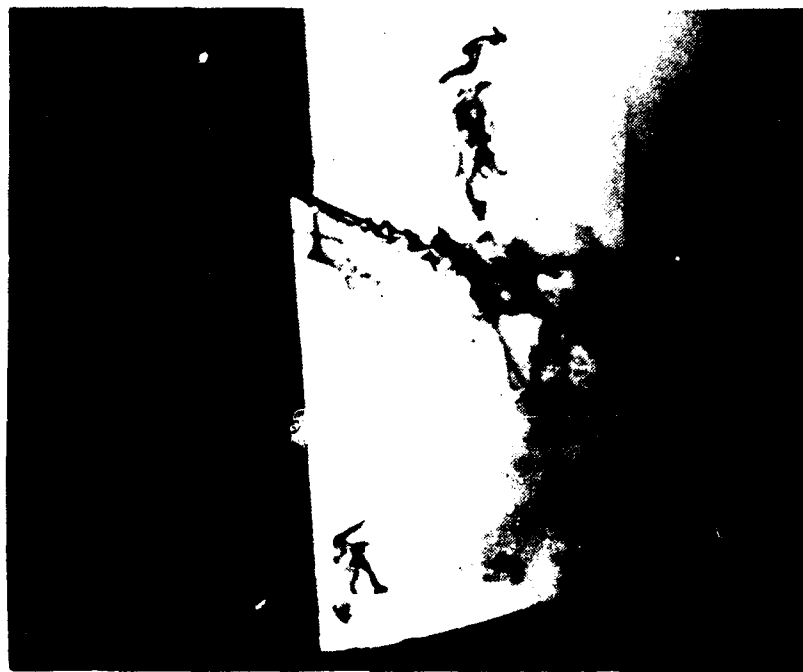


FIGURE 5. DLEE from 70 TO 100 Percent of Semi-Span.
 $\alpha = 20^\circ$



Figure 6. DLEE from 60 to 100 Percent of Semi-Span.
 $\alpha = 20^\circ$

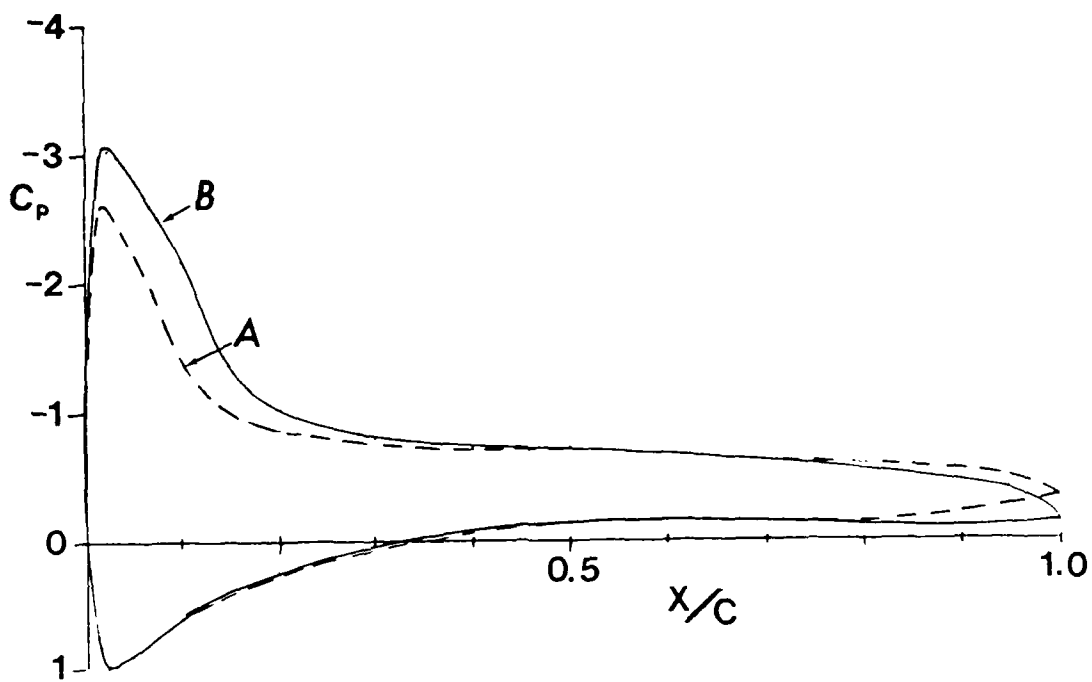
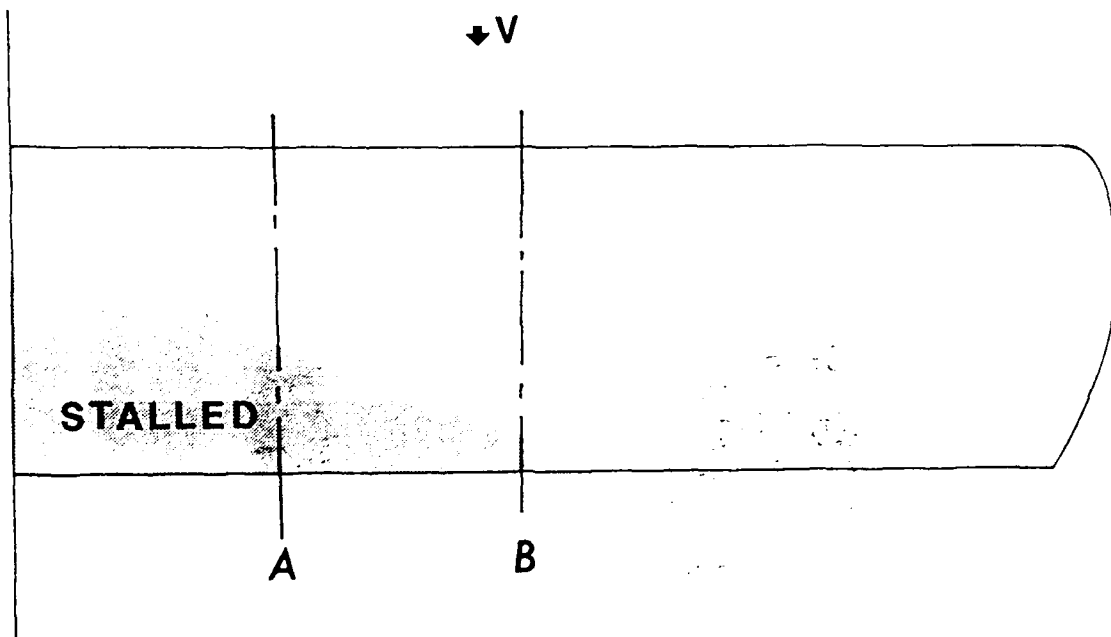
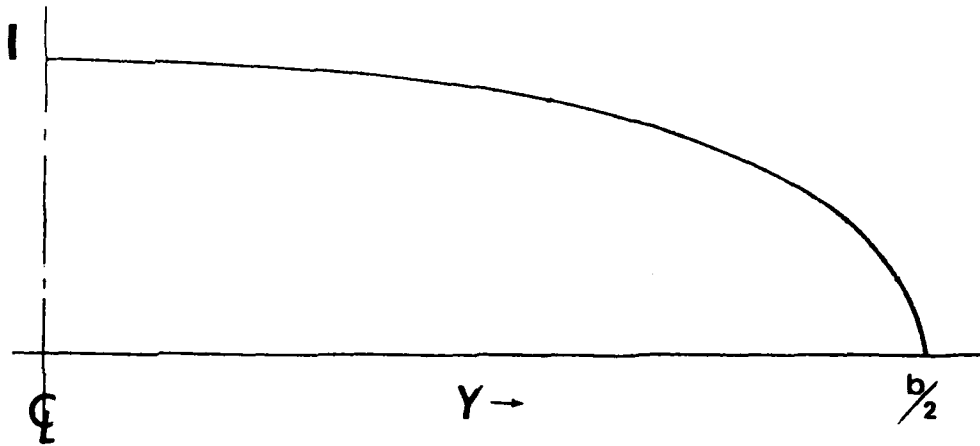
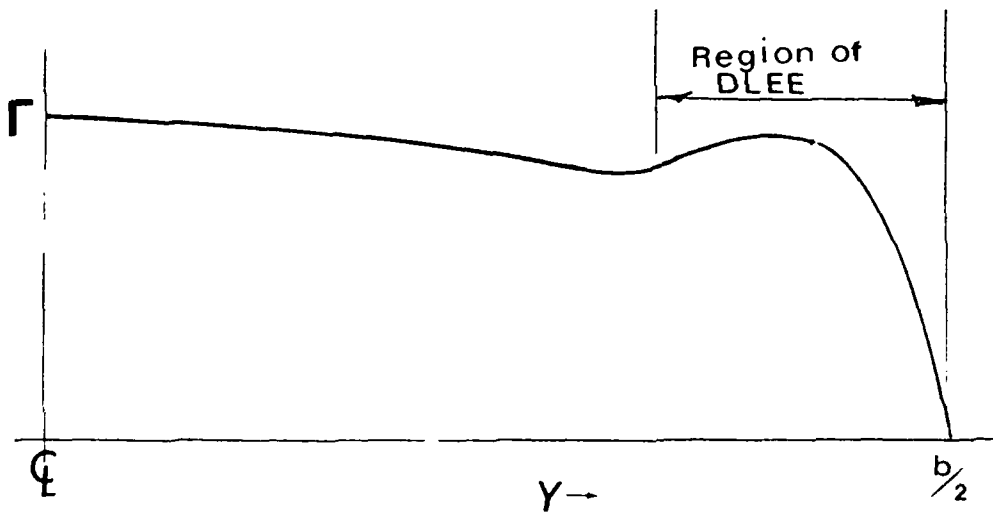


Figure 7. Origin of Pressure Gradient which Tends to Promote Spanwise Movement of Stalled Region on Straight Wing.

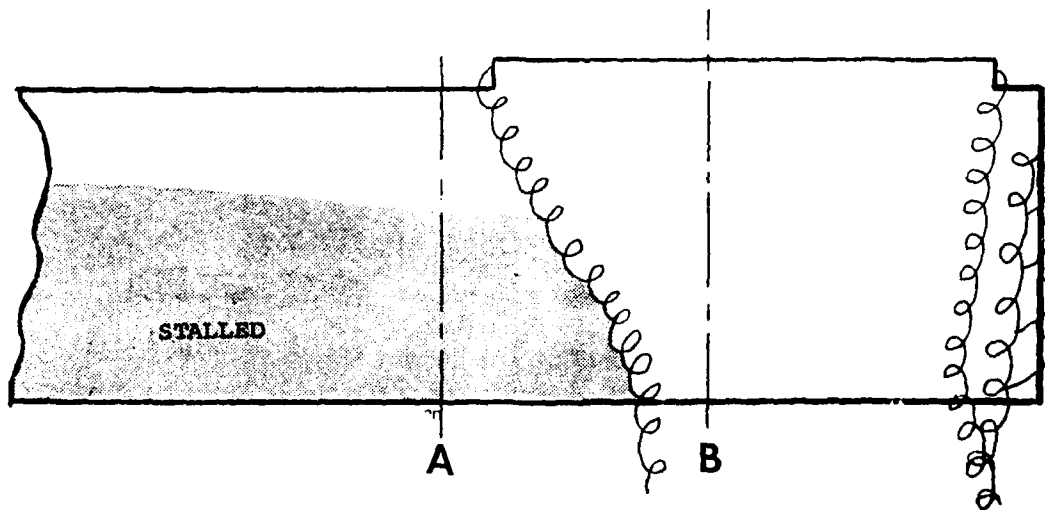


a. Lift Distribution on Straight, Constant-section Wing Below Stall.

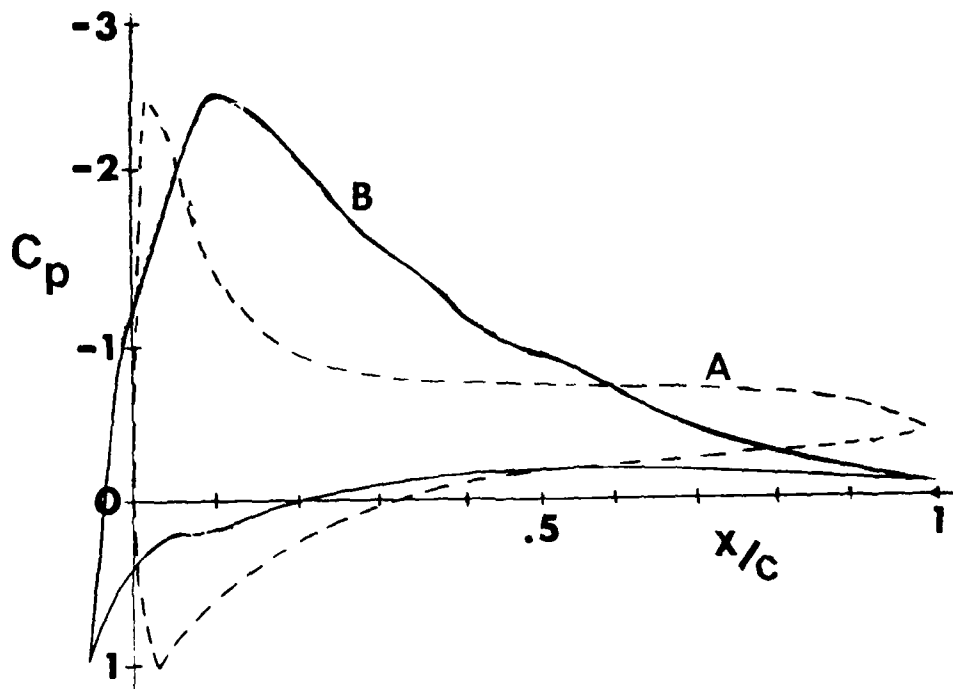


b. Lift Distribution on Wing with DLEE on Outboard Section.

Figure 8.



a. Wing with DLEE at Angle of Attack Producing Stalled Inboard Sections.



b. Pressure Distributions at Sections A and B.

Figure 9.

Appendix C

IAR 88-112

**EXPERIMENTAL STUDY OF SEPARATED
FLOW FIELD ON AN NACA 23024
RIGHT WING**

by

Yong Wang

and

Melvin H. Snyder

INSTITUTE FOR AVIATION RESEARCH

THE WICHITA STATE UNIVERSITY

WICHITA, KS 67208

September, 1988

ABSTRACT

Detailed experimental measurements have been made of the separated flow field on a right wing with an NACA 23024 airfoil at angles of attack from 4 to 40 degrees, at chord Reynolds number 0.9×10^6 , and Mach number 0.175. The data include force measurements by main balance, and surface pressure measurements at six spanwise stations obtained by use of pressure belts.

The results indicated use of pressure belts can produce good surface pressure distribution even at high angles of attack. The present tests reveal that the wing tip vortex has a very important influence on the wing forces.

LIST OF FIGURES

Figure		Page
1	Model Section Geometry and Coordinates	16
2	Model and Reflection Plane in Test Section	17
3	Wing Lift Coefficient for Three Tests	18
4	Wing Drag Coefficient for Three Tests	19
5	Wing Moment Coefficient for Three Tests	20
6	Wing Lift coefficient by Balance and Integration of Surface Pressure	21
7	Wing Drag Coefficient by Balance and Integration of Surface Pressure	22
8	Wing Moment Coefficient by Balance and Integration of Surface Pressure	23
9	Wing Sections Pressure Distribution; $\alpha = 4^\circ$	24
10	Wing Sections Pressure Distribution; $\alpha = 10^\circ$	25
11	Wing Sections Pressure Distribution; $\alpha = 20^\circ$	26
12	Wing Sections Pressure Distribution; $\alpha = 30^\circ$	27
13	Wing Sections Pressure Distribution; $\alpha = 40^\circ$	28
14	Lift Distribution in Spanwise Direction	29
15	Drag Distribution in Spanwise Direction	30
16	Moment Distribution in Spanwise Direction	31

LIST OF SYMBOLS

B	wing span
c	wing chord
C_L	wing lift coefficient
C_D	wing drag coefficient
C_M	wing moment coefficient
C_p	pressure coefficient
Re	Reynolds number based on wing chord
Y	spanwise coordinate
z	vertical coordinate
α	angle of attack, degrees

INTRODUCTION

High angle-of-attack aerodynamics has increased in importance over the last several years, because of the demand for greater maneuverability of space shuttle vehicles, missiles, military and commercial aircraft (both manned and remotely piloted), and also because the statistics of fatal general aviation accidents have shown that the stall/spin has been one of the most significant accident causes for the past decade. NASA Langley Research Center and Federal Aviation Administration (FAA) are conducting a large number of research programs to develop the technology required to improve stall/spin characteristics of light general-aviation aircraft [2].

In response to this interest, the Institute for Aviation Research at The Wichita State University has begun to investigate the fundamental aerodynamic characteristics of airfoils and wings at high angles of attack [11,12,14]. Some of this effort has focused on wing aerodynamics including a wing leading-edge modification, consisting of a discontinuous drooped leading edge added to the outer wing panel to enhance spin resistance [9].

As a part of the continuing stall/spin research program of the I.A.R. the main objectives of this research project are:

- a. obtaining experimental data to support the analytical work on high angle of attack airfoils and wings.
- b. to develop wind tunnel testing techniques and data acquisition and processing procedures.

- c. using experimental data to certify the technique of pressure belts for surface pressure measurement at high angles of attack.

EXPERIMENTAL INVESTIGATIONS

Facility And Instrumentation:

All tests were conducted in the WSU 7 x 10 ft. Walter Beech wind tunnel [3]. Instrumentation consisted of the tunnel main balance, on-line data acquisition and control system, manual five-hole probe traveling mechanism, five-hole probe and strip-a-tube pressure belts.

The model was an untapered, untwisted, reflection plane wing having NACA 23024 airfoil sections. The model has 9-inch chord and 60-inch semi-span, and was fabricated from solid aluminum. The basic NACA 23024 airfoil section is shown in Figure 1. The model was sized to permit testing through 360 degrees angle of attack with minimal wall interference. Force data corrections were small [13,14].

In order to minimize the floor boundary layer effects at the wing root, an 8-foot diameter circular reflection plane was installed 4 inches above the wind tunnel floor. This reflection plane was not attached to the balance. A small disk was fitted to seal the hole through the reflection plane. This disk was a 0.25 inch thick aluminum plate, 18 inches (2 chords) in diameter (as shown in Figure 2). The disk introduces a dynamic tare to the balance data which was evaluated by running the tunnel with the plate but without the wing panel.

In order to reduce the probe position shift error in Z direction, the manual five-hole probe traveling mechanism, with two supporting arms, used the same origin for motion in the Z direction for all tests. Two rigid supporting arms were used to

support the mechanism to reduce the probe vibration when it is in the turbulent wake from a separated boundary layer.

Forces and Surface Pressure:

Force measurements were obtained using the tunnel main balance for angles of attack from -8 to 44 degrees, and force results are presented in terms of coefficients of the usual wind-axis forces (C_L , C_D and C_M). The surface pressures were obtained by use of pressure belts at six span-wise stations (10%, 40%, 60%, 80%, 90% and 95%) and at five angles of attack (4, 10, 20, 30 and 40 degrees); each of these stations has 20 pressure measurement points. Surface pressure data are presented in terms of pressure coefficients.

Range of Tests

All tests were conducted at tunnel dynamic pressure of 45 psf which corresponds to chord Reynolds number of 0.9×10^6 and Mach number of 0.175.

Corrections and Data Reduction

The standard wind tunnel corrections [10] accounting for flow angularity, solid blockage, wake blockage, turbulence and horizontal buoyancy, are incorporated in wind tunnel data processing computer program [4,14].

The wind tunnel is equipped with an automated data acquisition system capable of real-time plotting and gives corrected force coefficients output as well as raw data. For high angles of attack, flow in the turbulent separated boundary layer and in the wake is basically unsteady, therefore, data recorded were time-averaged quantities.

RESULTS AND DISCUSSIONS

The reduced data are presented. Figures 3 through 8 are plots of wing force coefficients and moment coefficients measured by main balance and compared with values calculated from surface pressures. Figures 9 through 13 are the pressure distributions at different spanwise sections for various angles of attack. Figures 14 through 15 are spanwise distribution of the wing section force coefficients.

Force Results:

Figures 3 through 5 are the lift, drag and moment coefficients of NACA 23024 right wing for the angles of attack from -8 to 44 degrees at chord Reynolds number of 0.9×10^6 for different tests. Run No.1 is the first force measurement test and Run No.33 is the repeat force test after the surface pressure measurement tests were completed. The force data from reference [14] are the results of tests of the same model under almost the same Mach number and Reynolds number; the test was done in the same wind tunnel in 1985. All of the results were obtained from the computer controlled balance acquisition system. Blockage, buoyancy, and end plate corrections were made in the program in accordance with reference [15]. The agreement between the three sets of data, as seen in Figures 3 through 8, appears to be quite good over most of the test range. The agreement of the drag coefficient values is particularly surprising since the balance data was for total drag, but the pressure belt values were for pressure drag only, i.e., without viscous drag. The repeatability is very good up to angle of attack of 35 degrees. The greatest

deviation appears in these sets of data in the range of angles of attack from 35 to 45 degrees. In this region, flow is separated and the model vibrates. Repeatability of force data in this region is not very good.

Figure 3 is the lift coefficient results of the right wing for angles of attack from -8 to 44 degrees. This plot shows a smoothing of the normal sudden drop in lift coefficient after stall and comparatively large values of C_L at very high post-stall angles of attack. There appear to be three major reasons for this difference between 3-D post-stall lift and 2-D post-stall lift. First, NACA 23024 airofil is a very thick airfoil with big radius of leading edge. This prevents flow separation on upper surface near leading edge, and flow in this region can produce quite an amount of lift even when flow has been stalled near the trailing edge at angles of attack up to 20 degrees. Verification can be found from wing section pressure distributions in Figures 10 and 11. Second, for the finite span wing, the trailing vortices induce downwash at sections along the entire span which change the effective angle of attack along the span; the effective angle of attack at outboard sections is lower than that at inboard sections, so the flow near the tip is separated later than inboard. Third, at very high angles of attack, the wing tip vortex becomes very strong, even when the inboard section flow has been fully separated. The wing tip vortex still can create vortex lift near the tip sections [5,6,7]. All of these factors combine to prevent the sudden falling in lift coefficient as angle of attack increases. This can be seen by examining pressure distributions in Figures 11, 12 and 13.

Wing Section Pressure Distributions:

Figures 9 through 13 are the wing sections pressure distributions at angles of attack equal to 4,10,20,30 and 40 degrees. First, it should be pointed out that it is very difficult to obtain the surface pressure data at trailing edge by using the pressure belts in this test. The data points at trailing edge on the curves in these figures are not real measured data in the wind tunnel test. They are obtained by extrapolating and averaging the other data values around the trailing edge to make the curves of pressure distributions in closed form. From these figures, one can see that as angle of attack increases from 4 degrees to 40 degrees, the stagnation point, which corresponds to $C_p=1.0$ on the plots, moves backward from leading edge to 10% on the lower surface.

Figure 9 and 10 are the wing sections pressure distributions at angles of attack of 4 and 10 degrees. From these two plots it can be seen, the flow does not separate in this range of angles of attack, and the pressure distributions vary in the spanwise direction. The inboard section has a larger minimum pressure peak on upper surface than does the outboard section. As alpha increases from 4 degrees to 10 degrees, the pressure gradient in the spanwise direction increases. The effective angle of attack changes in the spanwise direction, and the effect of it is proportional to the lift coefficient, so as angle of attack increases, the effect increases as can be seen by comparing the two plots.

For angle of attack equal 20 degrees, flow at most sections of the wing has been separated. Figure 11 shows, in the 40% to 90% spanwise range, the separation points stay at about 30% chord aft of the leading edge. At inboard sections flow separated earlier at about 18% chord. At the wing tip section ($2y/B=95\%$), the flow does not appear to separate over the entire section. In the forward part of the section (40% chord), the peak and the range of low pressure is much greater than at inboard sections. The suction downstream of 40% chord is lower than that at inboard sections. The main reason for this pressure distribution is the existence of a wing tip vortex and its position and strength. Near the leading edge, the vortex is strong. The tip-vortex core is near the upper surface, so it can produce a high velocity flow in spanwise direction on upper surface, which can produce a high suction pressure peak. But, in the region far behind the leading edge, the core of the vortex is far from the surface when the angle of attack is large. The effects of the vortex are not as strong as near the leading edge. On the other hand, because the air with higher pressure on the lower surface has been rolled up to the upper surface, the difference of pressure between the upper and lower surface becomes smaller and smaller in the flow direction and is lower than that at inboard region.

For 30 degrees angle of attack, the separation point moves forward up to about 10% chord for all the inboard sections (to 80% spanwise). After the separation point, the pressure is almost constant for the following area. In the region near wing tip, the separation point is still at about 40% chord behind the leading edge, and the suction peak and area is still quite high and

large. From these results, we can conclude that the tip vortex has a strong influence on wing tip pressure distribution until angle of attack equals 30 degree. We can find the pressure distribution from the Figure 12 and 13.

For an angle of attack of 40 degrees, the wing tip vortex core is far away from the surface; the influence of the vortex on the surface pressure distribution is not so strong as at lower angles of attack, and the separation point moves forward to 5% chord after leading edge position for the all spanwise sections. From Figures 14 and 15, we still can find the influence of the tip vortex, which makes the suction pressure near the tip higher than on inboard sections.

Spanwise Section Force Coefficients Distributions:

Figures 14 and 15 are the wing sections force coefficient distribution in the spanwise direction, obtained by the integration of the pressure data in the chordwise direction. For angle of attack of 4 and 10 degrees, the flow is not separated, and the wing tip vortex is not very strong, the spanwise force distributions are almost elliptic; this result agrees well with finite span wing theories [1]. For higher angles of attack, these theories no longer can be used to estimate the spanwise force distribution because of large area flow separation and existence of strong wing tip vortices. For moderate angles of attack, both effects are of the same order, so it is more difficult to give an exact explanation for the test results, the lift distribution at $\alpha=20$ degrees is a result of this kind. The reason why the lift reaches its maximum value at 40% spanwise is not very clear. It needs further experimental test and analysis.

For angles of attack of 30 and 40 degrees, the inboard flow has fully separated, so the force does not change very much until near 80%. From Figure 14, we find that wing tip vortex influence region is from 80% to the tip, and the vortex makes the force coefficients in this region much higher than those at inboard sections. The lift coefficient near wing tip is about 40% higher than that at inboard sections.

CONCLUSIONS

1. Wing forces, surface pressure distributions, and velocity vectors have been obtained for NACA 23024 right wing and wing section at pre-stall, stall and post-stall angles of attack conditions. The velocity vector data do not include reversed flow regions of separated boundary layer and wake.
2. The results of force data, both from balance and surface pressure data integration, show that using pressure belts is a simple and effective method for getting surface pressure distribution even at post-stall angles of attack.
3. The wing tip vortex has an important influence on the force distribution at high angles of attack, which can induce high lift near the tip region that is about 40% higher than the inboard section at the same post-stall angle of attacks.

RECOMMENDATIONS

1. Flow visualization is recommended to investigate tip vortex position and its influence range at high angles of attack.
2. Some force measurements at other Reynolds numbers and Mach number are recommended to study the influence of both parameters on the aerodynamic properties of the wing.

REFERENCES

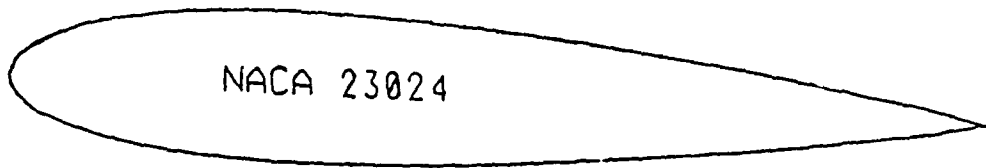
1. Abbott, Ira H. and Albert E. Von Doenhoff:
" Theory of Wing Sections "
Dover Publications, Inc. New York, 1959
2. Chambers, Joseph R. and H. Paul Stough, III:
" Summary of NASA Stall/Spin Research for General
Aviation Configuration "
AIAA Paper No. 86-2597, 1986
3. Davidson, M. L.:
" Facility Description of the 7 x 10 Feet W.H. Beech
Low Speed Wing Tunnel "
Wichita State University, AR 79-1, 1979
4. Habluetzel T.:
" Three-Dimensional Force Data Acquisition And
Reduction Routine for W.H. Beech Memorial 7 x 10 Foot
Low Speed Wing Tunnel "
Wichita State University, AR 80-1, 1980
5. Lamar, John E.:
" Extension of Leading-Edge-Suction Analogy to Wings
With Separated Flow Around the Sides Edges at
Subsonic Speeds "
NASA TR R-428, 1974
6. Lamar, John E.:
" Some Recent Applications of the Suction Analogy to
Vortex-Lift Estimates "
Part II, NASA SP-347, 1975, pp. 985-1011

7. Lamar, John E. and Luckring, James M.:
" Recent Theoretical Developments And Experimental Studies Pertinent to Vortex Flow Aerodynamics ---- With A View Towards Design "
AGARD-CP-247, Jan. 1979, pp. 24-1 - 24-31
8. Pfeiffer, Neal J. and Glen W. Zumwalt:
" Computational Model for Low Speed Flows Past Airfoils With A Spoiler "
AIAA 81-0253R, 1981
9. Pornchai Phutlek:
" Separated Flow Fields Measurements on a Wing With a Discontinuous Leading Edge "
Ph.D Dissertation, Wichita State University, 1987
10. Pope, A., and Harper, J. J.:
" Low-Speed Wind Tunnel Testing "
John Wiley, New York, 1966
11. Seetharam, H. C., and W. H. Wentz, Jr.:
" Studies of Flow Separation and Stalling on One-And Two-Element Airfoil at Low Speed "
SAE 770442, 1977
12. Seetharam, H.C., W.H. Wentz, Jr., and Walker, J.K.:
" Measurement of Post-Separated Flow Fields on Airfoils "
AIAA Paper No. 75-1426, 1975
13. Snyder, M. H., W. H. Wentz, Jr., and A. Ahmed:
" Reflection Plane Test of Control Devices on a Thick Airfoil at High Angles of Attack "
Wichita State University, WER-23 (Revised)

14. Wentz, W. H. Jr., and Fiscko, K. A.:

" Wing Tunnel Force and Pressure Tests of a 21%
Thick General Aviation Airfoil With 20% Aileron,
25% slotted Flap and 10% Slot-Lip Spoiler "

NASA-CR-3081, June 1979



Upper Surface		Lower Surface	
x/c	z/c	x/c	z/c
0.00000	0.00000	0.00000	0.00000
.00277	.04017	.02223	-.03303
.01331	.05764	.03669	-.04423
.03853	.08172	.06147	-.05862
.06601	.09844	.08399	-.06860
.09423	.11049	.10577	-.07647
.15001	.12528	.14999	-.08852
.20253	.13237	.19747	-.09703
.25262	.13535	.24738	-.10223
.30265	.13546	.29735	-.10454
.40256	.12928	.39744	-.10278
.50235	.11690	.49766	-.09428
.60202	.10008	.59798	-.08242
.70162	.07988	.69838	-.06664
.80116	.05687	.79884	-.04803
.90064	.03115	.89936	-.02673
.95036	.01724	.94964	-.01504
1.00000	.00000	1.00000	0.00000

Figure 1. Model Section Geometry and Coordinates

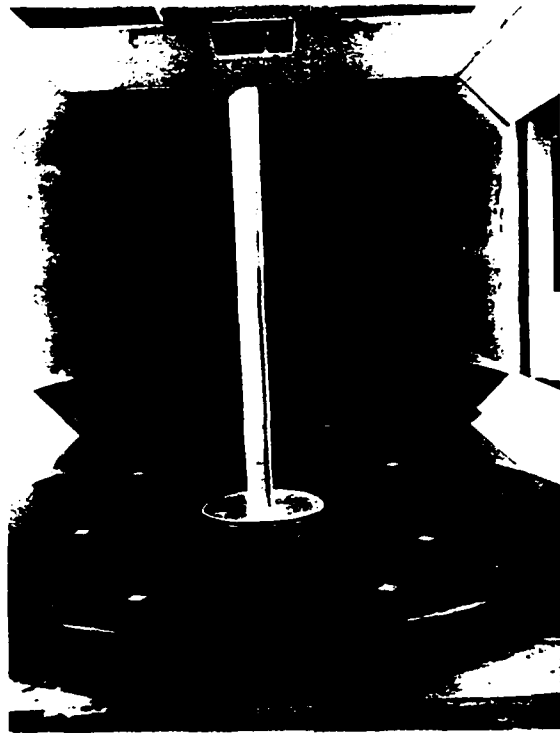


Figure 2. Model and Reflection Plane in Test Section

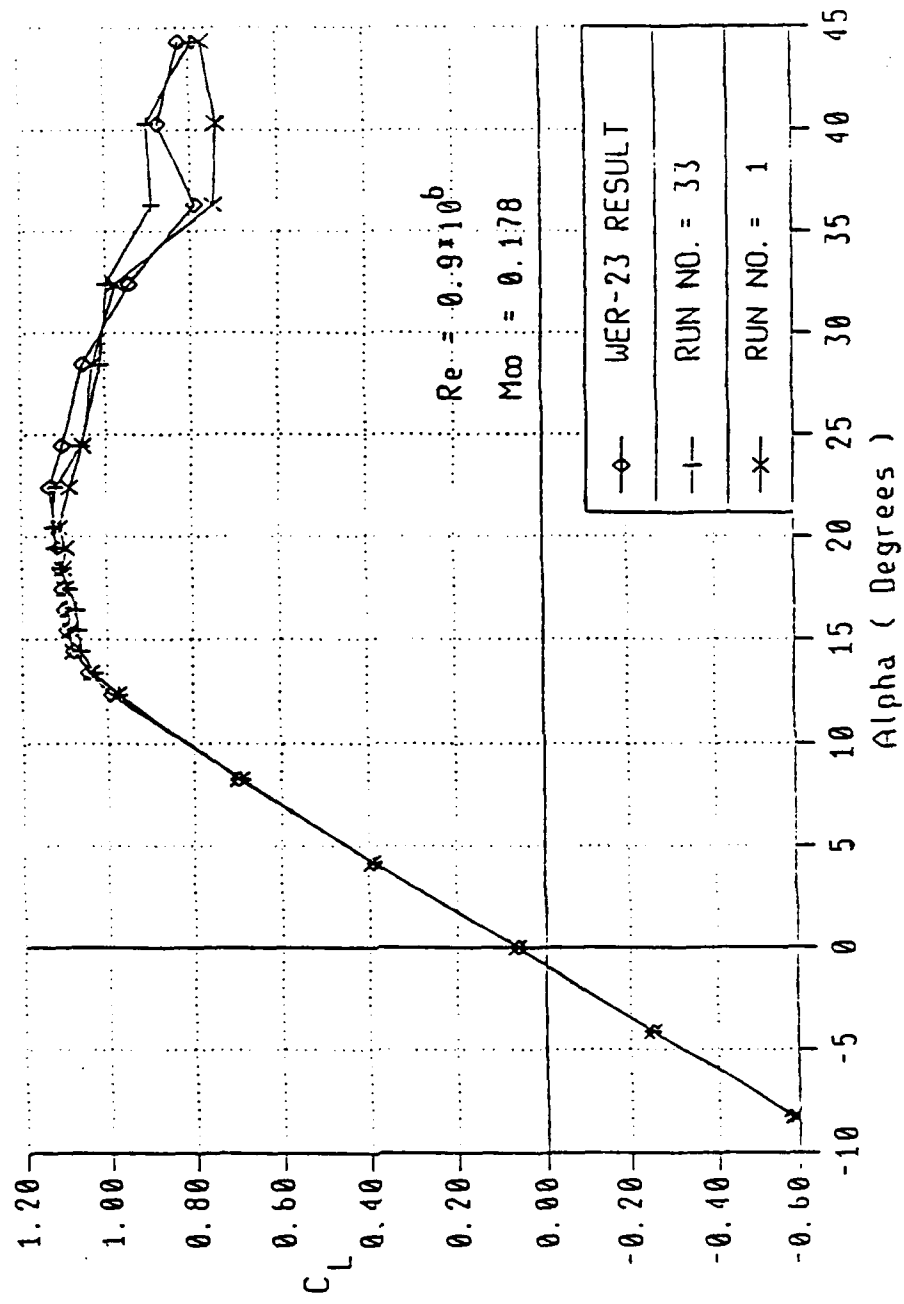


Figure 3. Wing Lift Coefficient for Three Tests

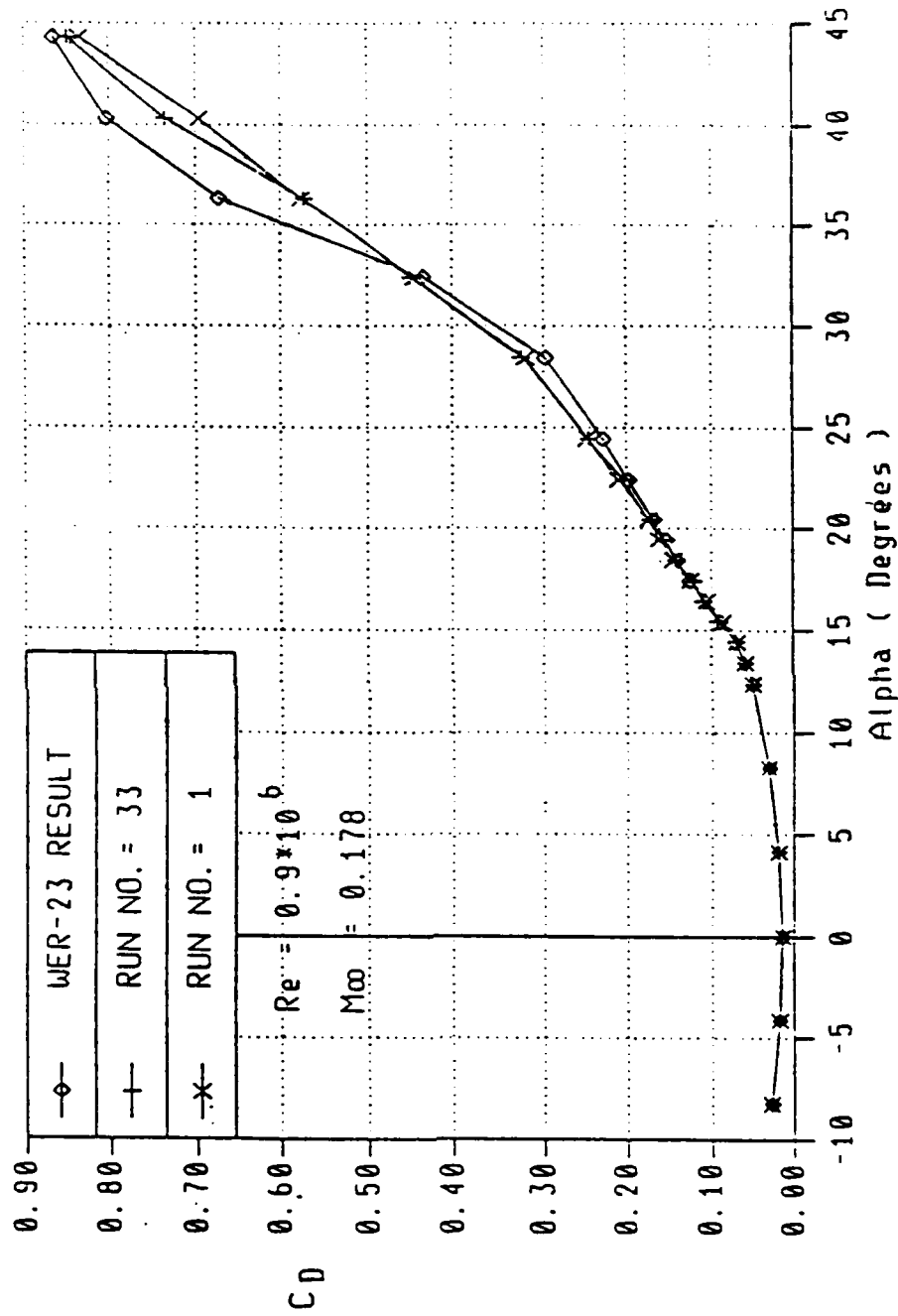


Figure 4. Wing Drag Coefficient for Three Tests

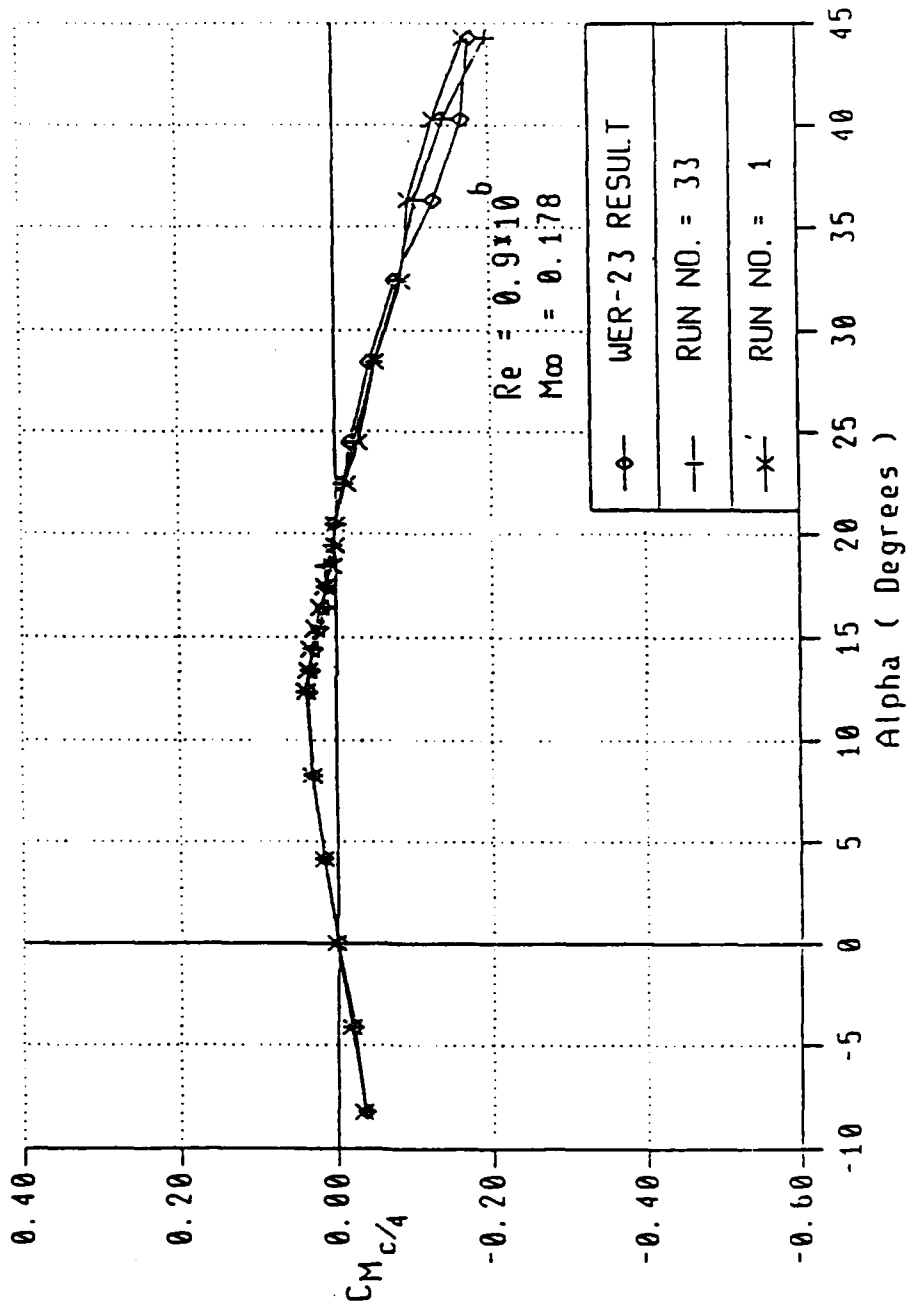


Figure 5. Wing Moment Coefficient for Three Tests

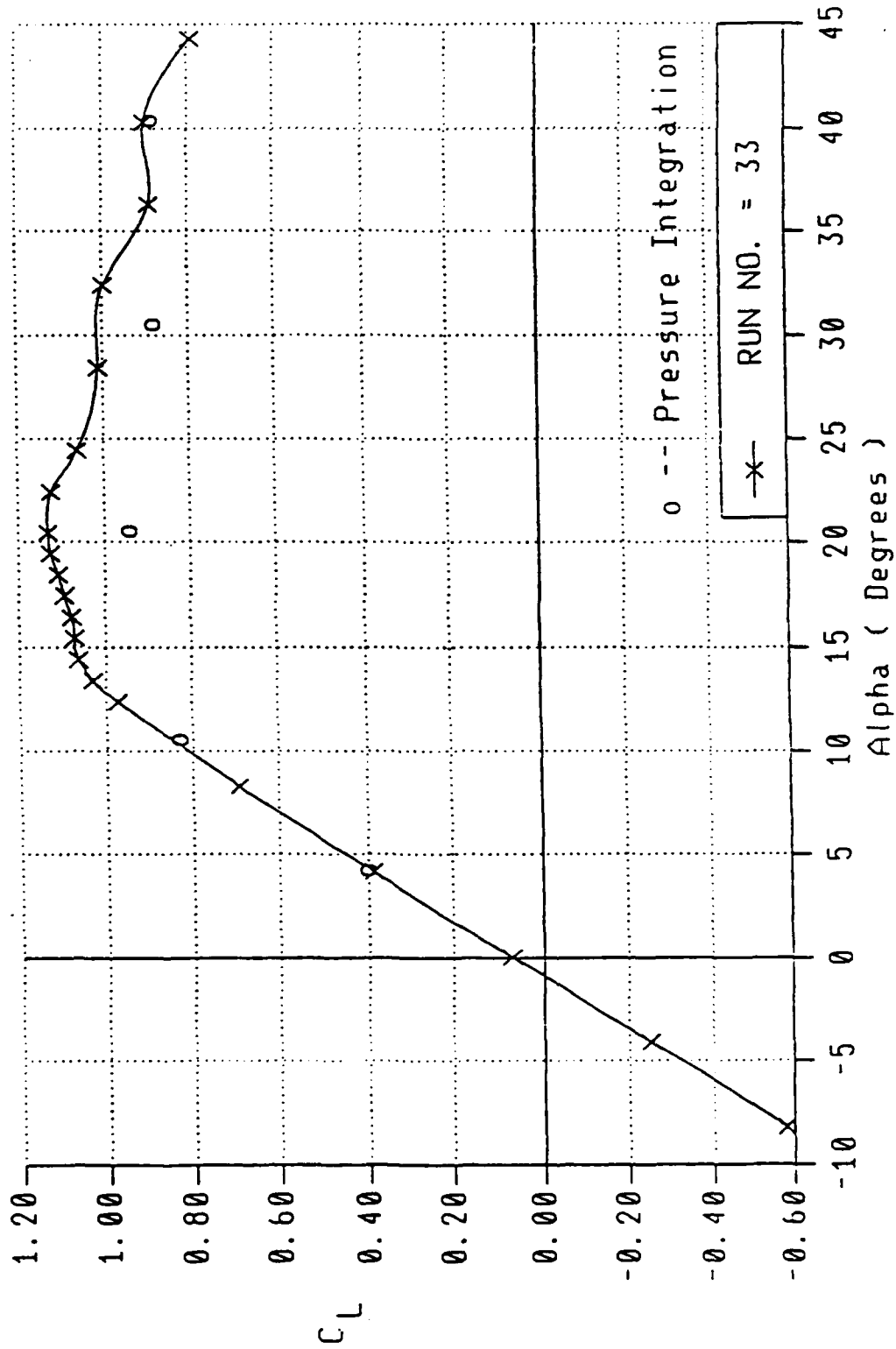


Figure 6. Wing Lift Coefficient By Balance and Integration of Surface Pressure

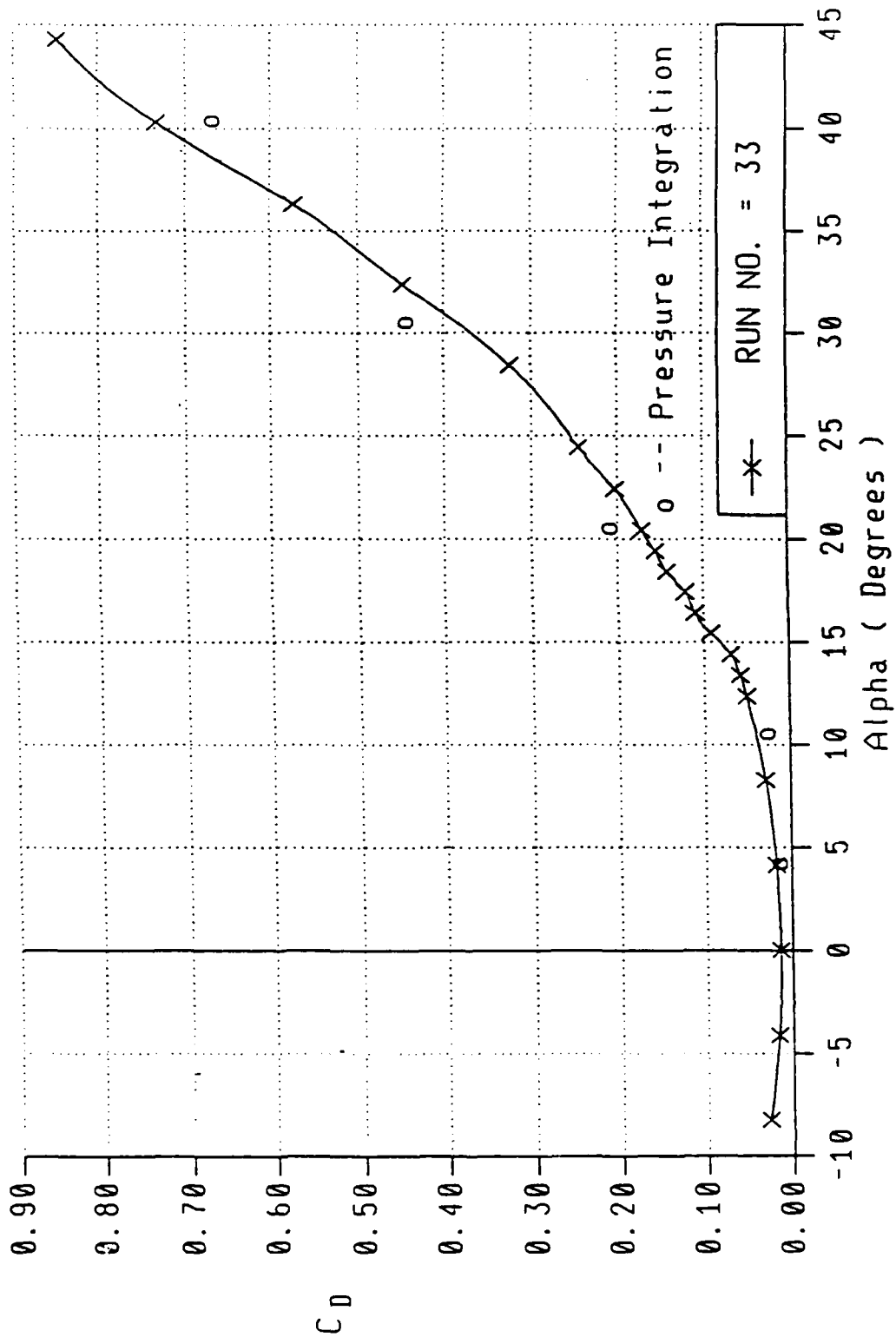


Figure 7. Wing Drag Coefficient By Balance and Integration of Surface Pressure

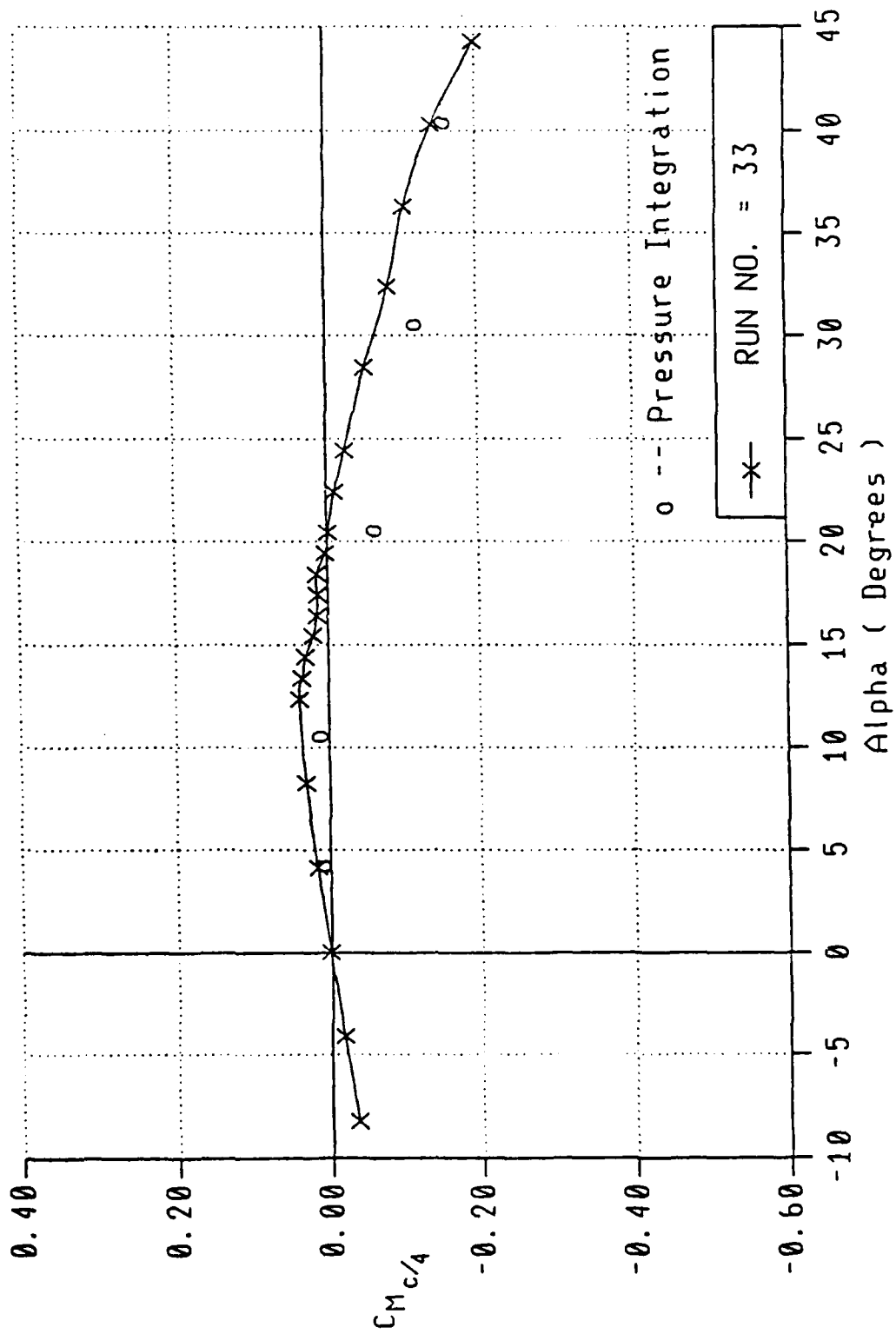


Figure 8. Wing Moment Coefficient By Balance and Integration of Surface Pressure

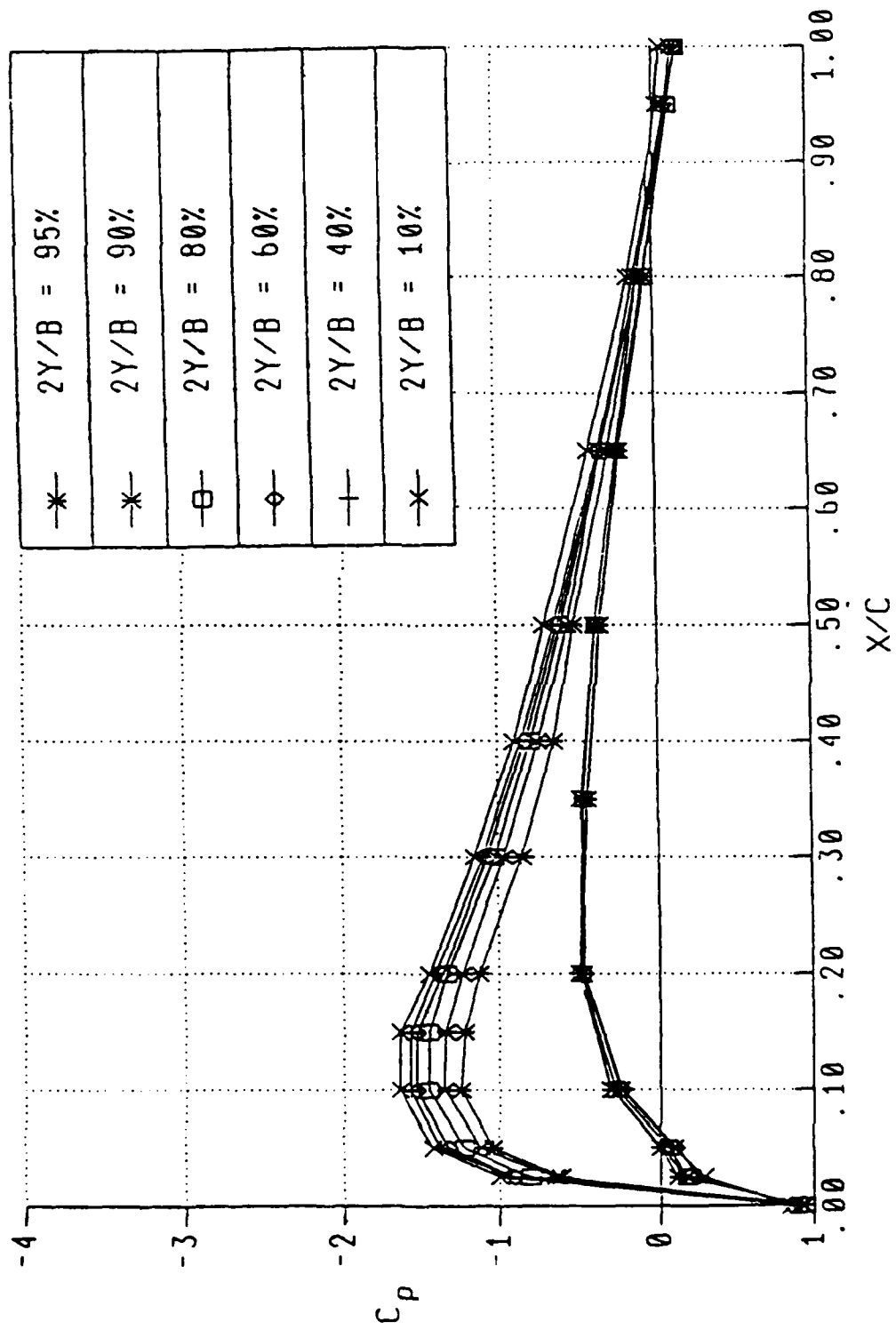


Figure 9. Wing Sections Pressure Distribution $\alpha = 4^\circ$

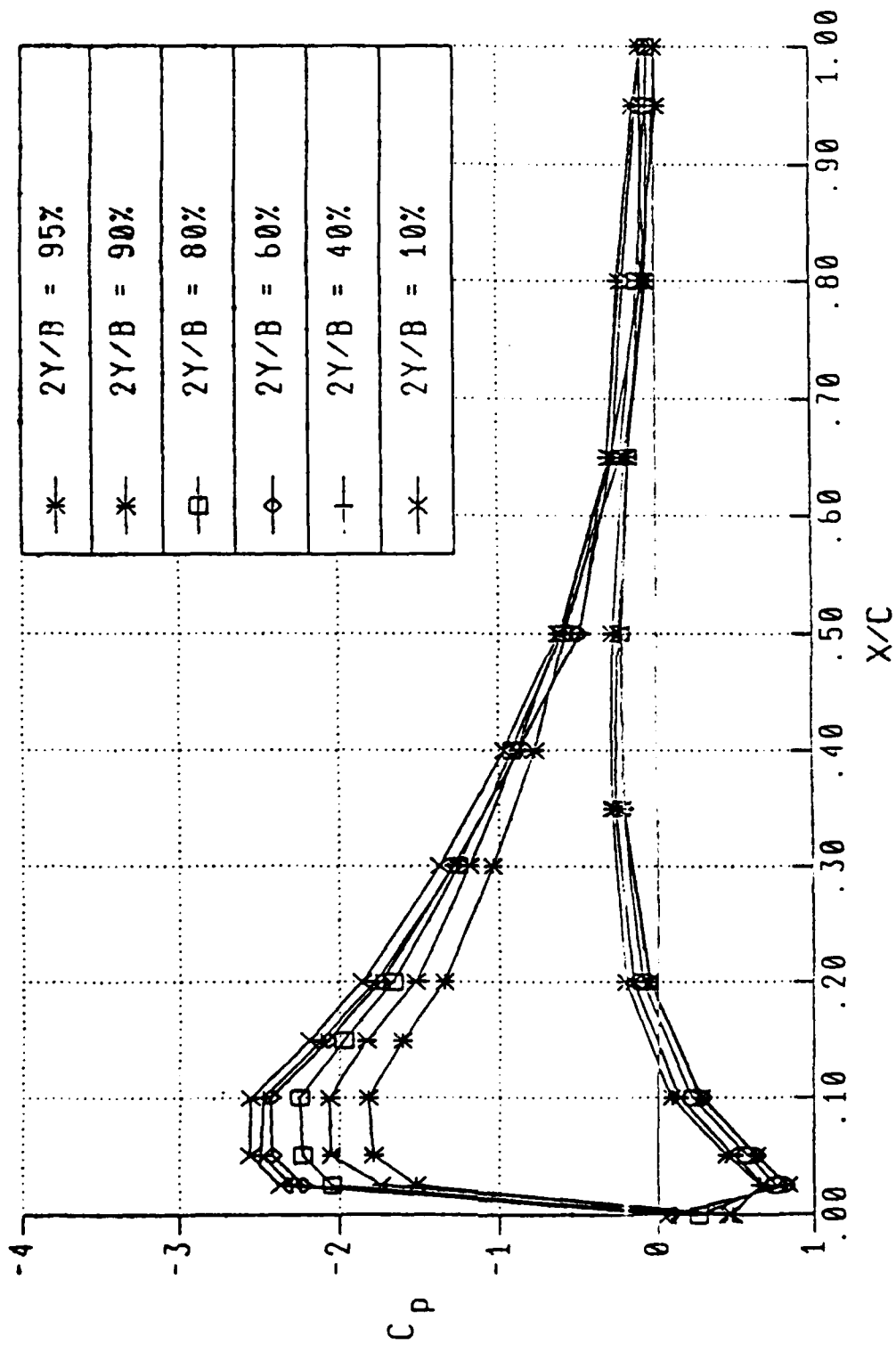


Figure 10. Wing Sections Pressure Distribution $\alpha = 10^\circ$

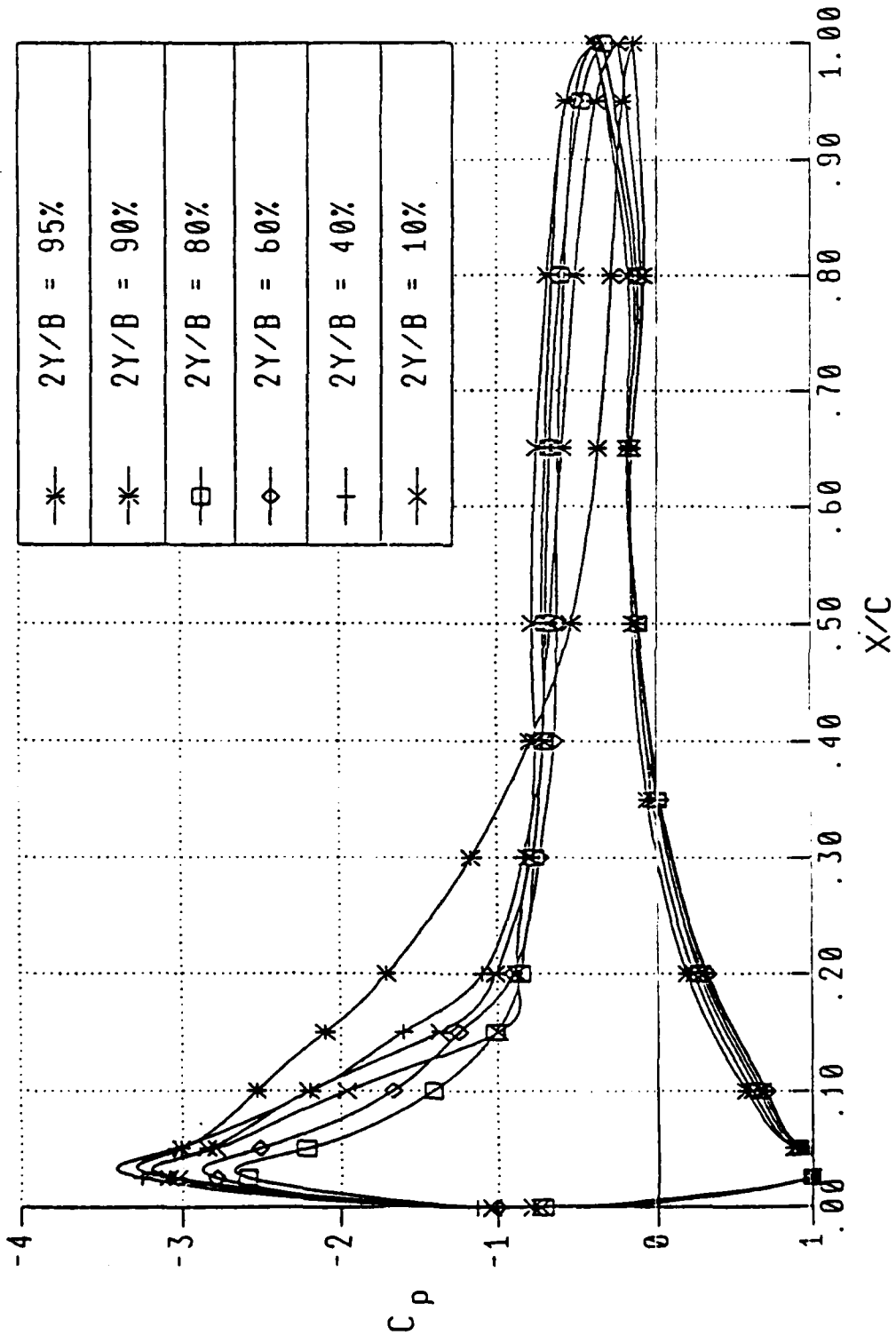


Figure 11. Wing Sections Pressure Distribution $\alpha = 20^\circ$

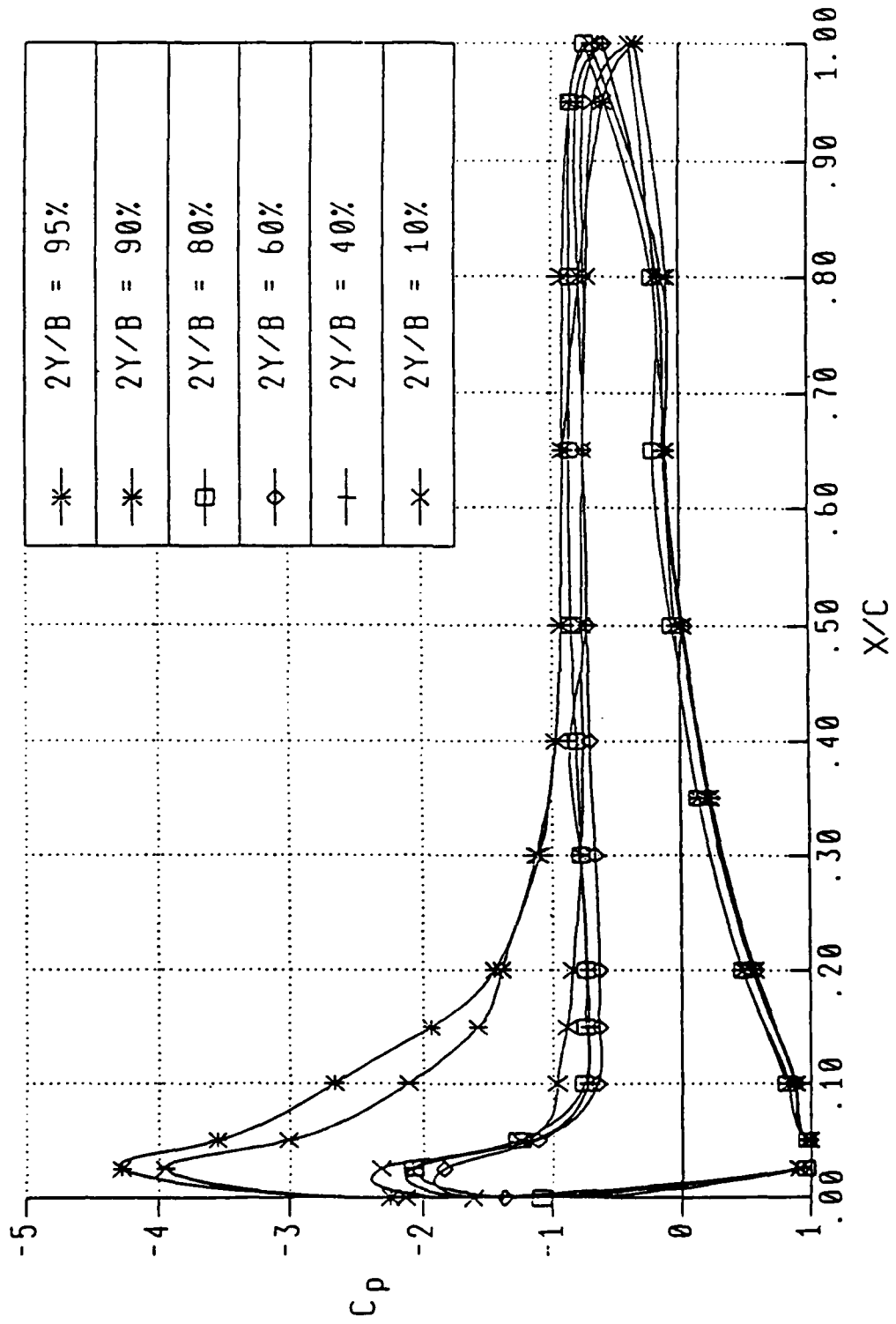


Figure 12. Wing Sections Pressure Distribution $\alpha = 30^\circ$

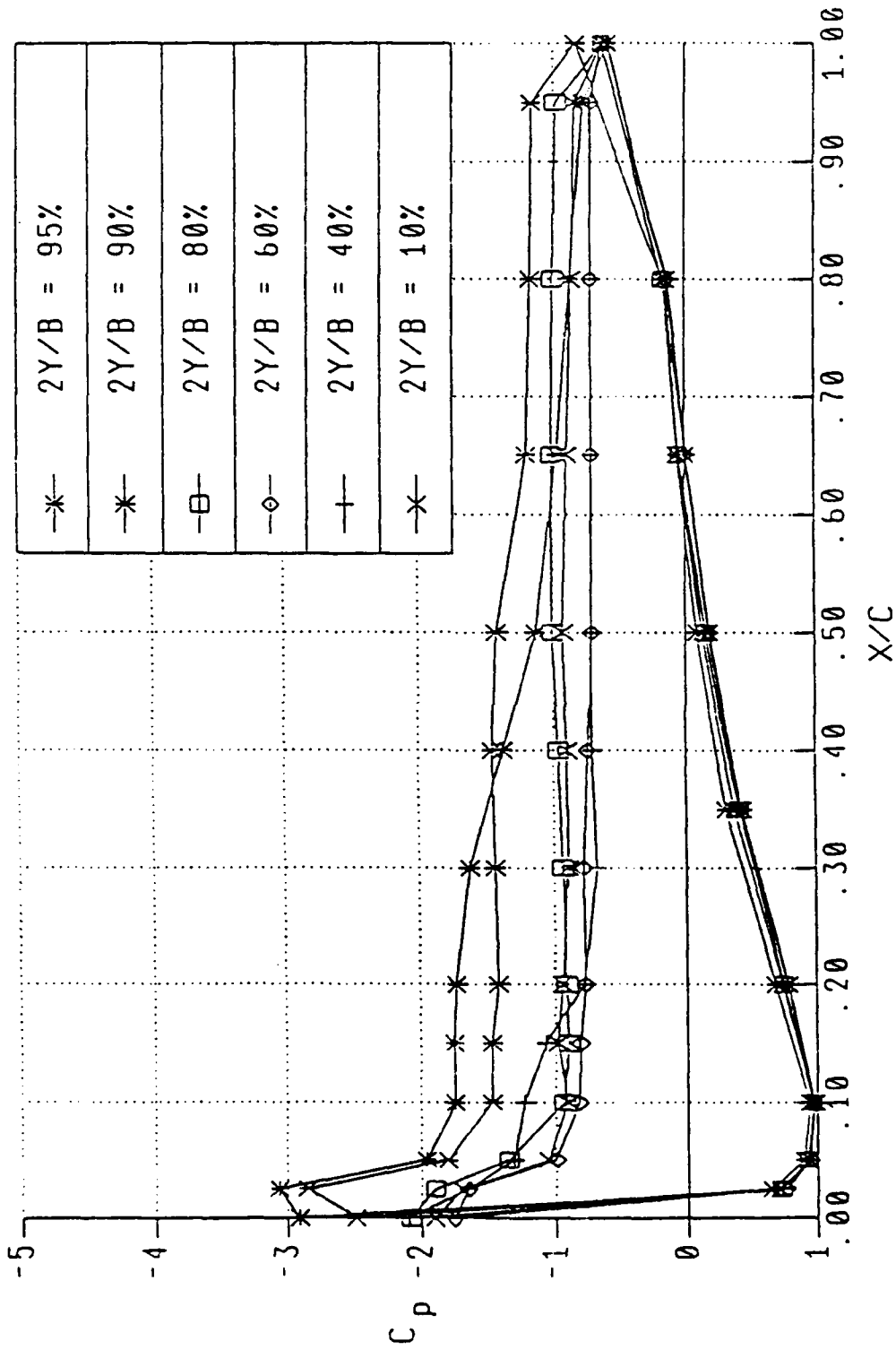


Figure 13. Wing Sections Pressure Distribution $\alpha = 40^\circ$

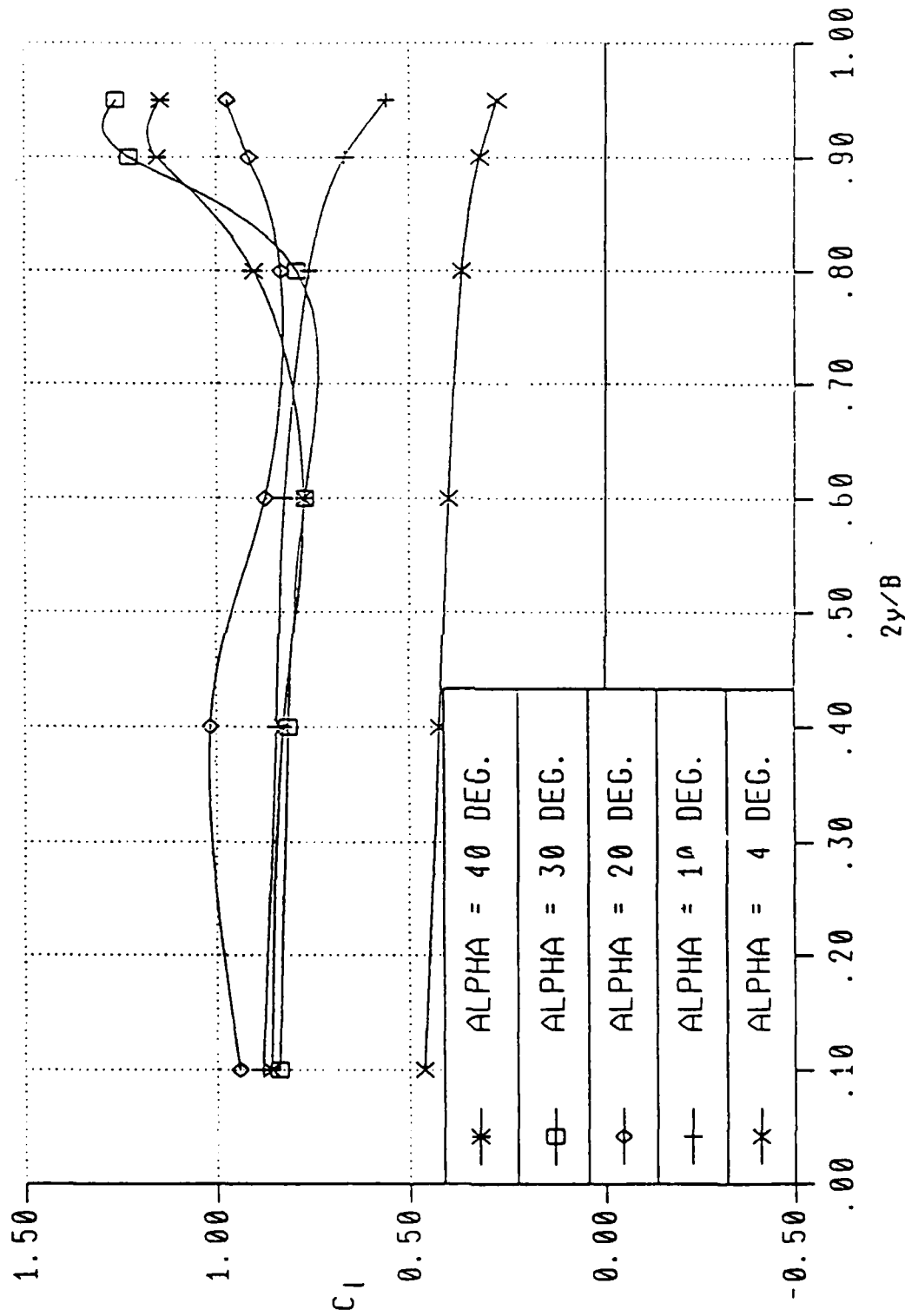


Figure 14. Lift Distribution in Spanwise Direction

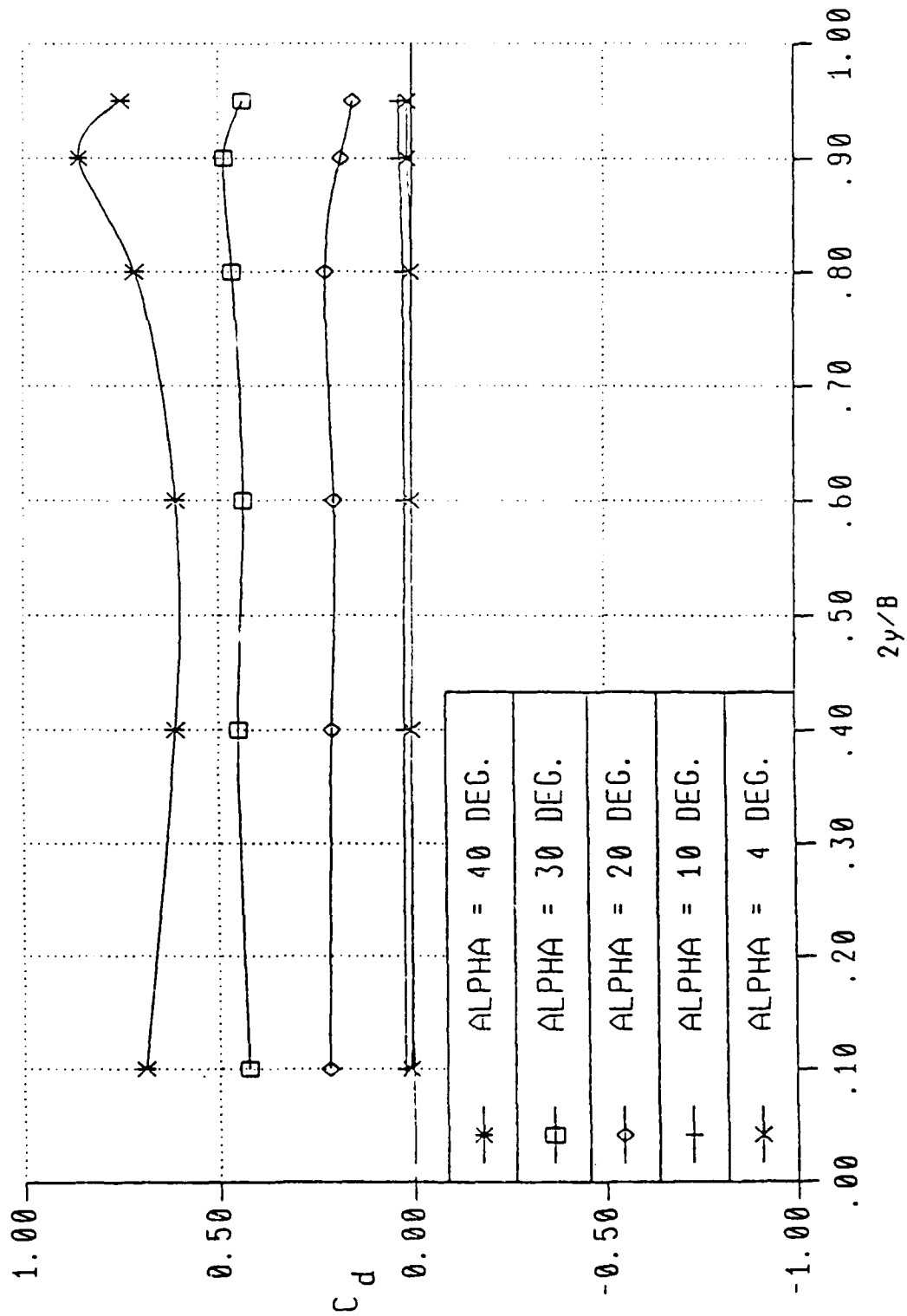


Figure 15. Drag Distribution in Spanwise Direction

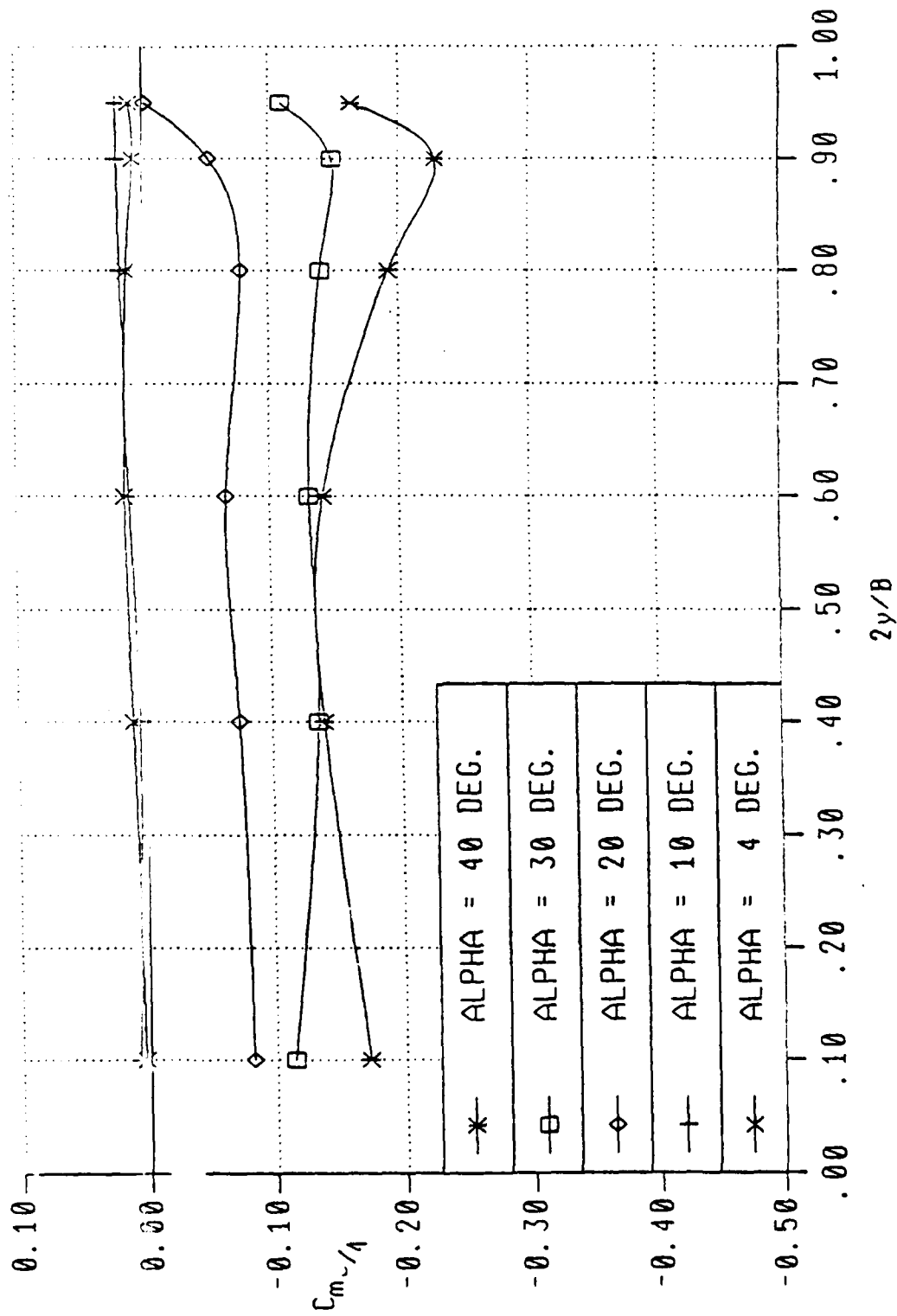


Figure 16. Moment Distribution in Spanwise Direction